

1-1-2014

Understanding the Mechanisms Leading to FSW Property Variations to Aid in Defect Formation Identification via Post-Weld Data Processing

Haley Rubisoff Doude

Follow this and additional works at: <https://scholarsjunction.msstate.edu/td>

Recommended Citation

Doude, Haley Rubisoff, "Understanding the Mechanisms Leading to FSW Property Variations to Aid in Defect Formation Identification via Post-Weld Data Processing" (2014). *Theses and Dissertations*. 4843. <https://scholarsjunction.msstate.edu/td/4843>

This Dissertation - Open Access is brought to you for free and open access by the Theses and Dissertations at Scholars Junction. It has been accepted for inclusion in Theses and Dissertations by an authorized administrator of Scholars Junction. For more information, please contact scholcomm@msstate.libanswers.com.

Understanding the mechanisms leading to FSW property variations to aid in defect
formation identification via post-weld data processing

By

Haley Rubisoff Doude

A Dissertation
Submitted to the Faculty of
Mississippi State University
in Partial Fulfillment of the Requirements
for the Degree of Doctor of Philosophy
in Mechanical Engineering
in the Department of Mechanical Engineering

Mississippi State, Mississippi

May 2014

Copyright by
Haley Rubisoff Doude
2014

Understanding the mechanisms leading to FSW property variations to aid in defect
formation identification via post-weld data processing

By

Haley Rubisoff Doude

Approved:

Judith A. Schneider
(Major Professor)

Rogelio Luck
(Committee Member)

Oliver J. Myers
(Committee Member)

Arthur C. Nunes, Jr.
(Committee Member)

Scott M. Thompson
(Committee Member)

Kalyan K. Srinivasan
(Graduate Coordinator)

Achille Messac
Dean
Bagley College of Engineering

Name: Haley Rubisoff Doude

Date of Degree: May 16, 2014

Institution: Mississippi State University

Major Field: Mechanical Engineering

Major Professor: Judith A. Schneider

Title of Study: Understanding the mechanisms leading to FSW property variations to aid in defect formation identification via post-weld data processing

Pages in Study: 126

Candidate for Degree of Doctor of Philosophy

The study of defect formation and identification is important to the further application of friction stir welding in industry. To better understand the topic, a systematic study was undertaken to describe material flow effects on the formation of defects, to list the various types of defects encountered across a parameter window, and to identify features in the weld force data that can then be used to recognize defects within the weld without destructive testing.

Tracer studies were used to determine the impact of the material flow on defect formation with a determination that proper shoulder contact is necessary to obtain sufficient material flow to fully consolidate the weld. A series of welds across a range of rotational speeds was used to identify mechanisms that led to variations in the mechanical properties of the welded panels. A balance between the x- and y-forces on the tool is needed to produce robust welds that were defect free. UMF was shown to identify regions of changing material flow conditions; however, the identification of intermittent defects was not as successful.

DEDICATION

I would like to dedicate this manuscript to my family for providing me with the opportunity to complete my education with this degree. My parents have provided me with a sound education that I appreciate more and more. They have also given me a wonderful example of what can be accomplished by hard work and have driven me to emulate them. My brothers have shown me that it is ok to follow my own path.

My extraordinary husband has been by my side for this entire process. He has been there when I had complicated engineering questions and to give me pep talks when I could not see the light at the end of the tunnel. He has sacrificed his time and energy to make sure I could continue my education even when it meant delaying his own. His family has also sacrificed to help me finish my studies. His wonderful parents have spent many days taking care of Sam so I could write a few more pages.

Sam's amazing smile makes the hardest day worth it all. He also pushes me to make the most of every minute (of his naps).

ACKNOWLEDGEMENTS

Firstly, I would like to thank my advisor, Dr. Judy Schneider, for all of her support for the last several years. She has constantly provided opportunities to expand my research by attending conferences, completing internships and supporting applications for fellowships. She has allowed me flexibility during my program to participate in these opportunities as well as during some major life events that occurred. Dr. Schneider is always available and always willing to offer advice and help which helped me get through graduate school. She has also shown me there is always a solution to any roadblock. Without Dr. Schneider's constant support, this dissertation would not have been completed.

Secondly, I would like to thank NASA Marshall Space Flight Center for the Graduate Student Research Fellowship that supported me during my doctoral degree program. Thank you Carolyn Russell and the welding team for providing me with the opportunity to come to MSFC for several summers to further my research and get exposure to an amazing area of engineering, America's space program. I would like to especially thank Dr. Art Nunes, Jr. for all of the conversations and deep thought about my research and ways to improve the scientific value of my study. Dr. Nunes has also driven me to improve my use of the English language and appreciate the nuances in the meanings of words.

Next, I would like to thank everyone in the Friction Stir Welding group at Mississippi State, especially the undergraduate (UG) researchers who have worked with me. Without Bryan Patton, Sylvester Stafford, Taylor Waters, and Clay Varner, the tedious job of serial sectioning and polishing several welds would have taken me years to complete. Thank you to Mike Brendel, Josef Cobb, and the UGs for helping me machine and weld panels. Also, thank you for all of the brainstorming and discussions about FSWing that have improved my understanding of the process.

Lastly, I would like to thank my committee for their willingness to sacrifice their time to help me improve my research and ensure that I have earned my Ph.D.

TABLE OF CONTENTS

DEDICATION	ii
ACKNOWLEDGEMENTS	iii
LIST OF TABLES	viii
LIST OF FIGURES	ix
ABBREVIATIONS	xii
CHAPTER	
I. INTRODUCTION	1
1.1 Literature and Background	3
1.2 Three-Prong Approach.....	7
1.2.1 What is a defect?.....	7
1.2.2 How do these defects change the load data collected during welding?.....	9
1.2.3 Can you use a data analysis technique to simplify the identification process?	10
1.3 References.....	12
II. CONTROL OF STRUCTURE IN CONVENTIONAL FRICTION STIR WELDS THROUGH A KINEMATIC THEORY OF METAL FLOW	15
2.1 Abstract.....	15
2.2 Introduction.....	16
2.3 Methods.....	18
2.4 Results and Discussion	20
2.5 Summary.....	29
2.6 Acknowledgements.....	29
2.7 References.....	30
III. INFLUENCE OF TOOL SHOULDER CONTACT CONDITIONS ON MATERIAL FLOW DURING FRICTION STIR WELDING	31
3.1 Abstract.....	31

3.2	Introduction.....	32
3.3	Methods.....	35
3.4	Results.....	37
3.5	Discussion.....	50
3.6	Summary.....	60
3.7	References.....	63
IV.	MECHANISMS OF FRICTION STIR WELD PROPERTY VARIATIONS	66
4.1	Abstract	66
4.2	Introduction.....	66
4.3	Methods.....	70
4.4	Results.....	73
4.5	Discussion.....	81
4.6	Summary.....	87
4.7	References.....	89
V.	IDENTIFICATION OF PERIODIC DEFECTS DUE TO MATERIAL FLOW VARIATIONS IN FSW USING POST-WELD DATA PROCESSING	91
5.1	Abstract	91
5.2	Introduction.....	92
5.3	Methods.....	97
5.4	Results.....	101
5.5	Discussion.....	106
5.6	Summary.....	108
5.7	Acknowledgements.....	109
5.8	References.....	110
VI.	CONCLUSIONS.....	112
6.1	References.....	114
VII.	FUTURE WORK.....	115
APPENDIX		
A.	TEMPERATURE AND STRAIN ESTIMATION.....	116
A.1	Shear Strain Rate Estimation	117
A.2	Temperature Calculation.....	118
B.	WELD PARAMETER WINDOW APPROXIMATION	119
C.	EXAMPLE DATA PROCESSING PROGRAM	121

D. COPYRIGHT PERMISSION.....125

LIST OF TABLES

2.1	Weld schedule for conventional and self-reacting friction stir weld panels	19
4.1	Weld parameter summary	71
4.2	Weld parameter window approximation based on nugget bulge (mm) [28].	71
4.3	Estimated temperature and shear strain rates for each weld.	81
5.1	Weld tool geometry.....	97
5.2	Weld parameters	99
5.3	Plunge parameters for Weld 1.....	99
5.4	Plunge parameters for Weld 2.....	99
5.5	Plunge parameters for Weld 3.....	99
5.6	Plunge parameters for Weld 4.....	100

LIST OF FIGURES

1.1	Schematic of FSW process	1
1.2	SR-FSW can be modeled as reflected C-FSW about the anvil when using a left-hand/right-hand tool.....	3
1.3	Increasing plunge force increases the shoulder contact and diminishes volumetric defects.	5
2.1	FSW pin tool flow.....	17
2.2	FSW panel layout showing run-on tabs on the 2 ends.....	19
2.3	Layout directions of x-ray radiographs were taken of the weld region.	20
2.4	Longitudinal views of material flow	21
2.5	Plan inverted x-ray of friction stir welds processed at 200 rpm, 4.5 ipm, and 8000 lbs plunge force.	23
2.6	Transverse radiographs with copper tracer at varying parameters	24
2.7	Transverse friction stir weld radiographs of the trace of the weld seam marked by a deposit of Cu at varying rotational speeds.	27
2.8	Projected trace of copper tracer coated on the faying surface prior to the FSW.	28
3.1	Conventional FSW terminology showing the tool during a weld.	32
3.2	Transverse view of a conventional FSW with regions of interest labeled.	33
3.3	Configuration of the metal plates for the butt welds.....	36
3.4	X-ray radiograph of plan view of FSW panel.....	37
3.5	Regions from Figure 3.4b that were sliced and prepared for transverse x-ray radiography and microscopy.	38
3.6	X-ray radiographs of transverse sections shown in Figure 3.5.	39

3.7	SEM images of the lighter regions of dispersed lead	40
3.8	Transverse SEM images with lead traces	42
3.9	Optical and corresponding transverse SEM image of LX-3	43
3.10	SEM image of LX-4.....	44
3.11	Color enhanced overlay images from slices LX-3 and LX-4	45
3.12	Optical and corresponding SEM image of longitudinal section of LX-3	46
3.13	Optical and corresponding SEM image of longitudinal section of LX-4	47
3.14	Longitudinal overlay of LX-3 and LX-4	48
3.15	Increasing magnification of lead rich region showing areas proposed as shear surface.	49
3.16	Close up of AS root surface from Section LX-14 (Figure 3.8e).....	50
3.17	Three incompressible flow fields.....	52
3.18	Resulting material flow as affected by the pin and shoulder.	54
3.19	Proposed variation in contact conditions at shoulder	56
3.20	Schema for the generation of lead wire traces in plan and transverse sections.....	58
4.1	Basic layout of the parameter window based in the literature.	69
4.2	The weld tool and shoulder detail.....	70
4.3	Representative cut plan for a weld.....	72
4.4	Macrographs of welded panels with the advancing side (AS) on the left.	74
4.5	Transverse macrographs of the weld structure	74
4.6	The mating transverse sections from the tool break location at 150 rpm 8.7cm into the length of the weld.....	75
4.7	A close-up of the layering of material from Figure 6a.	75
4.8	Total volumetric defect areas for each transverse section of the 200, 250, and 1000rpm welds.	77

4.9	Example volumetric defect images	78
4.10	Average ultimate tensile strength and hardness results	79
4.11	XRD data for 250, 400, and 600 rpm welds	80
4.12	X-force vs Y-force plot for each rpm.	84
4.13	Summary of the parameter window.	87
5.1	Shoulder contact comparison	94
5.2	Variation in plunge force as tool shoulder is seated	96
5.3	FFT results with and without shoulder contact	96
5.4	Weld schematic with x, y, and z forces and torque labeled [14]	98
5.5	As-welded panels	102
5.6	UMF analysis showing segment 16 as different from the other weld segments.....	103
5.7	Macro and micro results of transverse inspection.....	103
5.8	UMF results indicating segment 6 and 9 at different from the other segments.....	104
5.9	Macroscopic images of segments 6 and 9 from weld 2	104
5.10	Defect free macro images for weld 3 and 4.	105
5.11	UMF analysis results from slow plunge using the smaller tool	106
5.12	UMF analysis results from fast plunge using the smaller tool.....	106

ABBREVIATIONS

ANN	<i>Artificial Neural Network</i>
AS	<i>Advancing Side</i>
C-FSW	<i>Conventional Friction Stir Weld</i>
EDS	<i>Energy Dispersive Spectrometer</i>
FFT	<i>Fast Fourier Transform</i>
FSW	<i>Friction Stir Weld</i>
HAZ	<i>Heat Affected Zone</i>
ICA	<i>Independent Component Analysis</i>
LDA	<i>Linear Discriminant Analysis</i>
MMPM	<i>Millimeters Per Minute</i>
OM	<i>Optical Microscopy</i>
PCA	<i>Principal Component Analysis</i>
PM	<i>Parent Material</i>
PSA	<i>Phased-Space Analysis</i>
RPM	<i>Revolutions Per Minute</i>
RS	<i>Retreating Side</i>
SEM	<i>Scanning Electron Microscope</i>
SR-FSW	<i>Self-Reacting Friction Stir Weld</i>
SZ	<i>Stir Zone</i>

TMAZ	<i>Thermomechanically Affected Zone</i>
UMF	<i>Unsupervised Match Filter</i>
UTS	<i>Ultimate Tensile Strength</i>
XRD	<i>X-ray Diffraction</i>

CHAPTER I

INTRODUCTION

The field of friction stir welding (FSWing) has been established as a viable welding process in industry and academia despite the lack of complete understanding of material flow and how the flow is affected by processing parameters [1]. While several studies have used tracers to show orderly flow patterns of the weld material, only basic concepts of the material flow pattern can be deduced from the post weld placement as documented by x-rays and metallographs [2-7]. Due to the automated nature of FSWing, data can be collected from various transducers to monitor force in addition to torque. Thus, valuable information about the flow may be available in this data collected during FSWing. A schematic of the FSW process is available in Figure 1.1

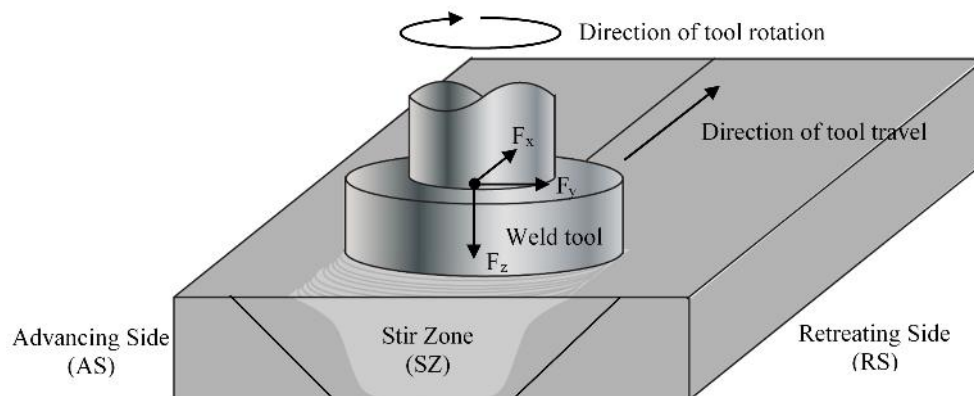


Figure 1.1 Schematic of FSW process

Often the assumption is made that FSW is a steady state process; however, this does not account for anomalies that have been noted in longer (>2ft) welds [8]. A dynamic “stick-slip” condition on the surface of the weld tool may be needed to match the model results to the observed results [9]. Kinematic approaches toward quantifying the material and contact conditions have been published recently which offer experimental evidence of the proposed stick-slip [10]. This matches assumptions made by numerical modeling in which the contact conditions alternate between fully sticking and fully slipping in order to match experimental results [9].

Considering that the FSW process is not static, but rather quasi-static in nature, post weld structure reveals little direct information about the dynamics of the process. Resolving the dynamic nature of FSWing, is the next step in understanding the flow patterns in an effort to optimize the process parameters and tool design. Thus, this study explored the dynamic nature of FSWing by combining aspects of material flow with signal processing of the force and torque data collected during FSWing of panels. Although research has been carried out on acoustic emission analysis [11], most research seems to be interested in signal processing of the force and torque data collected during FSWing of panels as a way to determine weld quality [12-24]. In the past, research has focused on identifying full panels as “good” or “bad” [12,14,15, 21], but work is beginning to move toward identifying isolated low strength regions in “good” welds [16,23,24]. Processing the force and torque signals obtained during a FSW should provide information on the changes in the forces which can be correlated with material flow. Non-optimized material flow has been correlated with defect formation which is detrimental to the FSW strength [25-28].

1.1 Literature and Background

Because FSW is a complex process in which very little is understood about the flow of material around the tool, some simplifications are made to more easily model the process and study the defect formation process. One such simplification is initially studying flow in conventional FSW (C-FSW) then applying that knowledge to self-reacting FSW (SR-FSWing). SR-FSWing has been kinematically modeled as two conventional FSWs reflected at the anvil to produce a SR-FSW with two shoulders and a pin as shown in Figure 1.2. Because of this assumption, the flow of the material was studied in a more simplified way, and the simplification allows for more testing of hypotheses since a C-FSW setup is available in the Mississippi State University lab.

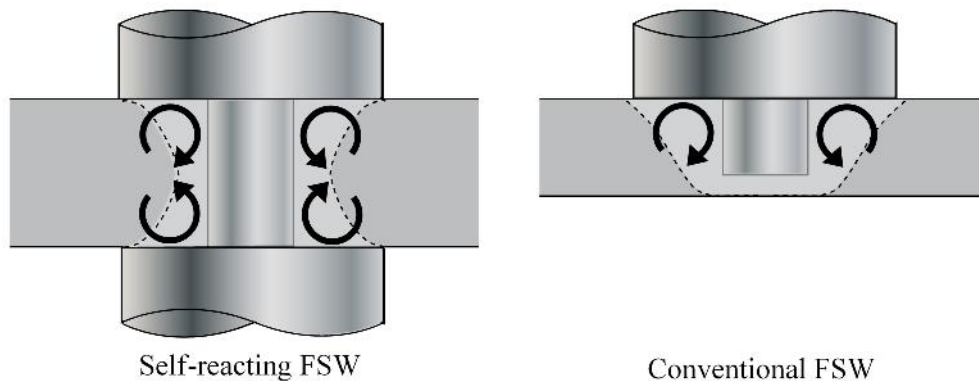


Figure 1.2 SR-FSW can be modeled as reflected C-FSW about the anvil when using a left-hand/right-hand tool.

Tracer studies [10] on C-FSW have led to a better understanding of material flow during FSW. Lead and tungsten tracers suggest a stick-slip boundary condition at the tool/ work piece interface. Even though the shoulder may appear to be in full contact with the work piece based on the tool marks on the surface, the shoulder may not be fully

engaging the material. An example of lack of shoulder engagement was seen in a series of self-reacting welds where the nugget showed evidence of less shoulder interaction in the weld with lower strength. No visible defects were present in the low strength weld, but the nugget had an advancing side bulge and decreased shoulder engagement when compared to the higher strength weld [24].

Voids are reported to form when the plunge force is insufficient to fully consolidate the material flowing around the tool [27, 29-36]. One suspected cause of the changes in the plunge force is changes in the amount of shoulder contact during welding as shown in Figure 1.3. McClure [37] has previously shown that material flow is strongly affected by shoulder contact. McClure completed several plunge tests where macroscopic images were taken from transverse samples at various times during the plunge phase. As the threaded pin is lowered into the work piece, material flow is concentrated around the pin tool/ work piece interface and very little if any material movement occurs through the material thickness. Once the shoulder contacts the crown surface, material begins to move in a through thickness pattern near the bottom edge of the pin. It appears that a vortex of material in the shape of a ring is moving around the threaded tool. The general shape of the vortex is similar to that of a doughnut revolving around the tool moving material through the thickness of the work piece. If the shoulder is not fully engaged, insufficient material flow may form voids. Because of this data, it was hypothesized that the force and torque data collected during welding may indicate this change in material flow and correlate with changing contact conditions.

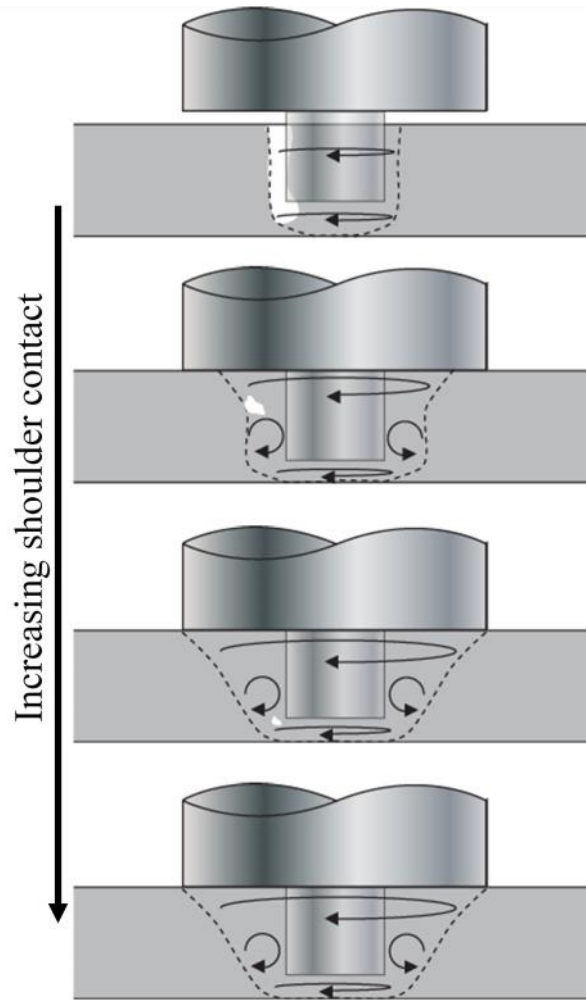


Figure 1.3 Increasing plunge force increases the shoulder contact and diminishes volumetric defects.

Most researchers are in agreement that the signals from the force and torque data hold more promise for detecting problems in the weld [12, 15]. Initial studies focused on determining which signals provided the most information about weld quality. Arbegast published a thorough study of all weld signals as well as weld parameters to determine which signals correlate to weld quality [15]. In this study, analysis of the tool rotation speed, travel speed and plunge force signals did not reveal indicators of problems in

known defective welds [15]. The torque and forge (z) forces did not show enough variation at problem areas to determine if welds contained small voids (0.05 mm diameter) [15]. Analysis of the side (y) force showed changes in the forces did indicate locations where weld defects were present. A drop in the y force corresponded with the formation of a void within the weld. Analysis of the travel (x) force did not show any correlation between fluctuations in the force and the occurrence of weld defects.

Morihara also studied the relationship between void formation and the x, y, and z forces [17]. The forces and the resultant force magnitude and direction were examined in frequency space using fast fourier transform (FFT). The occurrence of low frequency force events corresponded to locations of void defects in the welds [17]. In studies by Boldsaikhan, the x, y, z forces and torque were considered as indicators of weld quality based on welding experience [12]. Changes in the y force were found to be most strongly correlated to weld quality when comparing the 3 forces and torque [12]. Fleming was also able to locate defects in welds by analyzing the axial force data during lap welding [14]. Gimenez-Britos, et al. also had success identifying locations of weld defects by analyzing the y forces [16]. Jene has used x and y force frequency analysis to determine when welds contain voids and the location of tool breakage [18]. For self-reacting FSW (SR-FSW), the force correlations may not hold true due to the lack of a backing anvil. Further studies on SR-FSWs are needed to determine if other forces, such as the pinch force as found by others, will lead to indications of defects [19].

Several data processing schemes have been reported in the literature including phased-space analysis (PSA), artificial neural network (ANN), principal component analysis (PCA), and linear discriminate analysis (LDA) [12-18, 20]. Each of these

methods as well as others such as independent component analysis (ICA) and unsupervised matched filter (UMF) were compared using a previously acquired weld. Based on the results of the comparison, UMF and LDA was the most intriguing as they led to clear, concise results that could be easily used to locate defective regions of the weld [38]. Despite the good results for LDA with this weld, the need for well understood training data makes LDA less appealing when during the initial application of data analysis to welds. UMF on the other hand provides a similar result without needing training data.

1.2 Three-Prong Approach

A systematic approach to understanding defect formation and identification in FSWs was needed so three questions were asked in an attempt to clarify the research process.

1.2.1 What is a defect?

There are two general types of defects reported in FSWing: geometric versus material flow related. Geometric type defects include lack of penetration and lack of fusion and are caused by a misfit in the layup or geometry of the weld panel and weld tool. Lack of penetration defects generally occur when the weld tool is not deep enough to fully involve the material at the root of the weld leaving behind a small section of unconsolidated weld seam. Lack of fusion defects can also occur when the weld tool is offset from the weld seam during welding and the weld seam is not fully consumed [39]. Although both defect types can reduce the structural integrity of the weld, flow related

defects and their impact on the dynamics of the process are addressed in this study since geometric related defects can generally be mitigated during the weld fitup.

Flow related defects are more numerous in type and have been linked to specific weld parameters including travel speed, plunge force, and tool rotational speed [40-43]. Also included in this category are non-optimized tool geometry and improperly sized tool shoulder for the material thickness. If the weld parameters result in a FSW that is too hot (ex. high rotational speed and low travel speed) several defects can occur including: surface galling, excessive flash which may form a wormhole, and the root-flow defect where material flow patterns can be seen on the root side of the weld [39]. If the weld is too cold, lack of consolidation or intermittent void and scalloping defects are formed [39]. Also, cool welds can result in shingle lap defects or kissing bonds where the weld seam is not completely forged together [44]. Features of the FSW tool can also lead to defects in the FSW. One example is the wormhole defect found when the tip of the weld tool is not rounded or blunted leaving a point at the tip [45].

One difficulty in located defects in welds is the proper identification of a FSW defect. Volumetric type defects are easy to identify based on density differences in the area where material is missing. Although the missing area must be large compared to the wavelength of the source being used for inspection. Other types of defects related the resulting metallurgy maybe difficult to detect [46]. One example of this is softening of the welded material due to overheating during welding. This can occur in precipitation strengthened aluminum alloys including 2219 which is the material used in this study. If the weld temperature rises above a threshold for the material, coarsening of the precipitates may lead to a softening of the material or possible liquation at grain

boundaries [47]. This will give unexpectedly low tensile strength and hardness in a weld that appears visually to be a good weld. Destructive testing is usually required to identify this type of defect, although overheating may also lead to loss of shoulder contact which could be detected.

Chapter II and III of this manuscript describe the effect of weld parameters on material flow within the weld by using copper and lead tracers to map the material flow. Chapter III also explores the contact conditions between the tool and the workpiece and the resulting effect on material flow. Chapter IV uses the material flow information from Chapters II and III to better understand how defects are formed during the welding process and how to define a “good” FSW by determining the factors that lead to poor weld properties across a range of weld parameters.

1.2.2 How do these defects change the load data collected during welding?

Once the defects were fully described, the next step was to attempt to create flow related types of defects and determine what types of data signatures were present when these defects were formed. A few studies have used data analysis techniques to classify weld quality [12-24]. Most focus on classifying full weld panels as either “good” or “bad”[12,14,15,21]. Weld defects do not always run the full length of the weld, however, and most production welds are produced in a range where good welds are expected. Smaller type defects that occur in weld near the correct processing parameters can occur intermittently making them difficult to locate. There are some papers in the literature that are identifying intermittent type defects using a neural network approach [23]. This method requires the input of several characteristics so that the weld quality of different

segments can be determined; however, an understanding of the data features used to identify the defective regions is not required.

The change in flow due to a given type of defect may have a specific signature indicating that the defect has occurred. Identifying these regions in the data will provide insight into the material flow that is required to form a defect but will also provide an indicator that a defect has formed without needing destructive testing.

Chapter IV examines the high speed load data collected during FSWing panels across a range of parameters to determine what force characteristics are present for a good weld. Chapter V expands on the load data investigation by applying data analysis techniques.

1.2.3 Can you use a data analysis technique to simplify the identification process?

The large quantities of data that are collected during welding require some processing to ease inspection. Methods to extract the significant data can be used to reduce the dimensionality of the data file to make subsequent processing less computationally intensive. Reducing the time required for data processing will eventually aid in implementing the process as a real time process instead of post weld processing as is part of this research. This would enable defects to be identified early in development and corrective actions to be completed to prevent an entire weld from containing defects.

Therefore, it is important to consider processing methodologies while attempting to interpret the data collected. Once the signatures of defect formation are understood, analysis techniques can be used to automatically identify the regions with differences in the data. Chapter V investigates the use of unsupervised matched filter as a method for

identifying regions of the FSW with changing forces during welding. The method of analysis was applying FFT, PCA, and then UMF. UMF was selected because it does not require training data. For this work, data analysis techniques that required training data were not selected to simplify the analysis process.

1.3 References

- [1] J.A. Schneider. Friction Stir Welding and Processing. Ed. R.S. Mishra and M.W. Mahoney. Materials Park, OH: ASM International, 2007.
- [2] K. Colligan, Welding Res. Suppl., July (1999) 229s-237s.
- [3] T.U. Seidel, A.P. Reynolds, Met. & Mat. Trans., 32A (2001) 2879-2884.
- [4] M. Guerra, C. Schmidt, J.C. McClure, L.E. Murr, A.C. Nunes, Jr., Mat. Char., 49 (2003) 95-101.
- [5] F. Contreras, E.A. Trillo, L.E. Murr, J. Mat. Sci., 37 (2002) 89-99.
- [6] J.H. Ouyang, R. Kovacevic, J. Mat. Eng. & Perf., 11 (2002) 51-63.
- [7] J.A. Schneider, A.C. Nunes, Jr., 7th Intl. Conf. Trends Welding Research, 2005.
- [8] Personal communication. Dr. Arthur C. Nunes, Jr. NASA MSFC. Jan 29, 2010.
- [9] H.R. Shercliff and P.A. Colegrove, Friction Stir Welding & Processing II. TMS, 2003.
- [10] J.A. Schneider, R. Beshears, A.C. Nunes, Jr., Mat. Sci. & Engr. A, 435-436 (2006) 297-304.
- [11] Chen, et al., Intl J. Machine Tools and Manuf., 43 (2003) 1383-1390.
- [12] E. Boldsaikhan, et al., Friction Stir Welding and Processing IV, TMS 2007.
- [13] E. Boldsaikhan, E. Corwin, A. Logar, and W. Arbegast, Proc. 6th Intl. Sym. Friction Stir Welding, 2006.
- [14] P. Fleming, et al., Sensor Review. 28 (2008) 62-67.
- [15] W.J. Arbegast, Friction Stir Welding and Processing III, TMS 2005.
- [16] P. Gimenez-Britos, et al., 8th Intl. Sym. FSW, 2010.
- [17] T. Morihara, Masters of Science Thesis, South Dakota School of Mines and Technology, Rapid City, South Dakota, 2004.
- [18] T. Jene, et al., Welding in the World. 52 (2008) 47-53.
- [19] J.A., Schneider, Proc. from MS&T, 2009
- [20] H. Okuyucu, et al., Mat. Des. 28 (2007) 78-84.

- [21] P.G. Britos, et al., Friction Stir Welding and Processing V, TMS 2009.
- [22] E. Boldsaikhan, et al., Friction Stir Welding and Processing VI, TMS 2011.
- [23] E. Boldsaikhan, et al., Applied Soft Computing. 11 (2011) 4839-4846.
- [24] H. Doude, et al., 9th Intl. Sym. Friction Stir Welding, 2012
- [25] W.J. Arbegast, Hot Deformation of Aluminum Alloys, ed. Z. Jin., TMS, 2003.
- [26] Bendzsak, 2nd Intl. Sym. Friction Stir Welding, 2000.
- [27] K. Kumar and S. Kailas, Mat. Sci. Eng. A, 485 (2008) 367-374.
- [28] J.A. Schneider, A.C. Nunes, and M.S. Brendel, 8th Intl FSW Sym. 2010.
- [29] F. Gratecap, G. Racineux, S. Marya, Int. J. Mater. Form. 1 (2008) 143-158
- [30] K. Elangovan, V. Balasubramanian, Mater. Des. 29 (2008) 362-373.
- [31] K. Kumar, et al., Mat. Manuf. Proc. (2011).
- [32] Nunes, A.C., Automotive Alloys and Joining Aluminum Symposia, TMS 2001.
- [33] J. Seaman, B. Thompson, in:, Proc. Twenty-First 2011 Int. Offshore Polar Eng. Conf., International Society of Offshore and Polar Engineers, Maui, Hawaii, 2011.
- [34] Z.W. Chen, T. Pasang, Y. Qi, Mater. Sci. Eng. 474 (2008) 312.
- [35] K. Kumar and S. Kailas, Mat. Des. (2008).
- [36] A.J. Leonard, S.A. Lockyer, in:, Proc. 4th Int. Frict. Stir Weld. Symp., TWI, Park City, Utah, 2003.
- [37] J. McClure, Summer NASA Research Program 2004.
- [38] J.A. Schneider, H. Doude, and B. Ma., Proc. MS&T 2010.
- [39] W.J. Arbegast, Friction Stir Welding and Processing. Materials Park, OH: ASM International, 2007.
- [40] R.S. Mishra and Z.Y. Ma, Mater. Sci. Engr. R, 50 (2005), 1-78.
- [41] Y.H. Zhao, et al., Mater. Sci. Technol. 22 (2006) 45–50.
- [42] Y.G. Kim, et al., Mater. Sci. Eng. A 415 (2006) 250–254.

- [43] H.N.B. Schmidt, et al., *Acta Mater.* 54 (2006) 1199–1209.
- [44] A. Oosterkamp, et al., *Weld. J.* 83 (2004) 225s–231s.
- [45] J. Querin, and J. Schneider. Trends In Welding Research Conf, 2-6 Jun 2008.
- [46] J. Schneider, R. Stromberg, P. Schilling, B. Cao, W. Zhou, J. Morfa, O. Myers, *Weld. J.* (2013) 11s-19s.
- [47] B. Li, and Y. Shen. *Mat. Des.* 32 (2011) 3796-3802.

CHAPTER II
CONTROL OF STRUCTURE IN CONVENTIONAL FRICTION STIR WELDS
THROUGH A KINEMATIC THEORY OF METAL FLOW¹

2.1 Abstract

In friction stir welding (FSW), a rotating pin is translated along a weld seam so as to stir the sides of the seam together. Metal is prevented from flowing up the pin, which would result in plowing/cutting instead of welding, by a shoulder on the pin. In conventional FSW, the weld metal rests on an “anvil”, which supports the heavy “plunge” load on the tool. In this study, both embedded tungsten wires along and copper plating on the faying surfaces were used to trace the flow of AA2219 weld metal around the C-FSW tool. The effect of tool rotational speed, travel speed, plunge load, and pin thread pitch on the resulting weld metal flow was evaluated. Plan, longitudinal, and transverse section x-ray radiographs were examined to trace the metal flow paths. The results are interpreted in terms of a kinematic theory of metal flow in FSW.

¹ From *Friction Stir Welding and Processing V*, R.S. Mishra, M.W. Mahoney, and T.J. Lienert, eds., pp. 149-158. Copyright © 2009 by The Minerals, Metals & Materials Society. Reprinted with permission.

2.2 Introduction

FSW is a solid state joining process developed by The Welding Institute [1]. Since the development of FSW, researchers have worked to model weld metal flow in the vicinity of the tool and its relation to the weld structure. Early theories suggested a “chaotic-dynamic mixing” in the material [2]. Later tracer studies, using steel shot [3], aluminum shims [4], copper foil [5], bi-metallic welds [6-7], and tungsten wire [8], revealed defined streamline flow paths of the tracers interpretable in terms of an orderly flow of metal around the pin-tool. However, the effect of process parameters on the resulting metal flow is still not physically understood [9, 10]. This becomes increasingly important in designing robust tooling and process schedules to avoid defects such as wormholes.

The rotating weld tool used in FSW consists of a shoulder which rides along the workpiece surface, and a threaded cylindrical pin, which extends through the material thickness. As this weld tool rotates, the rotation motion causes deformation of the material adjacent to the surface of the shoulder and the intruding pin. This study considers the effects of process parameters and tool design on FSW microstructures and relates the microstructures to flow field components in a kinematic model of FSW metal flow.

Figure 2.1 illustrates the kinematic model of the FSW flow field [9]. The model decomposes the flow field around the pin into three incompressible flow field components, any combination of which yield an incompressible FSW flow field. These components are a rigid body rotation around the pin, a uniform translation as the tool transverses the weld seam, and a ring vortex flow field around the tool established by

threaded pin features. The flow components combine to create two currents in the flow field: a “straight-through” current of which the flow elements remain within the rotating flow for less than a complete rotation of the tool and a “maelstrom” current of which the elements remain within the rotating flow for multiple rotations [9].

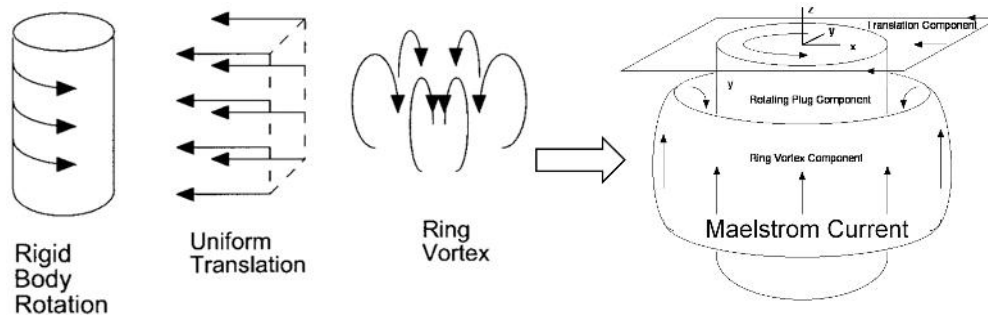


Figure 2.1 FSW pin tool flow

The flow around a FSW pin tool can be decomposed into three components: 1) a rigid body rotating plug component, 2) a translation component, and 3) a ring vortex component. Apparently, complex FSW structural features can be understood in terms of these three components and their interactions. These components can be related to welding parameters and tool design. The components present a conceptual bridge between weld process, which can be controlled, and weld structure (and weld properties).

The rigid body rotation field component comprises metal attached to the tool and rotating with the tool. It is bounded by a surface attached to the tool and a shearing surface, observed to be very thin, with the rotating plug of metal attached to the tool on one side and the body of weld metal moving at a relatively slow weld speed with respect to the tool on the other side. Metal crossing this boundary is subjected to extreme shear rates (typically 10^3 to 10^5 s^{-1}) comparable to those of metals crossing a similar shear plane in metal cutting operations. As the rotating field moves through the metal, it entrains elements of metal, rotates them, and abandons them in the wake of the weld tool.

The ring vortex field component superposes a radial velocity component and an axial velocity component on the flow field at the shearing surface. A negative radial velocity component retains metal elements longer in the rotating flow and tends to shift their exit into the weld cross section toward the advancing side (AS) of the tool. Some of the flow may be retained for many revolutions flowing axially and exiting only where the radial flow velocity component shifts from inward to outward. This effect has been reported in other studies where markers have traced out metal paths rotating multiple times around the weld tool [11]. The ring vortex flow field outside the shear surface adds distortions of its own to the weld structure.

It is generally possible, as will be demonstrated here, to attribute changes in tracer patterns to changes in the flow field components of the kinematic model, and to relate the flow field component changes to changes in weld parameters and tool geometry. Thus, through the kinematic model it is possible to relate weld parameters and tool geometry to weld structure and to control weld structure.

2.3 Methods

AA2219-T87 panels 6.35 mm thick were used in this study. The weld tool was machined from tool steel with a left hand pitch of 20 threads per inch. Pure copper (98.7%) was thermally sprayed to a thickness of 0.2 mm along the faying surface of one panel to mark the seam. Tungsten wires of 0.03 mm diameter were also placed longitudinally along the weld seam at depths of 20%, 50%, and 80% of the panel thickness or 0.13 mm, 3.30 mm, and 5.08 mm respectively from the shoulder surface. One panel was used for each wire depth providing 3 repetitions of processing parameters for each copper plated faying surface.

The weld parameters in this study included rotation speed, travel speed, and force. The weld schedule for each panel is described in Table 2.1. Each panel was welded using a systematic variation of one parameter as illustrated in Figure 2.2 to yield 3 weld specimens per panel. After the tungsten wire was positioned in a groove at the required depth, run on tabs were tack welded in place to hold the panels together.

Table 2.1 Weld schedule for conventional and self-reacting friction stir weld panels

Panel	Rotational Speed (rpm)	Travel Speed (mmpm)	Downward Force (kN)	Wire position (mm)	distance/rotation (mm/rev)
C7	200	114	29 , 31, 36	0.13	0.58
C8	200	114	29 , 31, 36	3.30	0.58
C9	200	114	29 , 31, 36	5.08	0.58
C22	150, 200, 300	114	31	0.13	0.38-0.76
C23	150, 200, 300	114	31	3.30	0.38-0.76
C24	150, 200, 300	114	31	5.08	0.38-0.76
C37	200	76, 114, 152	31	0.13	0.38-0.76
C38	200	76, 114, 152	31	3.30	0.38-0.76
C39	200	76, 114, 152	31	5.08	0.38-0.76

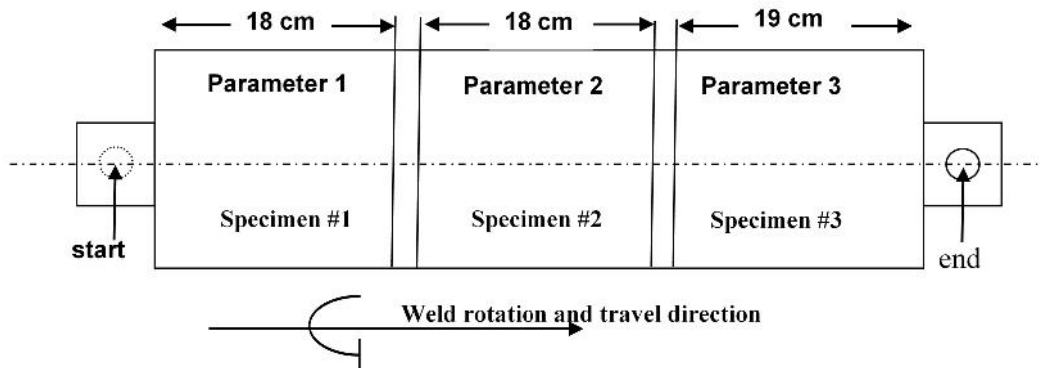


Figure 2.2 FSW panel layout showing run-on tabs on the 2 ends.

A 1" transition (T) section separates the parameter variations. One panel was used for each embedded wire placement depth.

Once all the panels were welded, x-ray radiographs of the welds were taken in 3 views, Figure 2.3. Plan x-rays recorded the as-welded panels. To radiograph in the longitudinal direction, the width of the weld panels was trimmed to isolate the weld region. Next, the samples were sectioned to an approximate thickness of 6.35 mm and radiographed in the transverse direction. The 6.35 mm transverse thickness captured 8-16 revolutions of the weld tool.

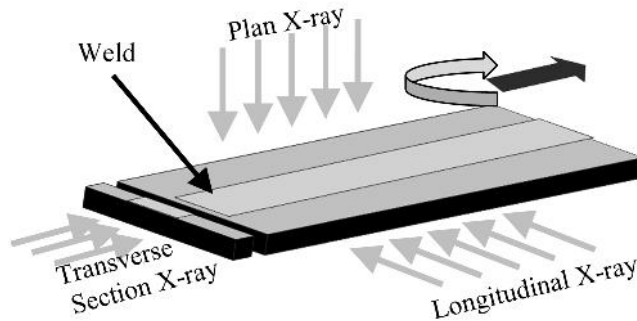


Figure 2.3 Layout directions of x-ray radiographs were taken of the weld region.

The x-ray radiographs were then examined to locate and highlight the post weld position of the tungsten wire and copper plating to determine what parameters affect material flow and how the process parameters move material through the weld nugget. Corresponding metallographic samples were prepared of the plan and transverse views to compare marker placement with variations observed in macro images.

2.4 Results and Discussion

Metal flow around the weld tool can be considered as a bundle of stream lines, Figure 2.4a. As the metal is wiped around with the weld tool, a shear zone exists in the

workpiece separating the region of fine metal grains from the relatively coarse grains of the parent material microstructure. Figure 2.4b is a plan view of a friction stir weld metallographically polished to remove the deformation induced by the shoulder. The fine grained region surrounding the cavity where the weld tool was removed is circular and displaced toward the RS so that a thicker region is noted on the RS than on the AS.

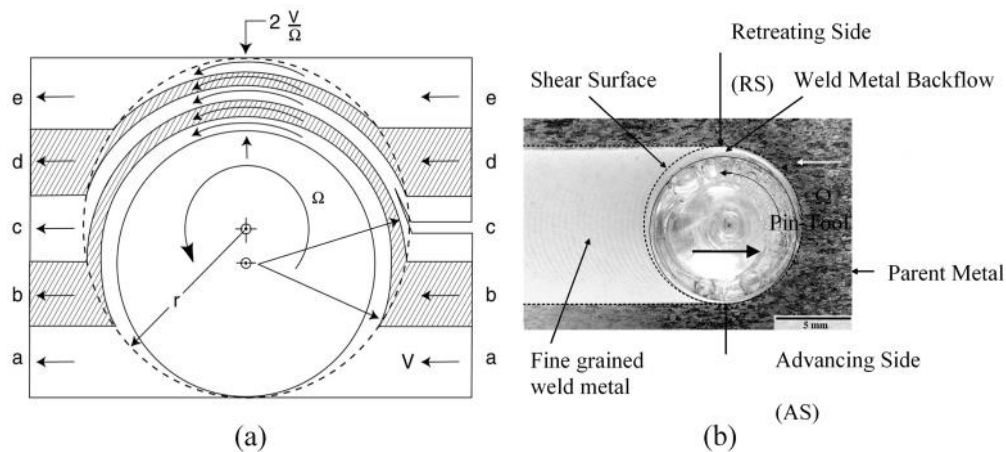


Figure 2.4 Longitudinal views of material flow

(a) Expected stream line flow of weld metal due to rotational motion of the weld tool. (b) Metallographic mount of the plan view of a friction stir weld termination showing differences in the refined metal region on the AS versus RS of the weld pin.

Weld markers introduced from the weld stream into the rotating flow are whisked around and deposited in the wake of the weld. Ignoring the effect of the ring vortex flow component, i.e., lateral and axial shifts, a wire marker exits along the same line as it enters the rotating flow. Figure 2.5 show plan views of tungsten wire markers introduced close to and distant from the shoulder. Two features are noteworthy. The wire is fragmented in the rotating flow. The fragments exhibit appreciable lateral scatter close to the shoulder.

Fragmentation occurs when the shear forces of the metal in the rotating flow on the segment of wire introduced into the rotating flow produce a sufficient load at the anchor point of the wire to tear the wire apart. When this happens, the wire segment is swept away in the rotational flow around the pin and out into the weld structure in the wake of the tool. Copper marker deposits on weld seam surfaces are torn apart into fragments in a similar fashion. Hence, in subsequent radiographs, streamlines are marked by discontinuous fragments of copper. Bundles of streamlines averaged in radiographs may look like a continuous line or, where broadly distributed, like a field of separate fragments. Metallographic images, which exhibit a very thin surface plane only, do not show continuous traces, but only discontinuous fragments from which drawing conclusions regarding streamlines may not be feasible.

Scatter occurs due to oscillation of the diameter of the shear surface. This varies the conditions of exit from the rotating field in a complex way and produces a complex series of lateral displacements in the tracer [12]. The shear surface is anchored to the tool shoulder at the edge of a no-slip surface for which the friction force is greater than the metal flow stress. Periodically, metal is emitted from under the shoulder. This periodic emission process forms the peaks and valleys of the “tool marks” on the weld surface and the band structures that appear as “onion rings” in weld transverse sections [13]. As metal escapes from under the shoulder edge, local normal pressure may drop making slip against the shoulder edge easier than shear within the metal. The anchor point of the shear surface follows the onset of slip on the shoulder and oscillates. The oscillation and the scatter induced by it are thus greatest at the shoulder and diminish away from the

shoulder. The scatter effect tends to produce broader distributions of marker fragments toward a tool shoulder.

For present purposes, marker fragmentation and scatter are artifacts that need to be recognized to avoid confusion but that do not significantly obscure the interpretation of the data in terms of the basic kinematic model.

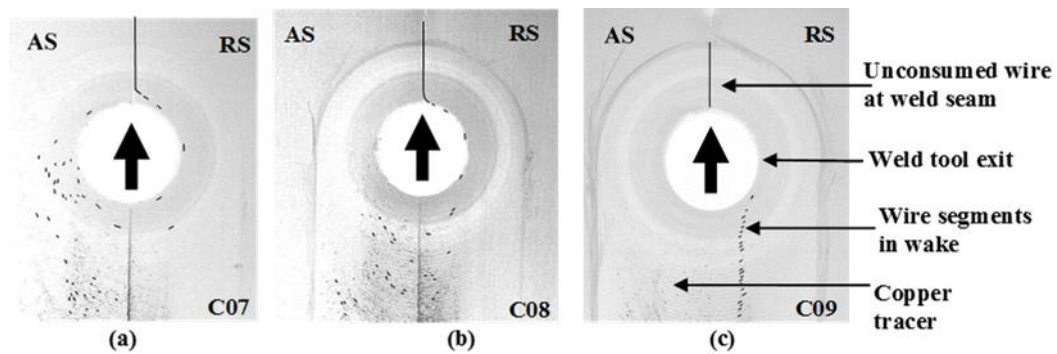


Figure 2.5 Plan inverted x-ray of friction stir welds processed at 200 rpm, 4.5 ipm, and 8000 lbs plunge force.

Tungsten wire segments have been digitally enhanced to document post weld position of (a) 0.05", (b) 0.13" and (c) 0.20" below shoulder surface.

Inverted x-ray radiographs of the transverse surface of a 6.35 mm thick friction stir weld are shown in Figure 2.6 for the range of travel and plunge force investigated in this study. The dark region corresponds to the deposit of copper originally located on the faying surface of the weld seam. Within the parameter range investigated for travel and plunge load, little variation in the resulting copper tracer placement is observed. If the copper on the faying surface were simply whisked around the pin tool, a vertical band of copper at the position of the initial weld seam location would be seen. Evidence of the trace from the former shoulder and pin surfaces can be observed on the AS of the

transverse section. The copper bands in Figure 2.7 show distortions from a purely vertical

band with the heaviest concentration of copper located on the RS. In all the weld sections of Figure 2.7, the expected trace loop is observed extending from the shoulder AS to the pin RS and back around to the original seam location. But this “primary loop” is somewhat obscured by a secondary distortion. This slight distortion is observed as a slight dip about mid thickness of the weld panel bringing the copper trace back to the position of the former seam location.

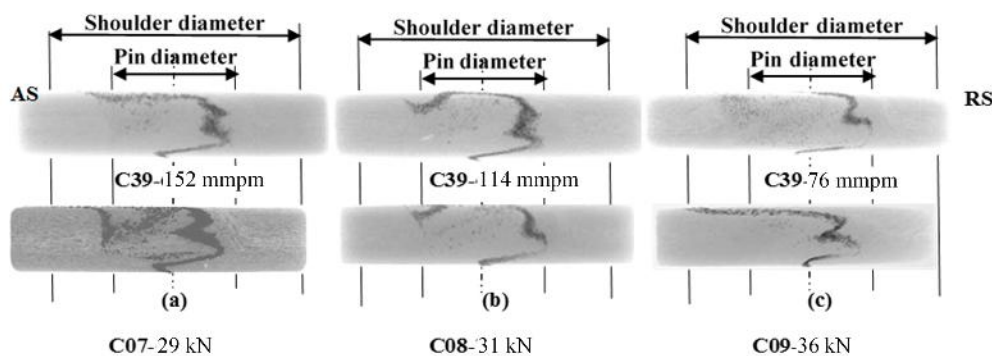


Figure 2.6 Transverse radiographs with copper tracer at varying parameters

Minimal variation observed in an inverted x-ray of post weld copper tracer due to variations in travel (a) and plunge force (b). Weld tool rotation was held constant at 200 rpm. As the weld travel was varied (a), the plunge force was held constant at 7000 lbs and as the plunge load was varied (b), the travel was held constant at 4.5 ipm. The dashed line indicates the centerline of the former weld seam location.

In comparison, Figure 2.7 shows changes in the shape of the copper tracer as the rpm is varied. Figure 2.7 also includes corresponding transverse section metallographs of the friction stir weld mounted, polished, and etched to reveal the microstructure. Banding (onion rings) and other etch-sensitive structures that do not show up on the radiographs are visible in the metallograph. Deformation of the band by the flow field around the pin can also be seen. A rise in the band in the outer portion of the ring vortex component of the flow field is conspicuous on the RS of the pin.

The copper is observed as dark particles in the weld zone of the metallographs shown in Figure 2.7. Although the copper particles fall along the trace of the weld seam identified in the radiograph, their density is insufficient to mark this trace very clearly. Hence, the complimentary radiographs of 6.35 mm thick transverse slices of the weld, which average the copper density, provide a more continuous marking of the former seam trace.

The radiographs and metallographs reveal distortions due to the flow field around the pin. At the edge of the ring vortex component, the flow is axially upward toward the tool shoulder. An axial displacement of the band toward the shoulder increasing with the rpm is conspicuous on the RS (right) of the pin, caused by a through thickness component.

Using the flow paths predicted by the Nunes model, illustrated in Figure 1, the ring vortex circulation can be envisioned to flow inward under the tool shoulder, down the threads on the pin, outward toward the bottom of the pin, and upward on the outside to complete the circulation with conserved weld metal volume. Inward flow delays the exit of weld metal from the rotating plug flow and shifts the trace metal toward the AS of the tool, Figure 8. Outward flow hastens the exit of weld metal from the rotating plug and shifts the trace metal toward the RS of the tool. Hence, because of the interaction of the rotating plug and ring vortex flow components, one expects to see the trace of the weld seam mark out a line from the shoulder AS to the pin RS. Since the outflow does not extend all the way to the bottom of the weld, the displacement effect on the seam trace vanishes at the anvil, and the seam trace reverts back to its original position.

Using the kinematic model, the seam trace at 150 rpm (Figure 2.7a), the left extending advancing arm of the seam trace, starts to show a swirl characteristic. The “notch” in the “primary loop” at 150 rpm can be attributed to a ring vortex secondary distortion. As the rpm is increased from 150 to 200 rpm (Figure 2.7b), this notch becomes more pronounced as the arm develops an axial characteristic. As the temperatures within the weld zone increase, the amount of softened material that can be drawn into the ring vortex increases. This increases until the notch is no longer observed at 300 rpm (Figure 2.7c) as the ring vortex flow appears to dominate the microstructure. It is also at the 300 rpm condition that a defect is observed to open up as a classic ‘wormhole’, Figure 2.7c.

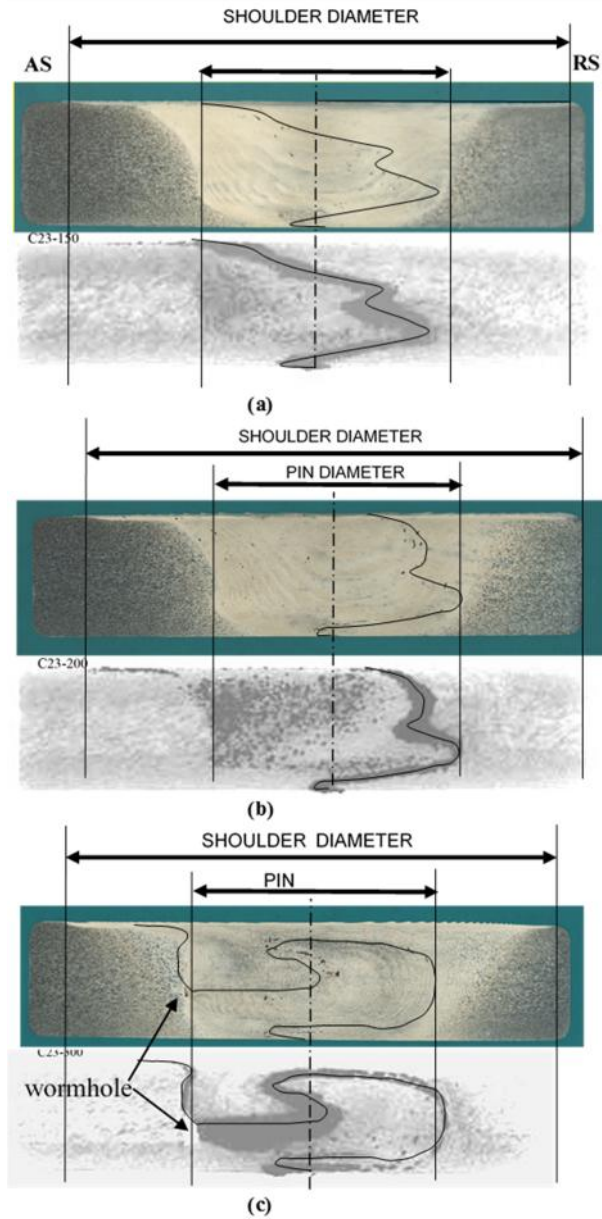


Figure 2.7 Transverse friction stir weld radiographs of the trace of the weld seam marked by a deposit of Cu at varying rotational speeds.

The travel speed was maintained at 4.5 ipm and the plunge force at 7000 lbs with the rotation varied from: (a) 150 rpm, (b) 200 rpm, to (c) 300 rpm. All welds show the basic advancing-(shoulder-side-to-retreating-(pin)-side-and-back-to-center loop due to the interaction of the rotating plug and ring vortex flow field components. At higher rpm, greater distortions of the basic loop appear as the ring vortex flow extends out from the shear surface.

To explain the variation observed in the traced flow, Figure 2.8 illustrates the metal at the former seam being influenced by a ring vortex flow. This causes metal to remain in the rotating plug longer as the weld tool transverse along the initial seam. Figure 8a illustrates a mild influence of the ring vortex flow on the metal in the rotational plug, where the effect is to move the material downward, but not necessarily remaining within the rotating plug for multiple weld tool rotations. As the region of plasticized metal increases in hotter welds to where the ring vortex flow exerts a stronger influence on the rotating plug (Figure 2.8b), regions of the metal would stay within the rotational plug flow longer, possibly for several rotations.

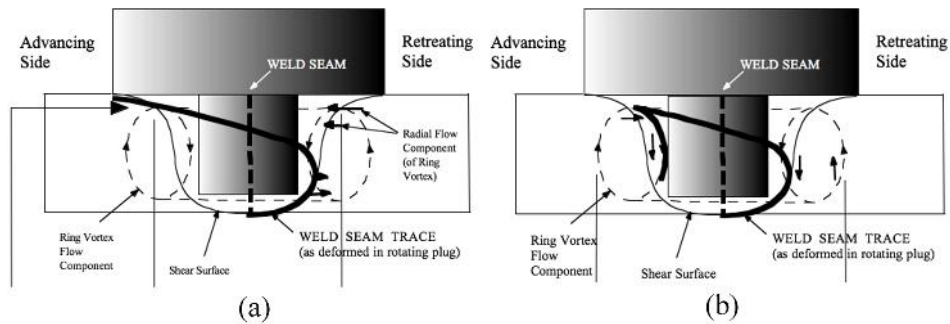


Figure 2.8 Projected trace of copper tracer coated on the faying surface prior to the FSW.

(a) In a colder weld, the ring vortex flow offers minimal distortion to the radial deformation. (b) As the weld becomes hotter and the zone of plasticized material increases, the ring vortex would be expected to draw more material into its flow path.

Once the rotational flow of the rotating plug has moved past the trace elements embedded in the tool wake, ring vortex circulations outside the rotating plug continue to distort the seam trace. If the outer edge of a ring vortex flow passes over a metal volume, it imparts a rotary swirl to that volume in the transverse plane. If the center of the ring

vortex flow passes over a metal element, it imparts an up-and-down axial motion to it in the transverse plane. There are temperature gradients in FSW [14], and plastic flow around the tool tends to be restricted to hotter regions where the weld metal flow stress is lower. Hence, in hotter (higher rpm) welds the ring vortex flow field is more broadly extended as can be observed on the RS of the metallograph in Figure 2.7c.

2.5 Summary

For FSW, the rotational speed affects how the shoulder interacts with the work piece. This interaction means that increasing the rotational speed results in a decreased impact on the weld metal path induced by the shoulder. As the weld heats, the shoulder and the bottom of the pin begin to have less effect on the material movement. This can also be considered to be the transition between sticking and slipping at these interfaces.

This understanding of the influence of process parameters on material flow during FSW also offers insight into defect formation. In a hotter weld, obtained by higher rpms, the vortex dominates the metal flow causing a disruption in the continuity of flow provided by the translational component.

2.6 Acknowledgements

The assistance of Carolyn Russell, Joseph Querin, Rhonda Lash, John Ratliff and Ronnie Renfroe is gratefully acknowledged. Funding from the Mississippi Space Grant and Marshall Space Grant Consortiums contributed to this study.

2.7 References

- [1] W.M. Thomas, E.D. Nicholas, J.C. Needham, M.G. Murch, P. Temple-Smith, and C.J. Dawes, *Friction-stir butt welding*. GB Patent No. 9125978.8, International Patent No. PCT/GB92/02203 (1991).
- [2] Y. Li, L.E. Murr, J.C. McClure, *Mat. Sci. Eng. A*, A271 (1999) 213-223.
- [3] K. Colligan, *Welding Res. Suppl.*, p. 229s-237s, July 1999.
- [4] T.U. Seidel, A.P. Reynolds, *Met. & Mat. Trans.*, 32A (2001) 2879-2884.
- [5] M. Guerra, C. Schmidt, J.C. McClure, L.E. Murr, A.C. Nunes, Jr., *Mat. Characterization*, 49 (2003) 95-101.
- [6] F. Contreras, E.A. Trillo, L.E. Murr, *J. Mat. Sci.*, 37 (2002) 89-99.
- [7] J.H. Ouyang, R. Kovacevic, *J. Mat. Eng. & Perf.*, 11 (2002) 51-63.
- [8] J.A. Schneider, A.C. Nunes, Jr., 7th Intl. Conf. Trends Welding Research, 2005.
- [9] J.A. Schneider, A.C. Nunes, Jr., *Met. Trans. B*, 35 (2004) 777-783.
- [10] W.J. Arbegast, *Hot Deformation of Aluminum Alloys*, ed. Z. Jin., TMS, 2003.
- [11] B. London, et al., *Proc. Friction Stir Welding Processing II*, eds. K.V. Jata, M.W. Mahoney, R.S. Mishra, S.L. Semiatin, T. Lienert, p. 3-12, 2003.
- [12] J.A. Schneider, R. Beshears, A.C. Nunes, Jr., *Mat. Sci. Engr. A*, 435-436 (2006) 297-304.
- [13] K.N. Krishnan, *Mat. Sci. Engr. A*, 327 (2002) 246-251.
- [14] M.W. Mahoney, et al., *Metall. Mater. Trans.*, 29A (1998) 1955-1964.

CHAPTER III

INFLUENCE OF TOOL SHOULDER CONTACT CONDITIONS ON MATERIAL FLOW DURING FRICTION STIR WELDING²

3.1 Abstract

Friction stir welding (FSWing) is a solid-state joining process of special interest in joining alloys that are traditionally difficult to fusion weld. In order to optimize the process, various numeric modeling approaches have been pursued. Of importance to furthering modeling efforts is a better understanding of the contact conditions between the workpiece and the weld tool. Both theoretical and experimental studies indicate the contact conditions between the workpiece and weld tool are unknown, possibly varying during the FSW process. To provide insight into the contact conditions, this study characterizes the material flow in the FSW nugget by embedding a lead (Pb) wire that melted at the FSWing temperature of aluminum alloy 2195. The Pb trace provided evidence of changes in material flow characteristics which were attributed to changes in the contact conditions between the weld tool and work piece, as driven by temperature, as the tool travels the length of a weld seam.

² A version of this chapter has been submitted for publication to Metallurgical and Materials Transactions A as: Doude, H.R., Schneider, J.A., and Nunes, A.C. "Influence of the tool shoulder contact conditions on the material flow during friction stir welding."

3.2 Introduction

Friction stir welding (FSW) uses a non-consumable, rotating tool which is plunged into the workpiece and translated along the weld seam to join pieces of metal [1]. Deformational and frictional heating resulting from the interaction of the rotating tool and the workpiece, soften the metal to produce a joint by stirring material from two pieces of metal together. Figure 3.1 summarizes the terminology associated with the FSW process. On the advancing side (AS) of the FSW, the tool feed and the tool rotation directions coincide. The tool feed direction and tool rotation direction are opposite on the retreating side (RS) of the FSW. The differences in the RS and AS movement result in an asymmetric flow field around the weld tool. A cross section of the FSW is referred to as the transverse view while the top surface is referred to as the plan view.

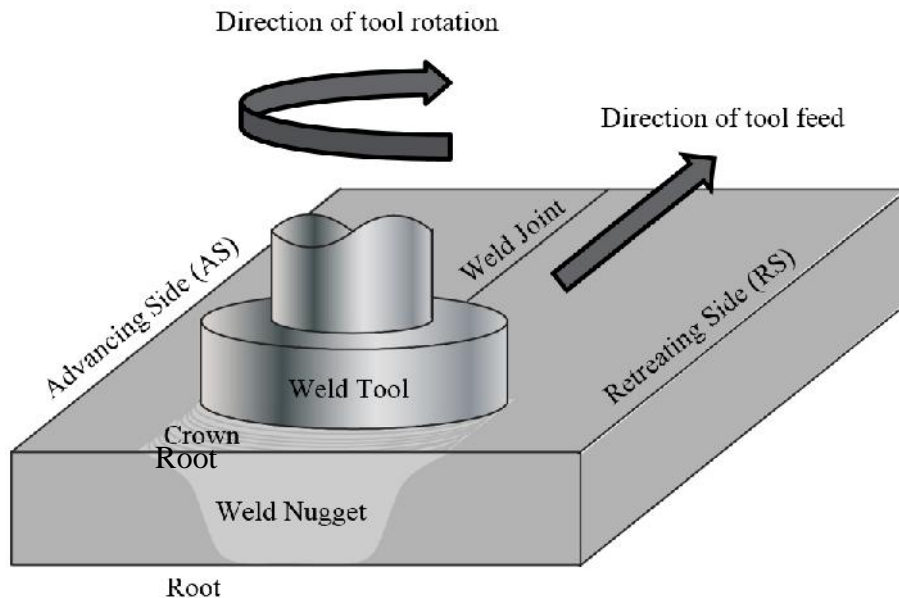


Figure 3.1 Conventional FSW terminology showing the tool during a weld.

The cross section (transverse view) of the resulting joint, shown in Figure 3.2, consists of three distinct metallographic regions outside of the parent material (PM); a stir zone (SZ), a thermo-mechanically affected zone (TMAZ), and a heat affected zone (HAZ). In the TMAZ, the PM grains show evidence of mechanical deformation as they elongate from the HAZ and bend toward the nugget region which consists of refined grains. The HAZ contains grains that have been heated but not mechanically deformed by the welding process.



Figure 3.2 Transverse view of a conventional FSW with regions of interest labeled.

The flow of material is reported to take place both in straight through flow, similar to slip line theory, as well as vertical or through material thickness flow [2-10]. As the material moves through the thickness of the workpiece, this gives rise to the observed marker flow occurring multiple times around the pin tool [11]. As the rotating tool moves along the weld seam, new material is drawn into the SZ and deposited in the wake of the weld in a layer by layer pattern giving rise to the onion ring structure observed [2, 12-15]. The spacing of the onion rings has been correlated with the distance

traveled by the tool during a single rotation [2, 7, 8, 10, 12, 13, 16-20]. Both the shoulder and the pin are reported to influence the flow patterns of the weld metal [3, 6, 7, 9, 14, 20-24].

Since the mechanical properties of the resulting weld are affected by the thermo-mechanical processing conditions, much effort has been concentrated on various numerical modeling approaches to define the material flow and temperature profile [2, 3, 5, 25-30]. The ability to link the process parameters with the resulting temperature profile rely on understanding how the heat is generated and dissipated. Heat generation considers either frictional contact between the workpiece and tool shoulder [25-27], shearing deformation between the workpiece and the pin [31-34], or a combination of both. How the heat dissipates also depends on the contact conditions between the workpiece and weld tool. The workpiece can either be considered to stick to the weld tool, slip at the interface, or alternate between sticking and sliding [16, 34]. Variations in stick-slip at the interface can be due to the varying contact conditions as the weld tool rotates and traverses down the weld seam. Often modeling efforts alter the contact conditions to match with experimental data observations. Although a more direct way to assess contact conditions considers the use of torque based models to estimate the friction coefficient and yield shear stress [32, 35], assumptions regarding contact conditions are still required. If contact conditions change during the weld, the assumed efficiencies of converting weld energy to thermal energy will be affected.

The use of marker studies has proven useful in identifying the metal flow patterns as orderly [4, 36-38]. As the FSW tool entrains the marker, the material flow is traced along a single flow line or plane of the metal flow which is visualized post weld using X-

ray radiography or metallographic techniques. This method coarsely captures the material flow due to discontinuous deposition. Thus while the tracer studies provide information on the macro-flow of the weld metal, solid tracers do not provide a continuous tracing which may provide information regarding the contact conditions experienced at the FSW tool/workpiece interface.

In this study, a 250 μm diameter Pb wire was embedded in the weld seam prior to a butt weld. At the temperatures predicted during FSWing of Al panels (70-90% Tmp) [39], the Pb wire was molten [40] and provided a continuous tracing of the metal flow during the FSW process. Traces of the molten Pb wire showed evidence of a cyclic periodicity not directly related to the process parameters.

3.3 Methods

A FSW butt weld was made using 2 panels of Al alloy 2195-T81 approximately 60cm long 10 cm wide and 0.82 cm thick. The weld tool incorporated a left hand $\frac{1}{2}$ -20 UNJF threaded pin 0.79 cm in length, 1.27 cm in diameter and made from H13 tool steel. A smooth shoulder was used with a diameter of 3.05 cm and made from MP159 Co-Ni-Cr alloy.

The panels were FSWed along the rolling direction with a continuous wire aligned along a scribe mark on one of the faying surfaces. The wire marker was positioned 0.13 cm below the shoulder surface and the plates were tack welded together to hold the wire in place as illustrated in Figure 3.3. After clamping in the FSW tool, the weld tool was offset to place the 250 μm diameter Pb wire on the AS of the panel joint.

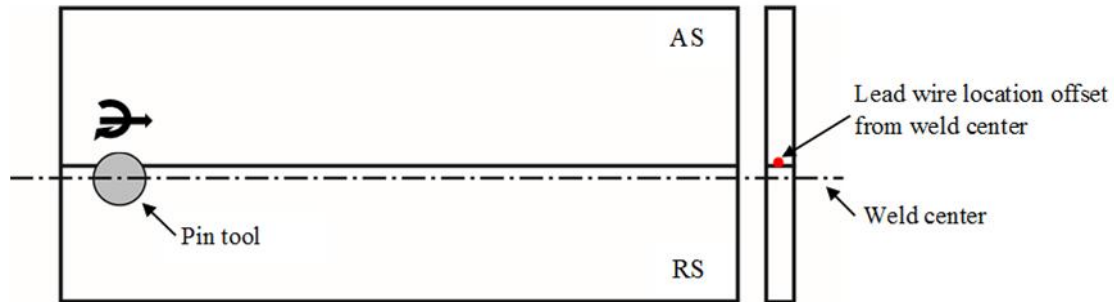


Figure 3.3 Configuration of the metal plates for the butt welds.

Prior to the weld, a continuous lead wire was placed in the scribed groove in the faying surface of the joint.

The panels were FSWed using a spindle rotational speed of 200 rpm and a traverse speed of 15 cm/min in displacement control. The tool was operated with a back tilt or "lead angle" of 2.5°. After the FSW, the crown surface was ground to remove the tool marks and enhance the ability for the X-ray radiography to document the post-weld wire placement in the plan view.

In a region where the Pb wire could be resolved in a plan view radiograph, a section ~8 cm long was removed from the weld panel and metallographically sliced into 6.4mm thick sections. The transverse orientation of each section was radiographically imaged and then mounted and polished using standard metallurgical procedures. Scanning electron microscopy (SEM) images were taken with an environmental, field emission (FE) FEI Quanta 600 operated at 8 and 15KeV and configured with an energy dispersive spectrometer (EDS) operated at 15KeV. Following the SEM imaging, the samples were etched using Keller's reagent to document the macrostructure which was recorded using a Nikon D1 camera. EDS was used to identify the element content of the microstructure observed in the SEM images.

3.4 Results

The inverted plan radiographs in Figure 3.4 contained Pb concentration variations which produce resolvable images in the center of the panel [16]. The apparently random swaths of Pb forming the images in Figure 3.4 were observed to bypass some rotations before reoccurring with no direct correlation between the spacing and the travel rate/tool rotation.

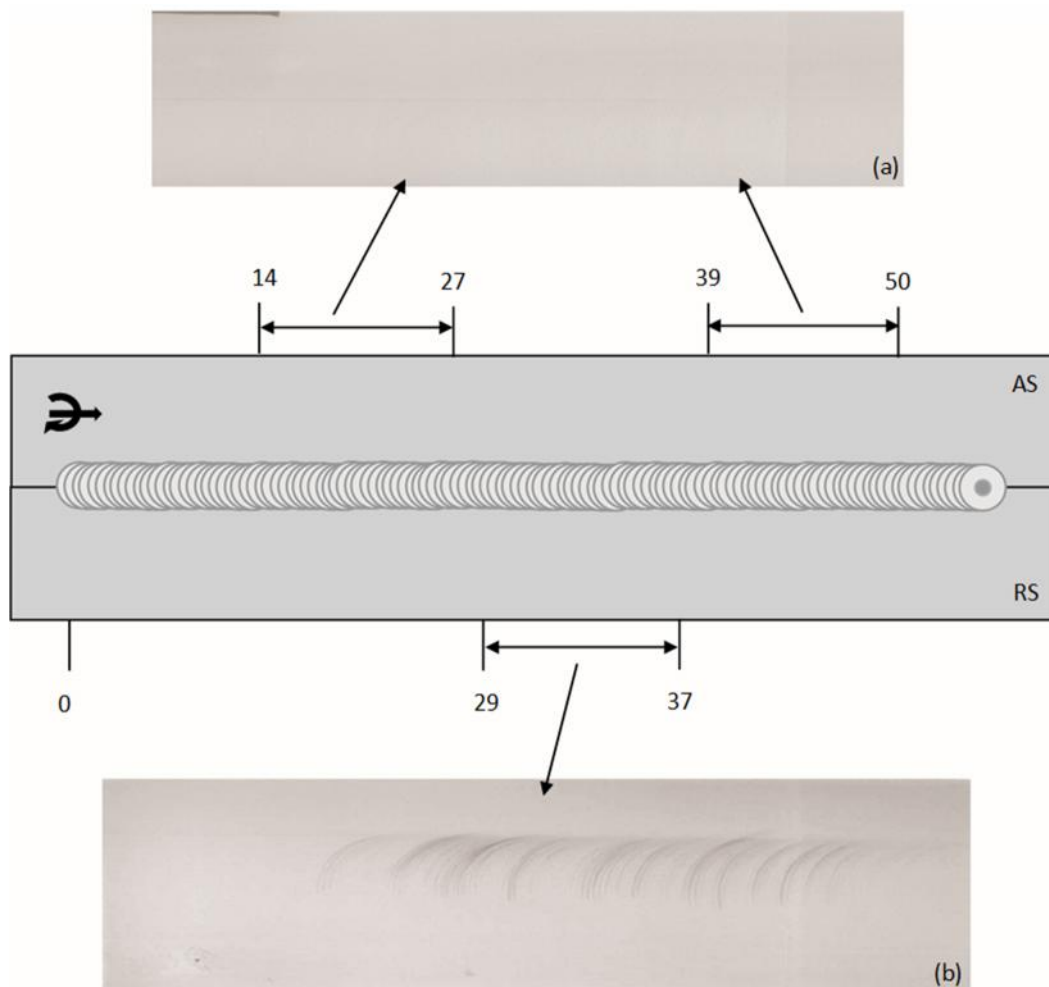


Figure 3.4 X-ray radiograph of plan view of FSW panel

The plan view radiographs are showing regions where lead wire is not resolved (a) and is resolved (b), Note all dimensions are in cm.

Figure 3.5 shows the 8 cm long weld, from Figure 3.4b, with the 6mm thick cut pattern superimposed. X-ray radiographs were taken of each transverse section and shown in inverted contrast in Figure 3.6 which revealed the higher density Pb as dark in contrast. In sections LX-6 to LX-9, the dispersal of Pb was on the AS, but spread through the material thickness. In sections LX-3 to LX-5 and LX-10 to LX-11, the dispersion of Pb was concentrated near the crown surface on the AS. These observations appeared just prior to the sections where the Pb tracer became less visible in sections LX-13 and LX-14, although a small trace of lead was noted at the AS crown surface.

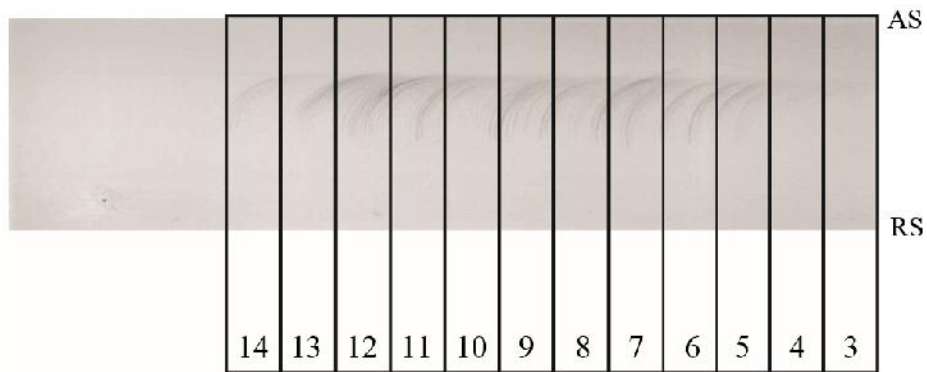


Figure 3.5 Regions from Figure 3.4b that were sliced and prepared for transverse x-ray radiography and microscopy.

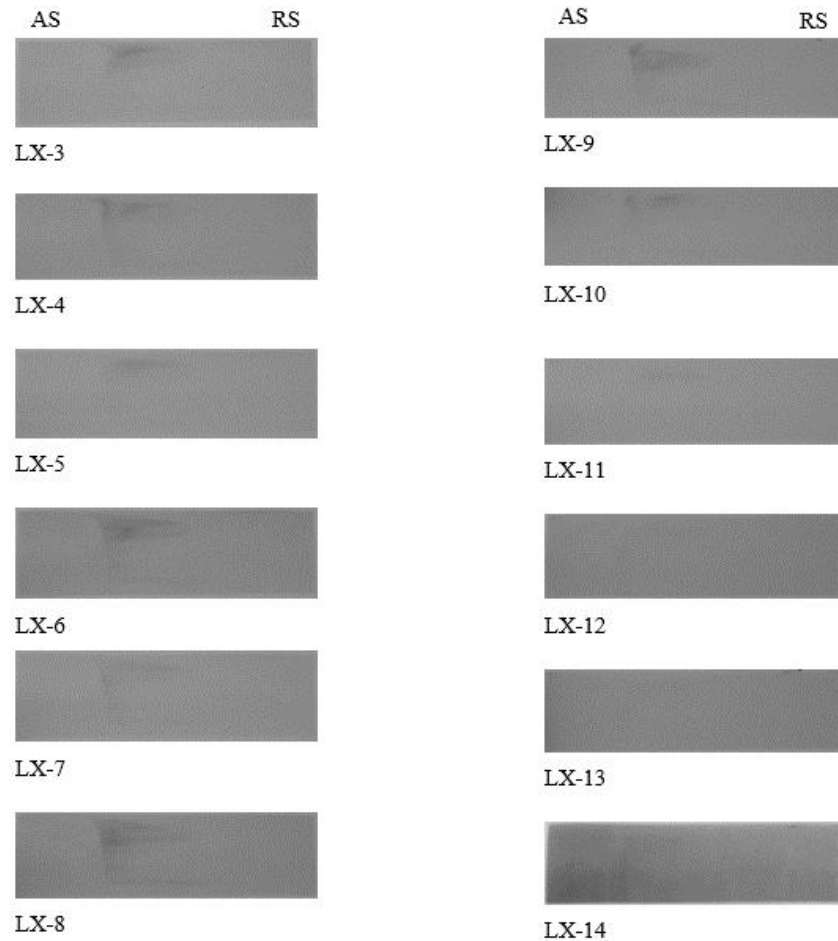


Figure 3.6 X-ray radiographs of transverse sections shown in Figure 3.5.

In sections LX-6 to LX-9, the dispersal of Pb is on the RS, but spread through the material thickness. In sections LX-3 to LX-5 and LX-10 to LX-11, the dispersion of Pb is concentrated near the crown surface on the RS. These observations appear just prior to the sections where the Pb tracer becomes less visible in sections LX-13 and LX14, although a small trace of lead is noted at the AS crown surface.

While radiography allowed a bulk view of the Pb tracer, SEM was used to obtain more detailed spatial resolution regarding the details of the observable traces of the finely dispersed Pb in the polished transverse and longitudinal specimens.

In the SEM, the higher density Pb tracer is lighter in color than the aluminum matrix. EDS was used to distinguish the chemistry of the different regions as shown in Figure 3.7. Since Pb is not soluble in the Al matrix [41], the molten Pb tended to form

small spheres upon solidification. Unlike the Pb spheres, copper rich particles found in these areas were evenly dispersed throughout the welded region.

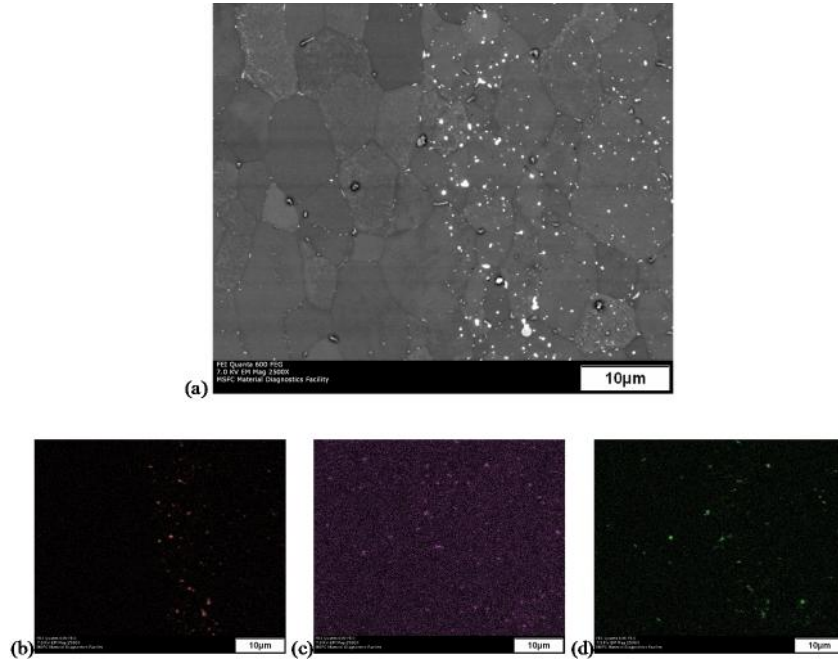


Figure 3.7 SEM images of the lighter regions of dispersed lead

The SEM image (a) shows the lighter regions of interest. The left most, smaller image (b) indicates the lead rich areas with pink. The middle image (c) indicates copper with purple and the right most image (d) indicates oxygen in green. The light regions in the SEM image are rich in lead.

Figure 3.8 compares selected SEM images from transverse sections with varying resolution of Pb from the x-ray radiographs shown in Figure 3.6. These sections include: LX-3 and LX-4, in which the inverted x-ray showed Pb concentrated near the crown surface; LX-7, where the Pb showed greater dispersion through the material thickness; and LX-14, in which Pb was only resolved at the RS crown surface. In section LX-3, patterns of Pb were observed within the material thickness, biased toward the crown

surface arching inward toward the weld center line. These arches appeared to straighten out toward the shoulder OD in sections LX-4 and LX-7.

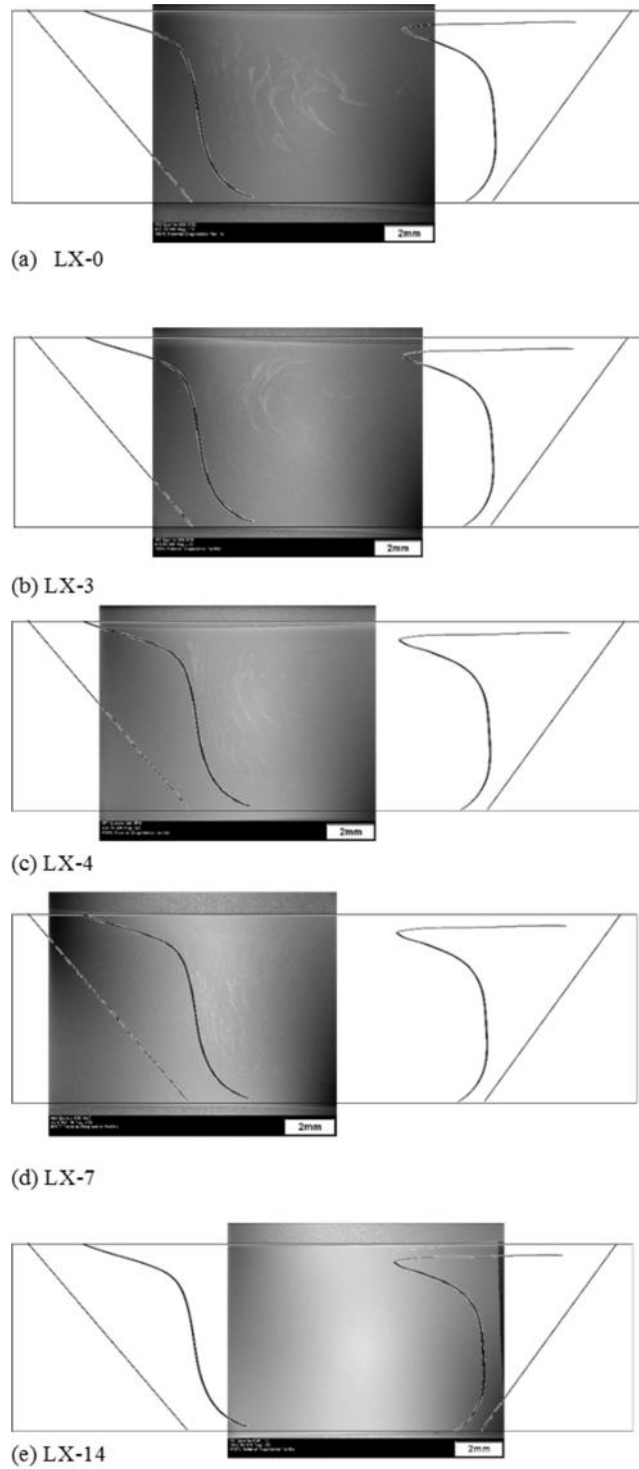


Figure 3.8 Transverse SEM images with lead traces

a-d) SEM images of the AS transverse sections shown in Figure 3.6. e) SEM images of the RS of the transverse sections shown in Figure 3.6.

Figure 3.9 compares the optical macrograph (a) and SEM image (b) of the transverse section of weld segment LX-3. The Pb concentrations appeared light in the SEM image and correspond with dark regions in the OM. The SEM image showed a bright region of Pb with wisps that follow the contour of the onion rings. Near the AS shoulder and surface of the weld, the Pb was located towards the center of the weld and then arched outward and downward coming back toward the center of the weld towards the mid-thickness of the weld.

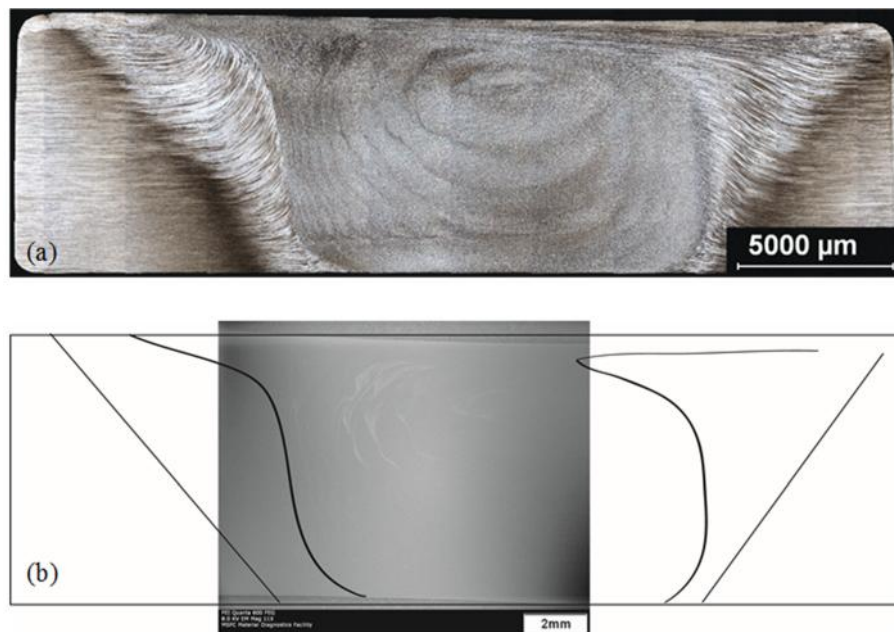


Figure 3.9 Optical and corresponding transverse SEM image of LX-3
Optical (a) and corresponding SEM (b)

Examination of the next transverse section of the weld (LX-4) showed differences in Pb trace. Figure 3.10 shows the SEM image of the resulting macrostructure and Pb trace, respectively. In the SEM image of section LX-4, the Pb tracer moved outward near the surface towards the edge of the shoulder unlike sample LX-3. The Pb trace appeared

to be drawn up towards the shoulder induced flow and was pulled outward toward the AS shoulder edge. The tracer was also seen following the elliptical onion rings towards the center of the SZ like LX-3; however, the brightest concentrations of Pb were located toward the outside of the nugget in LX-4. Similar patterns were observed in Figure 3.8 for sections LX-7. Figure 3.11 shows an overlay of SEM images from LX-3 and LX-4, which highlights the differences in the Pb trace patterns.

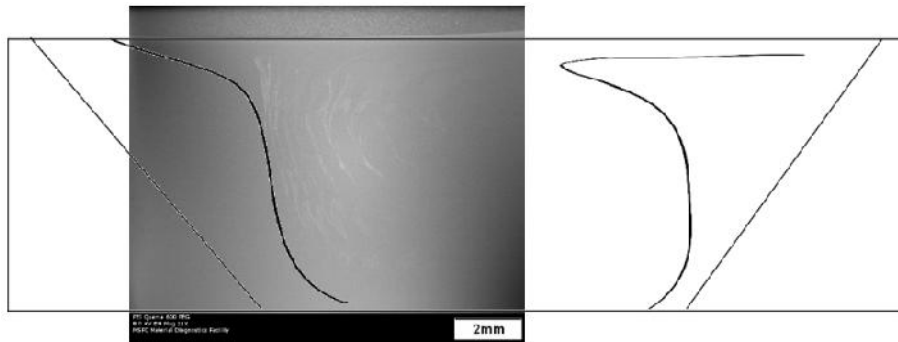


Figure 3.10 SEM image of LX-4

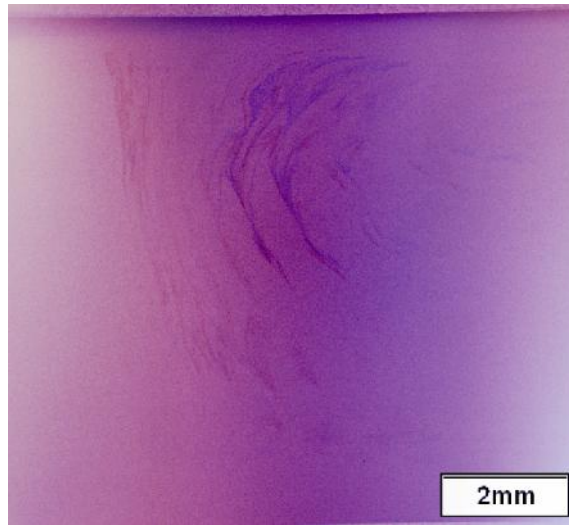


Figure 3.11 Color enhanced overlay images from slices LX-3 and LX-4
LX-3 (blue) and LX-4 (pink)

Examination of longitudinal images from segments LX-3 and LX-4, shown in Figure 3.12 and 3.13, respectively, show similar flow patterns with differences in Pb density near the crown surface. The Pb tracer was contained within the material thickness, with no lead resolvable at either the root or crown surfaces. The Pb was observed to show a broad loop pattern near the crown and a narrow loop pattern near the root. Figure 3.14 shows an overlay of these two transverse sections showing the similarities in the Pb trace patterns. Circular swirls were also noted near the root surface at an offset distance of ~1mm.

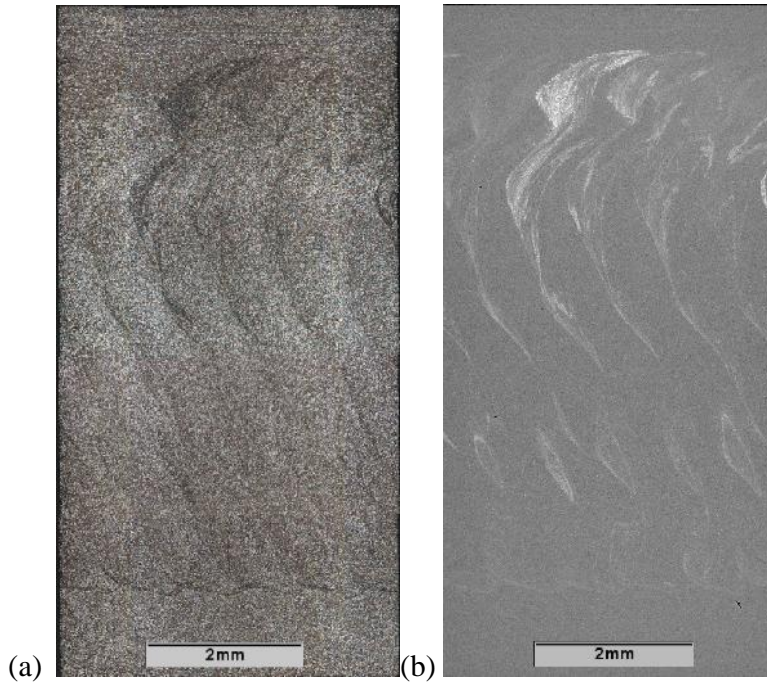


Figure 3.12 Optical and corresponding SEM image of longitudinal section of LX-3
Optical (a) and corresponding SEM image (b)

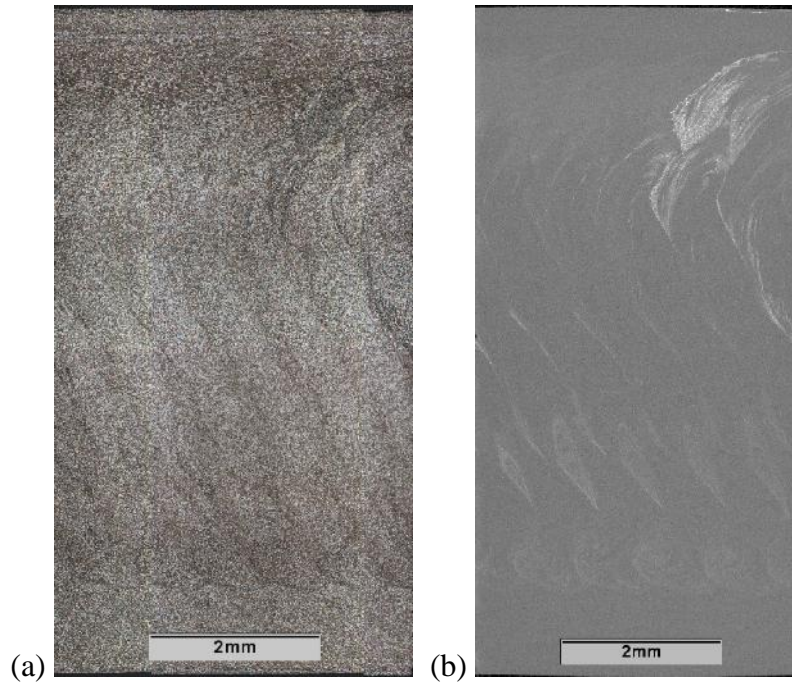


Figure 3.13 Optical and corresponding SEM image of longitudinal section of LX-4.
Optical (a) and corresponding SEM image (b)

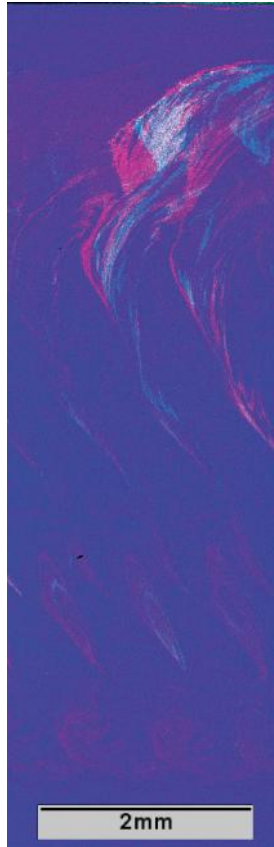


Figure 3.14 Longitudinal overlay of LX-3 and LX-4
LX-3 (blue) and LX-4 (pink)

Figure 3.15 shows a magnified region from the root/AS corner of the transverse section of the FSW. Flow patterns were similar to the "vortices" reported by Murr, et al [6, 41]. The loops of Pb, observable in both the transverse and longitudinal sections, showed regions of flow reversal. This occurred as the threads pushed material down into the thickness of the material which then reacted against the backing anvil to begin the upward flow toward the shoulder. The Pb tracer moved from the original location at 0.13cm from the crown surface to a location closer to the root of the weld or about 0.67cm from the crown surface.

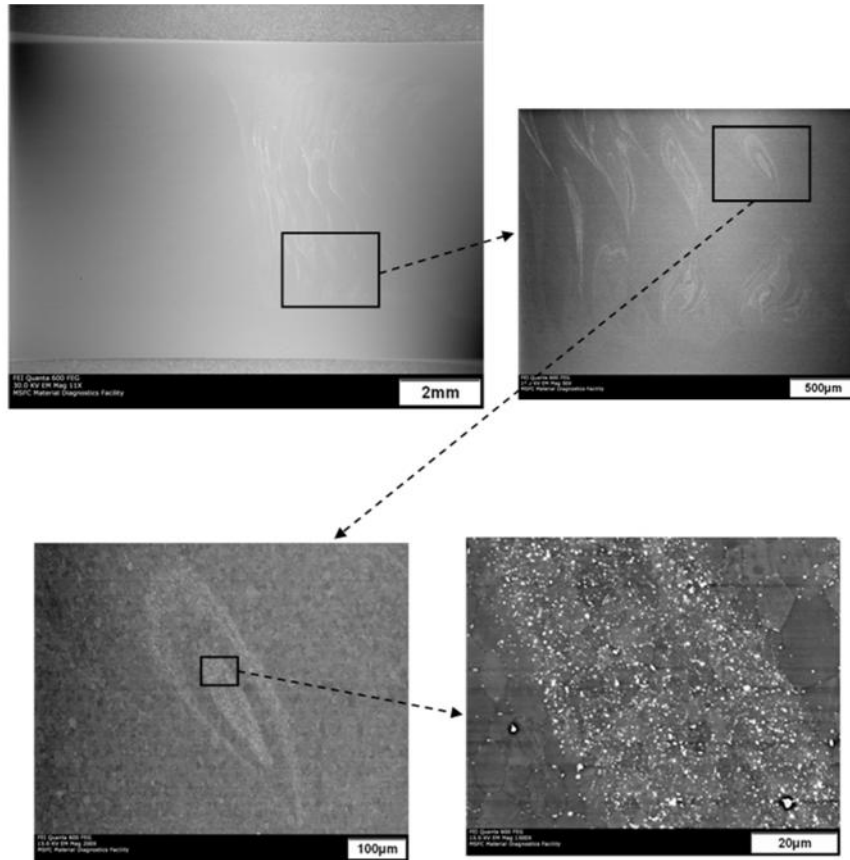


Figure 3.15 Increasing magnification of lead rich region showing areas proposed as shear surface.

In the SEM image of LX-14, shown in Figure 3.16, the Pb tracer was only observed at the crown and root surfaces and not within the material thickness. The Pb was observed in the x-ray radiograph of Figure 3.6, near the RS crown surface. The surface lead suggested the Pb was allowed to escape along the root weld seam and crown surfaces in sections where the Pb tracer was not resolvable in the x-ray radiography images.

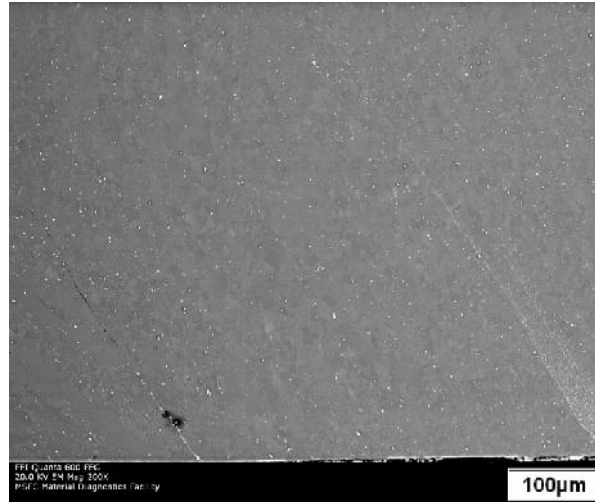


Figure 3.16 Close up of AS root surface from Section LX-14 (Figure 3.8e).

3.5 Discussion

FSWing has been modeled as an extrusion dominated [42] versus a mixing dominated [3] process. It maybe that depending on the tool design and process parameters, different mechanisms of material transfer dominate [43]. Modeling as an extrusion dominated process assumes the material flow is similar to that in a die cavity wall. This type of process would explain regions where the Pb was concentrated and shown to extend from near the crown to near the root surfaces. Thus in regions where slipping occurred at the shoulder and the SZ contracts, it may be that the material in this region was simply extruded around the tool. As this region of resolvable Pb tracer was near the end of the panel, it was conjectured that the heat buildup increased the temperature and caused the shoulder to slip. The tool was only partial slipping as regions are still observed where the Pb traced out a mixing dominated path.

In either case, the extrusion model [42] provided a basis for a pressure gradient which varied as a function of temperature. The pressure gradient was reported to correlate with the occurrence of wormhole features near the root surface on the AS of a FSW. Close-up of the root surface in Figure 3.16 showed an incomplete sealing of the shear contours.

In contrast to numerical models which rely on assumptions regarding material properties as influenced by the strain and strain rate of the process, contact conditions, and heat generation, a simple kinematic approach was used to consider the metal flow as influenced by the tool and processing parameters and not the material properties [2, 3]. While the model cannot predict temperatures, it does provide a basis for visualizing the contact conditions between the tool and the workpiece. The basic flow of metal in the vicinity of the friction stir tool can be decomposed into three components pictured in Figure 3.17. These components are set to match particular boundary conditions. The components can then be superposed (like Fourier components) to approximate the flow field around the friction stir tool. The components have been designed to represent incompressible flows, and when superposed the resultant flow must be incompressible due to the linearity of the divergence operator. The effect of each flow component and their combinations upon the weld macrostructure are understood. The model can be used to relate the effects of boundary conditions, for example tool geometry, to weld macrostructure. It can also be used to relate macrostructural observations, for example tracer patterns, to tool surface conditions, which is the concern of the present paper.

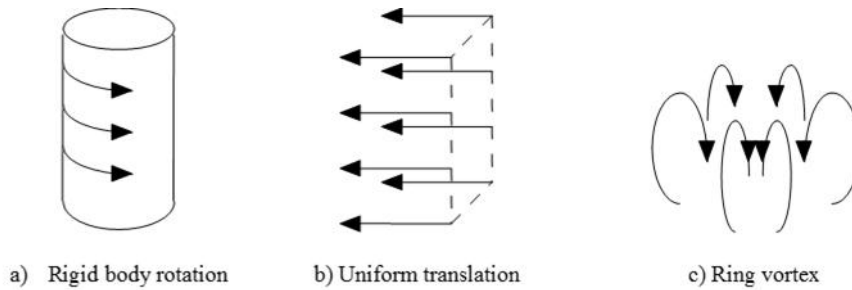


Figure 3.17 Three incompressible flow fields

a) rigid body rotation, b) uniform translation, c) ring vortex.

The heavy pressure at the surface of a typical friction stir tool may be expected to require very high shear stresses to cause slip, higher than the shear stress of the metal itself. Hence the weld metal is expected to seize to the tool surface. The attached weld metal must then transition to the stationary weld metal environment through an interval of shearing metal. It turns out that this interval is very narrow, an “adiabatic shear band”, effectively a “shear surface”. The shear surface is cylindrical with a radius that enlarges as one moves from the end of the pin to the shoulder. The shear surface is not confined to the tool-metal interface as a slip surface would be. Its shape is selected by nature to minimize torque. The rotating plug of metal between the tool surface and the shear surface is represented by the “rigid body rotation” of Figure 3.17a for a straight sided cylinder. The actual rigid body rotation flow component is conceived as a flared cylinder enclosing the pin and attached to the edge of the seized area on the tool shoulder.

The uniform translation flow component of Figure 3.17b is set to the long range boundary condition where the flow moves toward the tool on one side and away from it on the other. This component interacts with the rotating plug component to produce a flow field that carries the weld metal around the tool on the retreating side.

Threads on the pin, scrolls on the shoulder (not present in this study), and tilt on the FSW tool drive weld metal downward near the tool pin, outward near the bottom of the workpiece, upward along the outside of the nugget region, and inward near the shoulder of the tool as illustrated in Figure 3.18 [3] so as to produce the ring vortex flow component (Visualize this as a smoke ring around the pin.) as illustrated in Figure 3.17c and 3.18a. The ring vortex circulation is set by radial (on the shoulder and backing anvil) and axial (on the pin) boundary conditions. Figure 3.18b shows a side view of the ring vortex component interacting with the shoulder features to drive the material through the thickness, react against the backing anvil and the shoulder, prior to exiting in the wake of the weld as the tool travels down the length of the weld seam [43]. It should be noted that, unlike the discontinuous flow at the shear surface, the ring vortex flow component represents a continuous deformation field, presumably a viscous creep type flow.

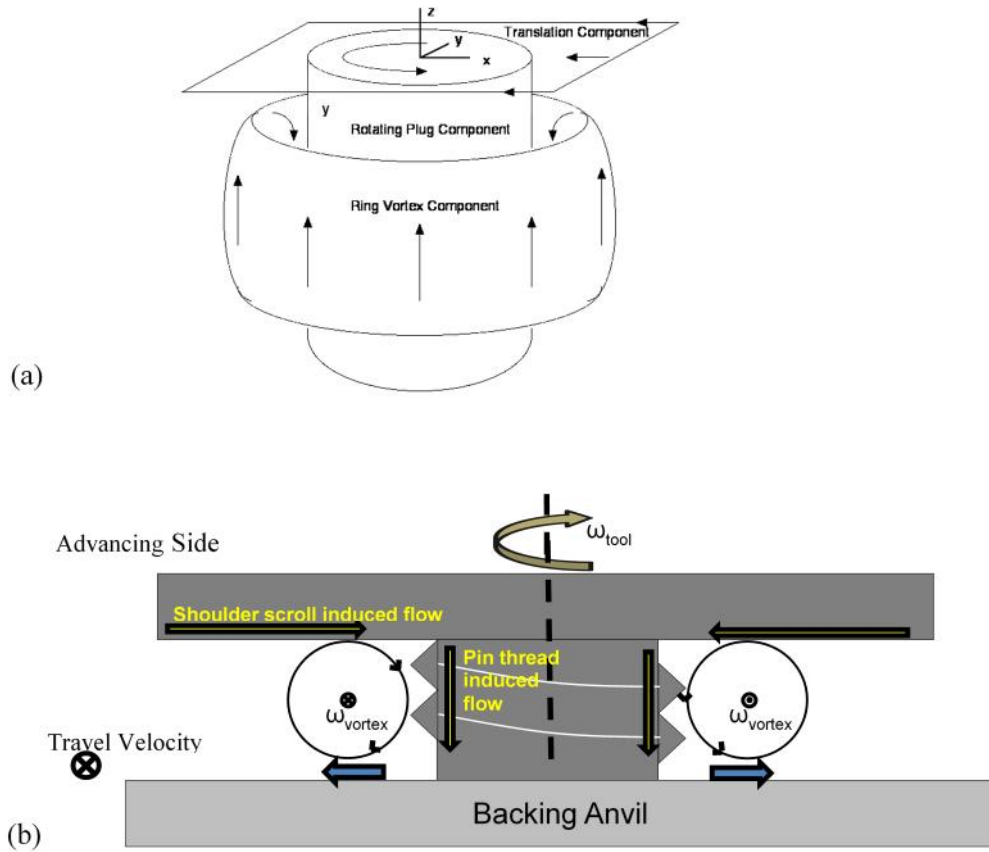


Figure 3.18 Resulting material flow as affected by the pin and shoulder.

(a) The pin dominated flow forms a ring vortex component within the thickness of the weld panel. (b) A side view shows how the pin dominated ring vortex component interacts with the shoulder features to drive the material through the thickness, reacting against the backing anvil and the shoulder prior to exiting in the wake of the weld as the tool travels down the length of the weld seam.

There is a fourth flow component that plays an important role in the determination of friction stir macrostructure, the oscillatory flow component that gives rise to the internal banding which forms the onion ring structure [12, 13, 43]. Pumping of metal by tool eccentricity back and forth along the hot, soft metal channels following the shear surface gives a texture to the metal that, when polished and etched, presents a band structure in the bulk of the weld and a ripple structure, often called “tool marks” on the weld surface.

Indirectly, the oscillatory component can punctuate the appearance of the lead wire tracer within the weld. At the edge of the shoulder, the pressure on the weld metal drops to zero. Close to the edge, the pressure is low enough for slip to be easier than shear. The top of the shear surface, joined to the edge of the seized area on the shoulder, does not extend into the slipped region. If the shoulder pressure distribution changes with the rotation of the tool due to the eccentric pumping effect, the width of the slip area and the radius of the upper region of the shear surface may change slightly with tool rotation. Any shear surface radius changes will correspond to a change in SZ area [16]. During these decreases and increases of the shear surface radius, the shear surface shrinks away from (Figure 3.19a) and then expands into (Figure 3.19b) the wire tip so as to leave a gap and engulf a substantial amount of wire as shown in Figure 3.19. The absence of lead tracer near the shoulder in transverse LX-3 section shown in Figures 3.6 and 3.8 also suggests a gap region due to a small increase in slipped area at the edge of the shoulder. The location of the point on the shoulder where the seized area stops and slip begins is marked on the advancing side by the edge of the SZ; this location does not appear to change very much.

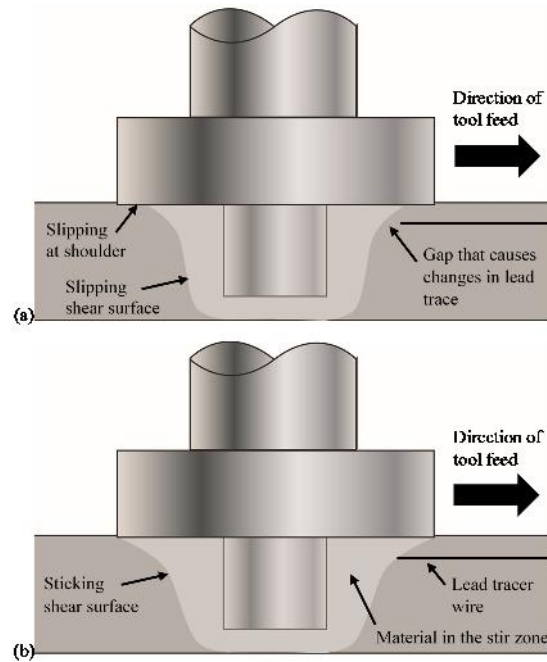


Figure 3.19 Proposed variation in contact conditions at shoulder

For a weld speed of 15 cm/min and a rotation speed of 200 rpm, the tool advance per cycle is 0.75 mm. For a gap extending a whole tool rotation, an extension of the slipped region by 0.75 mm or roughly 5% of the shoulder radius would be sufficient to cause gaps in the lead trace, other things being equal. Gaps in the wire trace due to eccentric pumping occur within a tool rotation cycle; wider gaps over multiple cycles should be attributed to other causes. The lead is confined to a narrow portion of the banding that would correlate with a particular part of the pumping cycle. This would suggest a sudden forward motion of the shear surface (increase of seized area), followed by a retreat (increasing slip area) at a faster rate than the weld speed of advance.

The shear surface spreads out the lead, which is molten at welding temperature, parallel to the band structure, where it will be seen to follow the onion rings, etc. in the

band structure. The melting temperature of Pb is 600K (327°C) and the expected range of temperatures reached in FSWing of aluminum is between 653-840K (380-567°C) (70-90% absolute melting temperature) [25, 39, 44]. Figure 3.20 illustrates the expected periodic deposition of Pb, but much greater axial dispersion is evident in the longitudinal sections, particularly in Figures 3.11 through 3.14. Pressure on the molten lead, both steady and oscillating, can be visualized as spreading the lead axially along the hot, soft, least resistive path following the shear surface, the way a dollop of ketchup would spread over your hand if you push it against a table. (Eccentric pumping could also disperse the lead up and down the banding, but judging from the amplitude of the ripple marks this displacement would be much smaller than observed.) Lead, be it noted, is not soluble to an appreciable state in aluminum [40], and dispersion takes place by flow and not dissolution. Narrower traces were observed for greater axial extensions in Figure 3.8. The axial extension is observed to be so great that lead can emerge at the weld surface as seen in Figure 3.16. Variation in lead expulsion is a good candidate for the cause of coarser gaps (over multiple tool revolutions) in lead traces, such as those between the discrete wisps of lead observed in the plan view in Figure 3.5. Variation in lead expulsion could be caused by local temperature variation, and local temperature variation could be a result of local variation in contact resistance at the anvil and hold-down clamp surfaces.

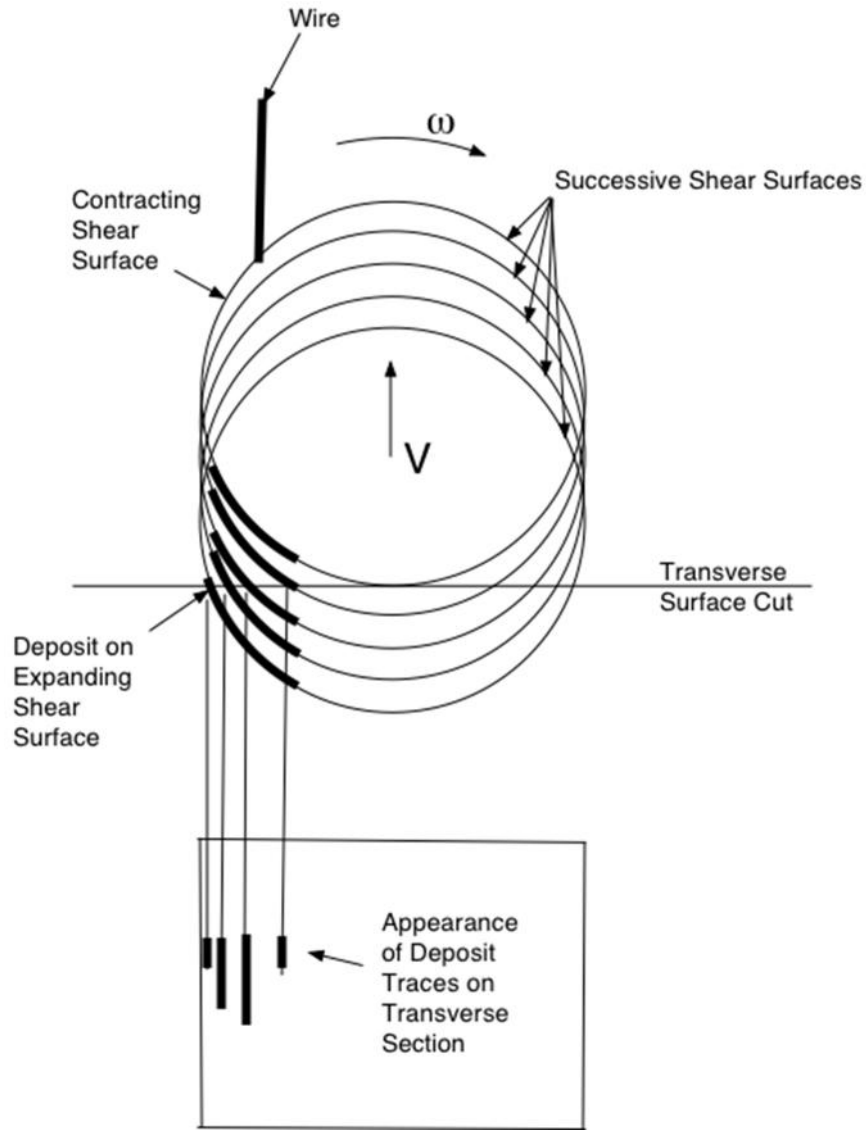


Figure 3.20 Schema for the generation of lead wire traces in plan and transverse sections.

The shear surface traces are taken as vertical lines, sections of cylinders here. In a more precise model the shear surface traces would be distorted into a bulge by the ring vortex circulation. A transverse cut through the bulge would produce the familiar onion ring pattern, along which the lead traces would lie. The longitudinal traces are generated in a similar way.

More variation at coarser scale is seen in Figure 3.11, where two sets of traces from transverse sections LX-3 and LX-4 are directly juxtaposed. The LX-3 trace is more curved than the LX-4 trace. The curvature of a trace in transverse section is an effect of the ring vortex flow component, which is driven by boundary conditions on shoulder and pin. Assuming that the weld metal has seized to the pin and shoulder, variation of the ring vortex could be attributed to temperature variations and their effect upon deformation within the weld metal, i.e. hotter, softer metal responds more easily to surface forces. Or it could be attributed to the effect of molten lead emerging at the tool-weld metal interface and lubricating the surface, i.e. inserting itself between tool and workpiece and shearing much more easily than the replaced solid workpiece metal, and so effectively reducing resistance of the shoulder surface to the pin driving force.

Temperature variations could also cause variations in shoulder slippage that would give rise to gaps in lead distribution, but the variation would need to be of the same order of magnitude as the gap (between 5 and 10 mm), and this magnitude of lateral variation in the upper SZ is not seen.

The lead wisps in the plan view of Figure 3.5 did not emerge in the early portions of the weld and disappeared at the end of the weld. This, too, can be attributed to temperature variations along the weld panel. The panel is presumably somewhat hotter at the ends, due to less metal bulk to absorb welding heat at the ends as well as an initial dwell in place during the tool insertion phase, and cooler in the middle, with small temperature variations along the way due to variations in thermal contact resistance. It is possible that a slight increase in temperature could result in significant loss of lead from

surface extrusion (Figure 3.16). Temperature variations are also thought to be responsible for the macrostructural variations seen in Figures 3.8 and 3.10.

The above picture is simplified and conjectural pending further study. One complication that has not been taken into account is the interaction between shoulder slippage and temperature. As slippage increases and the shear surface at the shoulder retreats, the slightly reduced deformation region (shear surface) produces slightly less heat and a slight reduction in temperature (as if the shoulder had been reduced).

3.6 Summary

Radiographic and SEM imaging of a lead wire tracer were used to obtain information about the internal structure of a FSW. From the internal structure certain tentative conclusions about shoulder contact were drawn:

1. The point where the SZ joins the shoulder on the advancing edge remains close to the shoulder edge with only small displacements. This indicates that most of the shoulder is seized to the workpiece, driving with the pin a rotating plug of metal attached to the tool.
2. The plan view radiographic image of the lead wire trace is divided into a pattern of wisps separated by intervals substantially greater than the distance travelled by the tool in a single revolution. The traces are not resolvable at the start of the weld and become resolvable at the midpoint of panels which is thought to be the result of temperature variations.
3. In the panel interior variation in proximity to clamps or other surface contact conditions can cause periodic variations in temperature. This is

thought to account for the irregular separations of the lead wisps observed in the middle of the weld panel.

4. At a finer scale, lead trace variations over the distance traversed in a single revolution of the tool are attributed to variations in slip at the edge of the shoulder and to their effect on the location of the shear surface in relation to the end of the wire. A sudden reduction of the slipped area extends the shear surface out into the wire and rapidly incorporates wire into the shear surface. The high pressure beneath the shoulder squeezes the molten lead out over the hot shear surface. The lead trace appears limited to a narrow line on the band width, so that it appears that the wire is incorporated in sudden jumps as if the slipped area on the shoulder edge suddenly gives way, retreating back a distance close to the distance traversed by the tool during a rotation (~ 0.75 mm), and then suddenly advancing when the shear surface reencounters the wire.
5. Subtle differences in distortions of the shear surface and internal banding in the wake of the tool are seen in longitudinal sections. The sections compared in Figure 3.11 are about 6.4 mm or 8.5 tool revolutions apart. The differences are thought to result either from variations in lubrication of the radial flow of weld metal beneath the shoulder by lead expelled over the weld metal-shoulder interface or from direct flow stress effects of local temperature variations. Both of these mechanisms would be expected to affect the ring vortex bulk flow component around the tool in a similar way.

6. It has been shown that tools are available to make inferences about FSW tool contact conditions from interior tracer observations. Melting tracers yield particularly complex and informative results. It is recommended that further study of this nature be carried out with a view to updating the techniques (in particular detailed observation of surface extrusions of the tracer) and to developing the understanding necessary to design optimal FSW tools and select optimal FSW weld parameters.

3.7 References

- [1] W.M. Thomas, E.D. Needham, M.G. Murch, P. Templesmith, C.J. Dawes, International Patent Application No. PCT/GB92/02203 and GB Patent Application No. 9125978.9, 1991.
- [2] A. C. Nunes, Jr., Proc. Aluminum 2001, Pub. TMS Intl., Materials Park, OH, (2001) 235-248.
- [3] J.A Schneider, A.C. Nunes, Jr., Metall. Mater. Trans. B 35 (2004) 777-783.
- [4] K. Colligan, Weld. J. Supp. (1999) 229-237.
- [5] T.U. Seidel, A.P. Reynolds, Sci. Tech. Weld. Joining 8 (3) (2003) 175-183.
- [6] M. Guerra, C. Schmidt, J.C. McClure, L.E. Murr, A.C. Nunes, Mater. Charact. 49 (2003) 95-101.
- [7] Z.W. Chen, T. Pasang, Y. Qi, Mater. Sci. Eng. A 474 (2008) 312-316.
- [8] A.P. Reynolds, Scripta Mater. 58 (2008) 338-342.
- [9] Y.H. Zhao, S.B. Lin, F.X. Qu, L. Wu, Mater. Sci. Technol. 22 (2006) 45-50.
- [10] K. Kumar, S.V. Kailas, Mater. Sci. Eng. A 485 (2008) 367-374.
- [11] B. London, M. Mahoney, W. Bingel, M. Calabrese, R.H. Bossi, D. Waldron, Friction Stir Welding Processing II, Pub. TMS Intl., Materials Park, OH, (2003) 3-12.
- [12] F. Gratecap, M. Girard, S. Marya, G. Racineux, Int. J. Mater. Form 5 (2011) 99-107.
- [13] K.N. Krishnan, Mater. Sci. Eng. A 327 (2002) 246-251.
- [14] R.M. Leal, C. Leitão, A. Loureiro, D.M. Rodrigues, P. Vilac, Mater. Sci. Eng. A 498 (2008) 384-391.
- [15] P.F. Mendez, K.E. Tello, T.J. Lienert, Acta Mater. 58 (2010) 6012-6026.
- [16] J.A. Schneider, R. Beshears, A.C. Nunes, Jr., Mater. Sci. Eng. A 435-436 (2006) 297-304.
- [17] S. Xu, X. Deng, Acta Mater. 56 (2008) 1326-1341.
- [18] H. Zhang, S.B. Lin, L. Wu, J.C. Feng, Sh.L. Ma, Mater. Design 27 (2006) 805-809.

- [19] B. Yang, J. Yan, M.A. Sutton, A.P. Reynolds, *Mater. Sci. Eng. A* 364 (2004) 55–65.
- [20] Z.W. Chen, S. Cui, *Scripta Mater.* 58 (2008) 417–420.
- [21] A. Scialpi, L.A.C. De Filippis, P. Cavaliere, *Mater. Design* 28 (2007) 1124–1129.
- [22] H.N.B. Schmidt, T.L. Dickerson, J.H. Hattel, *Acta Mater.* 54 (2006) 1199–1209.
- [23] S. Muthukumaran, S.K. Mukherjee, *Sci. Technol. Weld. J.* 11 (2006) 337–340.
- [24] S. Muthukumaran, S.K. Mukherjee, *Int. J. Adv. Manuf. Technol.* 38 (2008) 68–73.
- [25] J.C. McClure, W. Tang, L.E. Murr, X. Guo, *Proc. 5th Int. Conf. Trends in Welding Res.*, Pine Mountain, GA, June 1998.
- [26] Y.J. Chao, X. Qi, W. Tang, *Trans. ASME* 125 (2003) 138–145.
- [27] O. Frigaard, O. Grong, O.T. Midling, *Metall. Mater. Trans. A* 32 (2001) 1189–1200.
- [28] P. Colegrove, M. Painter, D. Graham, T. Miller, *2nd Int. Symp. FSWing*, Gothenburg, Sweden, June 2000.
- [29] P.A. Colegrove, H.R. Shercliff, *Sci. Tech. Weld. Joining* 9 (6) (2004) 483–492.
- [30] P.A. Colegrove, H.R. Shercliff, *J. Mater. Proc. Technol.* 169 (2005) 320–327.
- [31] H. Schmidt, J. Hattel, J. Wert, *Modelling Simul. Mater. Sci. Eng.* 12 (2004) 143–157.
- [32] M.Z.H. Khandkar, J.A. Khan, A.P. Reynolds, *Sci. Tech. Weld. Joining*, 8 (3) (2003) 165–174.
- [33] C.M. Chen, R. Kovacevic, *Int. J. Mach. Tools. Manuf.* 43 (2003) 1319–1326.
- [34] H. Schmidt, J. Hattel, *Scripta Mater.* 58 (2008) 332–337.
- [35] J.A. Querin, J.A. Schneider, *Weld. J. Supp.* 21 (2012) 76s–82s.
- [36] J. Sanders, "Understanding the Material Flow Path of the Friction Stir Weld Process," MSME Thesis, Mississippi State University, 2005.
- [37] T. U. Seidel, A. P. Reynolds, *Metall. Mater. Trans. A* 32 (2001) 2879–2884.
- [38] H.A. Rubisoff (Doude), J.A. Schneider, A.C. Nunes, Jr., *FSW&P-V*, Pub. TMS Intl., Materials Park, OH, 2009.

- [39] J.A. Schneider, "Temperature distribution and resulting metal flow," Chapter 3, FSW&P, Pub. ASM International, Materials Park, OH, 2007.
- [40] W.G. Moffet, "The Handbook of Binary Phase Diagrams," Genium, New York, 1984.
- [41] L.E. Murr, Y. Li, R.D. Flores, E.A. Trillo, J.C. McClure, Mater. Res. Innovat. 2 (1998) 150-163.
- [42] W.J. Arbegast: Hot Deformation of Al Alloys, TMS Int., Materials Park, OH, 2003.
- [43] M. Brendel, J.A. Schneider: Proc. 9th Int. FSWing Symp., TWI, May 2012.
- [44] W. Tang, X. Gui, J.C. McClure, L.E. Murr, A.C. Nunes, Jr., J. Mater. Proc. Manuf. Sci. 7 (2) (1998) 163-172.

CHAPTER IV

MECHANISMS OF FRICTION STIR WELD PROPERTY VARIATIONS³

4.1 Abstract

Depending on the parameter window used when friction stir welding (FSWing), property variations can occur due to changes in the flow of the material around the weld tool. A series of welds were completed across the parameter window for a threaded tool in AA 2219-T87. The panels were sectioned transversely along the entire panel and characterized by tensile tests, hardness, and macrostructure imaging. High speed data acquisition collected the force data during the welds. X-ray diffraction was used to understand the precipitate state. Variations in the mechanical properties were correlated with volumetric defects and changes in the precipitate state.

4.2 Introduction

Friction stir welding (FSWing) has grown in popularity in manufacturing due to its repeatability and low environmental impact [1–3]. Despite its increasing usage, the mechanics of the process are still not fully understood. Without this knowledge, the process cannot be used to its full potential [4].

³ A version of this chapter was submitted for publication to *Welding Journal* as: Doude, H.R. and Schneider, J.A. “Mechanisms of friction stir weld property variations.”

One area of limited understanding is defect formation. There are two general types of defects reported in FSWing: geometric and material flow related. Geometric type defects include lack of penetration and lack of fusion and are caused by a misfit in the layup or geometry of the weld panel and weld tool. Lack of penetration defects generally occur when the weld tool is not deep enough to fully involve the material at the root of the weld leaving behind a small section of unconsolidated weld seam. Lack of fusion defects can occur when the weld tool is offset from the weld seam during welding and the weld seam is not fully consumed [3]. Although both defect types can reduce the structural integrity of the weld, flow related defects and their impact on the dynamics of the process are addressed in this study since geometric related defects can generally be mitigated during the weld fitup.

Flow related defects are more numerous in type and have been linked to specific weld parameters including travel speed, plunge force, and tool rotational speed [1, 5–8]. The plunge force is especially considered important in the process of defect formation [8–13]. Volumetric defects as well as reduced material properties (ex. softening due to overheating [14, 15]) are due to material flow issues. Also included in flow related defect category is non-optimized tool geometry including improperly sized tool shoulder for the material thickness because tool design affects material flow and can lead to defect formation [6, 9, 10, 16–18]. One example is the wormhole defect found when the tip of the weld tool is not rounded or blunted leaving a point at the tip [17].

There are various theories about how the material moves around the tool including the metalworking model [19], kinematic model [20, 21], and stacked layers

model [22, 23]. All of these theories agree that without sufficient material movement, defects occur within the weld nugget [22–25].

Material movement within the weld depends on how the tool interacts with the workpiece material based on the rate of rotation of the weld tool, the speed at which the tool travels along the weld seam, and the amount of force on the work piece by the tool. The tool rotation rate and tool travel speed are used to develop a two dimensional parameter window in which defect-free welds can be formed. An example of the parameter space with a nominal parameter window is shown in Figure 4.1. Volumetric defect formation is often attributed to welding outside of the acceptable weld parameter window on the “cool” side of the parameter space [5, 8, 24, 26]. The cool side of the parameter space includes a region where the travel speed is faster than the acceptable weld parameter window and the rpm is lower than the acceptable weld parameter window. If the weld is too cold, lack of consolidation or intermittent volumetric defect and scalloping defects are formed [3]. Also, cool welds can result in shingle lap defects or kissing bonds where the weld seam is not completely forged together [27]. By going to the “hot” side of the parameter space where the travel speed is lower and the rpm higher than the acceptable parameter window, excessive flash which may form wormhole and shallow weld nuggets are expected as well as the root-flow defect where material flow patterns can be seen on the root side of the weld [5, 18, 24]. Some researchers have also found that in high rpm and high travel speed welds, volumetric defects can occur [5]. The reported reason for these defects is “abnormal stirring” of the material within the weld nugget caused by a temperature gradient between the material near the crown and near the root of the weld [5].

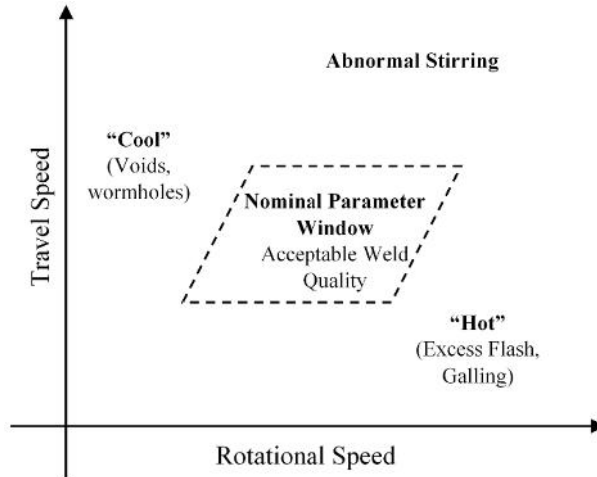


Figure 4.1 Basic layout of the parameter window based in the literature.

This study characterized the defects encountered when welding at various rotational speeds and a constant travel speed in an attempt to better understand what constitutes a “good” FSW and the effect of material flow on weld quality. Welds were formed with tool rotation rates ranging from the “cool” side of the parameter window to the “hot” side of the window in order to get a full range of material movement while holding the travel speed and plunge depth constant. It was expected that volumetric defects would occur in the “cool” range of the parameters and excess flash would occur with tool rotation rates above the nominal parameter window. Ultimate tensile strength, hardness, and transverse macrographs were used to determine weld quality for each weld panel. The precipitate state of selected panels was investigated using x-ray diffraction (XRD).

4.3 Methods

A series of butt joints were FSWed in 6.35mm thick AA2219-T87 panels (10 cm x 61 cm) with a range of tool rotational speeds and a constant tool travel speed. The weld tool, machined from H13 tool steel, Figure 4.2, had a shoulder diameter of 15 mm with a counter-clockwise scroll and the threaded pin was 6 mm in diameter with a 2 mm pitch. The panels were welded under tool depth position control with electronic deflection control which maintained a constant tool depth within the panel regardless of the associated plunge force and deflection of the weld machine. The FSWs were performed on an MTI RS-1 machine with high speed data collection. Digital data was collected at a rate of 1024 Hz using a National Instruments PXI 6123 data acquisition system. Table 4.1 displays the range of weld parameters. The rotational speed range was chosen based on nugget bulge estimates for conventional welds, Table 4.2, to give a range of welds across and outside of the expected parameter window [28].

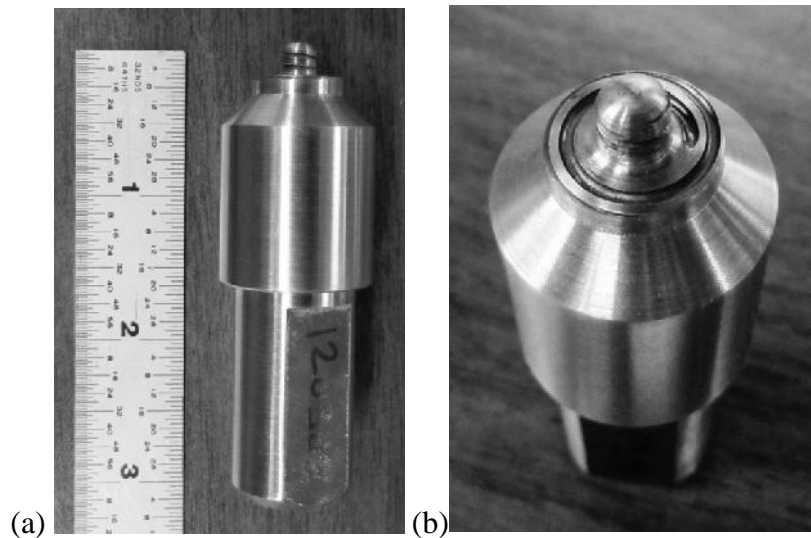


Figure 4.2 The weld tool and shoulder detail

The tool (a) with a close-up of the shoulder and pin (b)

Table 4.1 Weld parameter summary

Joint type	Travel speed	RPM range	Average plunge depth	Pin length	Control mode	Tool offset from weld seam
Butt joint	100 mmpm	150, 200, 250, 400, 600, 800, 1000	6.1 ± 0.1 mm	6 mm	Position Control	1 mm (AS)

Table 4.2 Weld parameter window approximation based on nugget bulge (mm) [28].

Travel (mmpm)	Tool Rotation (rpm)										
	150	200	250	300	400	500	600	700	800	900	1000
500	0.051	0.102	0.152	0.229	0.381	0.584	0.838	1.118	1.422	1.778	2.134
450	0.076	0.127	0.178	0.279	0.483	0.711	1.016	1.372	1.727	2.134	2.540
400	0.076	0.152	0.229	0.330	0.584	0.914	1.270	1.676	2.134	2.591	3.073
350	0.102	0.203	0.305	0.432	0.762	1.168	1.626	2.134	2.667	3.200	3.759
300	0.152	0.279	0.406	0.584	1.016	1.549	2.134	2.769	3.404	4.013	4.597
250	0.229	0.381	0.584	0.838	1.422	2.134	2.896	3.632	4.369	5.004	5.486
200	0.330	0.584	0.914	1.270	2.134	3.073	4.013	4.851	5.486	5.893	5.994
150	0.584	1.016	1.549	2.134	3.404	4.597	5.486	5.944	5.893	5.309	4.318
100	1.270	2.134	3.073	4.013	5.486	5.994	5.309	3.708	1.829	0.406	0.025

The panels were sectioned into 25 sections 19.5mm in width to provide a complete view of the resulting weld, Figure 4.3. Half of each section (6.35mm wide after machining) was used for tensile testing and half was hardness tested using an Instron Model RS 574 with a 1/16 in ball indenter on the Rockwell B scale. The hardness specimens were then mounted, polished and etched using Keller’s reagent to reveal the macrostructure of the FSW for metallographic inspection. When volumetric defects were

present within the weld nugget, ImageJ software was used to measure the area of the volumetric defect in the transverse section.

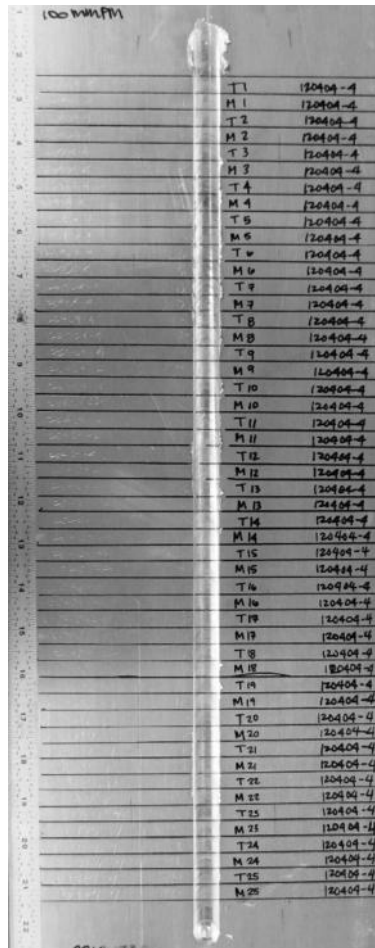


Figure 4.3 Representative cut plan for a weld.

A Rigaku Ultima III was used to determine the precipitate state of the 250, 400, and 600 rpm panels. A continuous scan rate of 0.35deg/min was used with a step size of 0.02 degrees over a 2 range of 18-55 degrees using a Cu-K source.

The shear strain rate of the material in the shear zone was estimated by approximating

$$\dot{\gamma} = \frac{R*\omega}{\delta} \quad (4.1)$$

where $\dot{\gamma}$ was the strain rate in s^{-1} , R was the radius of the shear surface which was estimated to be equal to the radius of the pin, ω was the rate of material movement which was estimated to be the tool rotation rate, and δ was the thickness of the shear surface which was approximated as 0.01 times the diameter of the pin [21]. The temperature of the material during welding was estimated using the alternative heat index which uses the torque to determine the temperature during weld by

$$T = T_{mp} - \frac{T}{2\pi m_t R^3 \left[\frac{1}{3} \left(\frac{R_s}{R} \right)^3 + \frac{H}{R} \right]} \quad (4.2)$$

where T was the temperature of the shear surface, T_{mp} was the melting temperature of the material, T was the torque, m_t was the change in the shear stress due to the increased material temperature, R was the radius of the pin, R_s was the radius of the shoulder, and H was the pin length [29].

4.4 Results

The resulting transverse macrographs of the panels, Figure 4.4, show the changing stir zone shape as the rotational speed was increased.

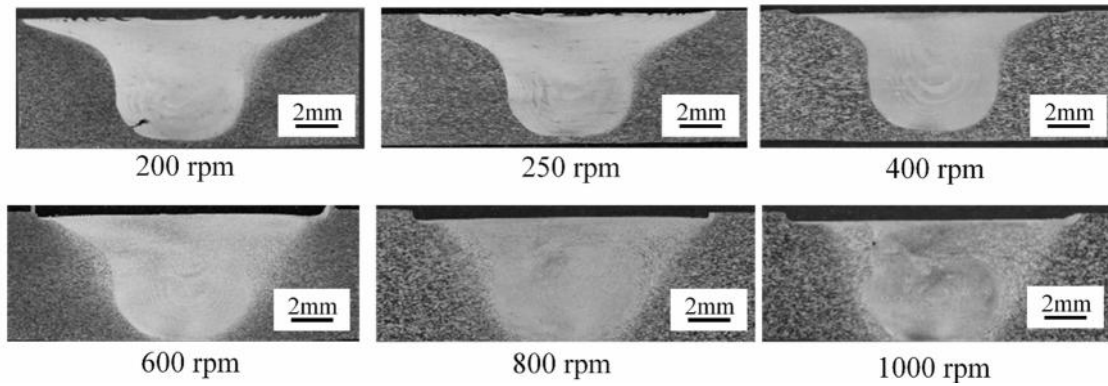


Figure 4.4 Macrographs of welded panels with the advancing side (AS) on the left.

The 150 rpm weld, lowest rpm in the series, was not completed due to breakage of the tool during welding. The rate of 150 rpm did not allow for enough softening of the material for the H13 weld tool to withstand the forces during welding. The pin separated from the shoulder at approximately 8.7 cm from the start of the weld and was embedded in the weld nugget. Figure 4.5a contains the transverse section of the panel before the tool broke and Figure 4.5b shows the transverse section of the weld after the tool broke. The tool was located and sectioned through to determine the material flow at the time of the tool break. The mating surfaces of that cut are available in Figure 4.6 a and b. Figure 4.7 contains a magnified view of Figure 4.6a.

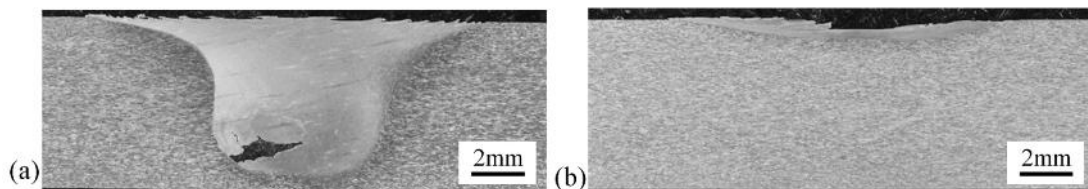


Figure 4.5 Transverse macrographs of the weld structure

(a) before and (b) after the tool broke at 150 rpm.

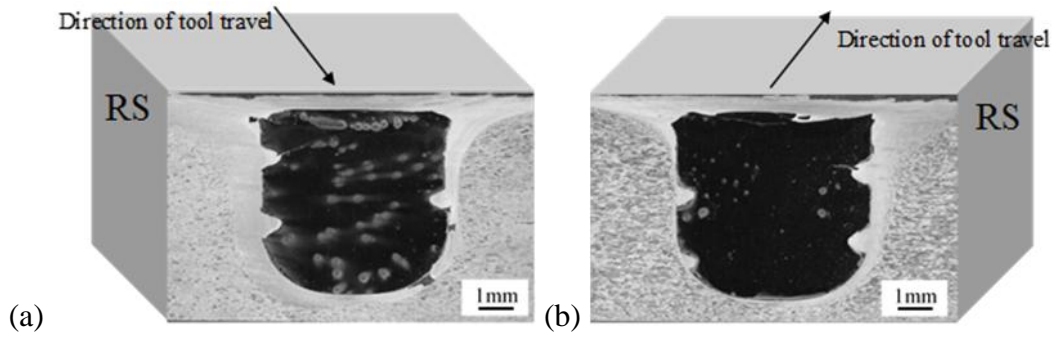


Figure 4.6 The mating transverse sections from the tool break location at 150 rpm 8.7cm into the length of the weld.

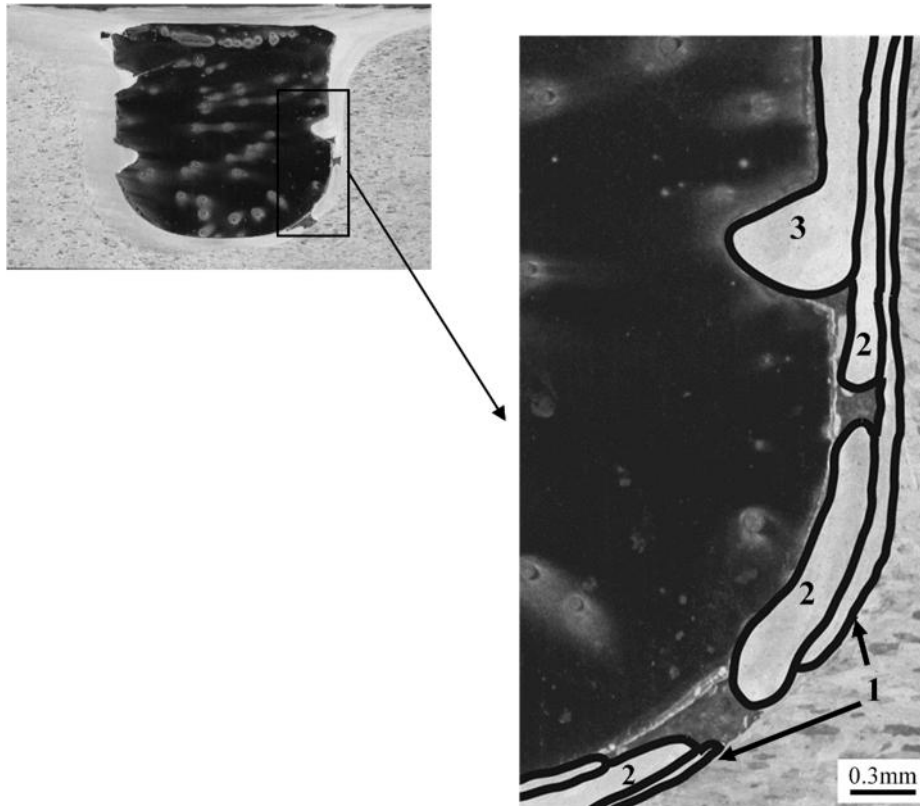


Figure 4.7 A close-up of the layering of material from Figure 6a. The numbers indicate the assumed order of deposition of the layers.

Welds at 200, 250, and 1000 rpm contained volumetric defects on the advancing side of the stir zone. Figure 4.8 contains the total volumetric defect area for the 3 panels containing volumetric defects. Optical microscopy images of the largest volumetric defects from each panel are presented in Figure 4.9. The 200 rpm weld resulted in volumetric defects on the advancing side of the weld located toward the bottom edge of the pin tool. The volumetric defects average size was $0.25 \pm 0.12 \text{ mm}^2$ with a maximum volumetric defect size of 0.54 mm^2 and a minimum volumetric defect size of 0.01 mm^2 . The 250 rpm weld was fully consolidated until the reaching the end of the panel where sections 23-25 contained volumetric defects. The volumetric defects increased in size from segment 23 to 25 with segment 25 having the largest total volumetric defect area of 0.038 mm^2 . At 1000 rpm, volumetric defects were present in clusters and located on the advancing side of the weld toward the mid-thickness of the transverse specimen. The volumetric defect average area was $0.09 \pm 0.07 \text{ mm}^2$ with the maximum volumetric defect area of 0.28 mm^2 and a minimum volumetric defect area of 0.01 mm^2 . Welds completed at 400, 600, and 800 rpm were full consolidated, containing no volumetric defects.

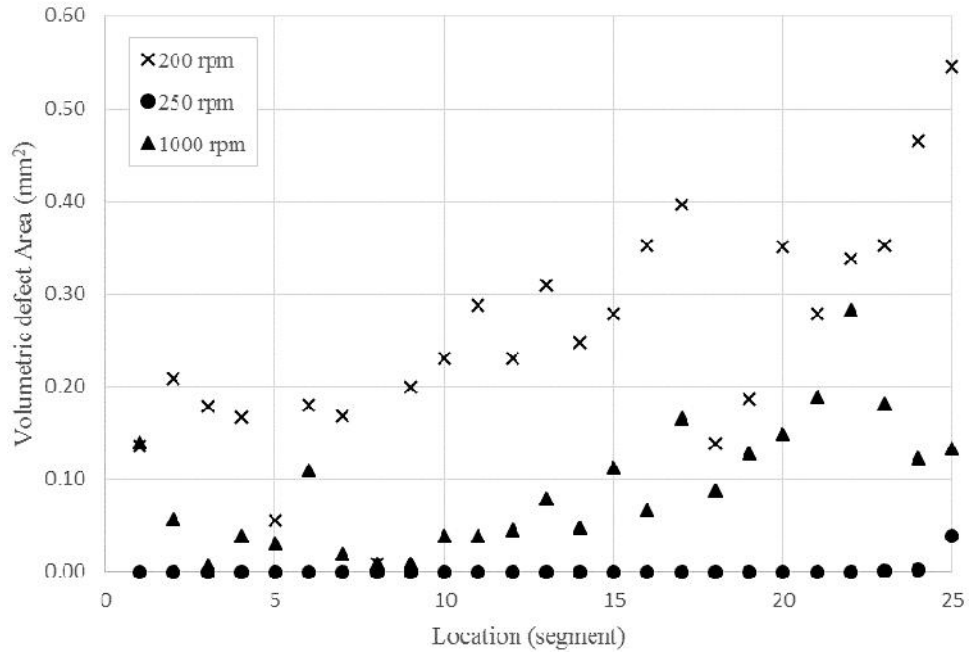


Figure 4.8 Total volumetric defect areas for each transverse section of the 200, 250, and 1000rpm welds.

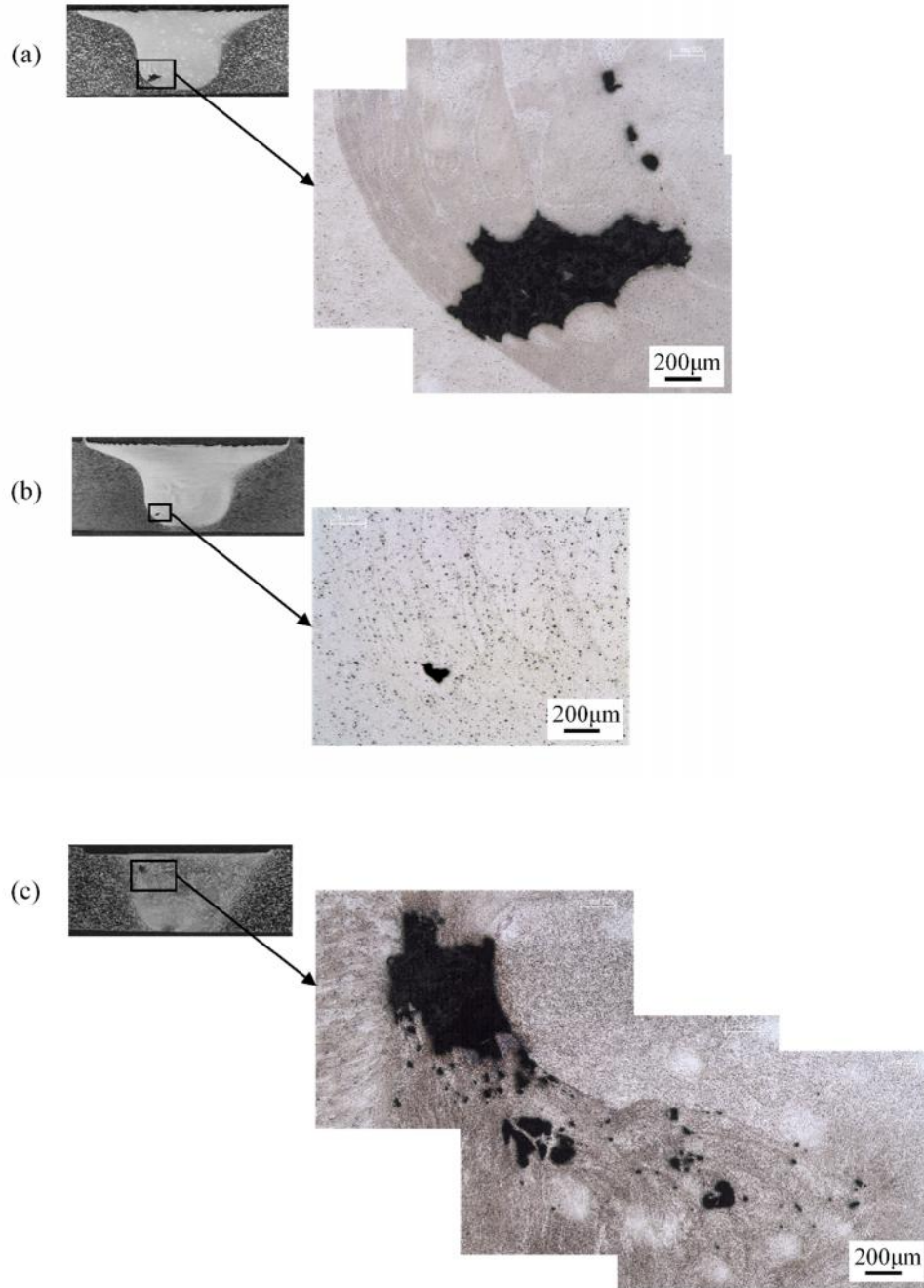


Figure 4.9 Example volumetric defect images

(a) 200, (b) 250, and (c) 1000 rpm welds.

The average ultimate tensile strength (UTS) for each panel is located in Figure 4.10 and showed an increase in ultimate tensile strength in the panels up to 800 rpm. At 1000 rpm, the tensile strength drops back to the UTS of 240 MPa which was below the UTS of the 200 rpm weld. The hardness measured at the center of the weld stir zone is also available in Figure 4.10 and indicates the lowest hardness values at 250 and 400 rpm with an increasing hardness from 600 to 1000 rpm.

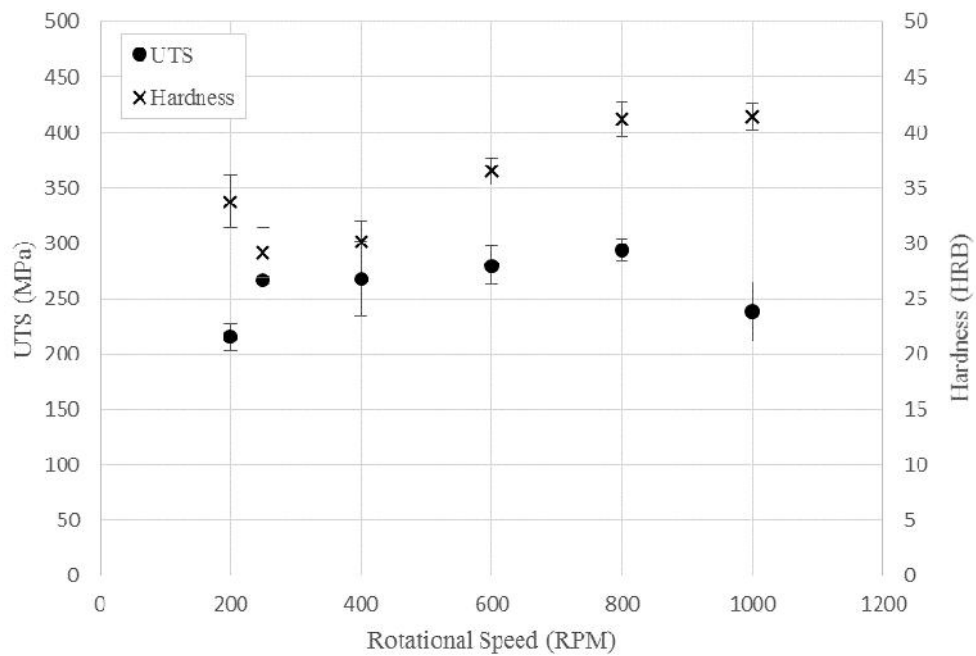


Figure 4.10 Average ultimate tensile strength and hardness results

Since the 400 rpm weld showed a drop in hardness, XRD was used to further investigate the precipitate state of the 250, 400, and 600 rpm welds to determine if there were differences in the precipitates. Slow scans have been previously correlated with the presence of coarsened precipitates [15]. The XRD scans, Figure 4.11, showed a

coarsening of the precipitates in the 250 and 400 rpm panels and reduction in the amount of copper-rich precipitates at 600 rpm. The Al_2Cu peaks increased from the 250 rpm panel to the 400 rpm panel and then decreased in the 600rpm panel to levels below the 250 rpm results.

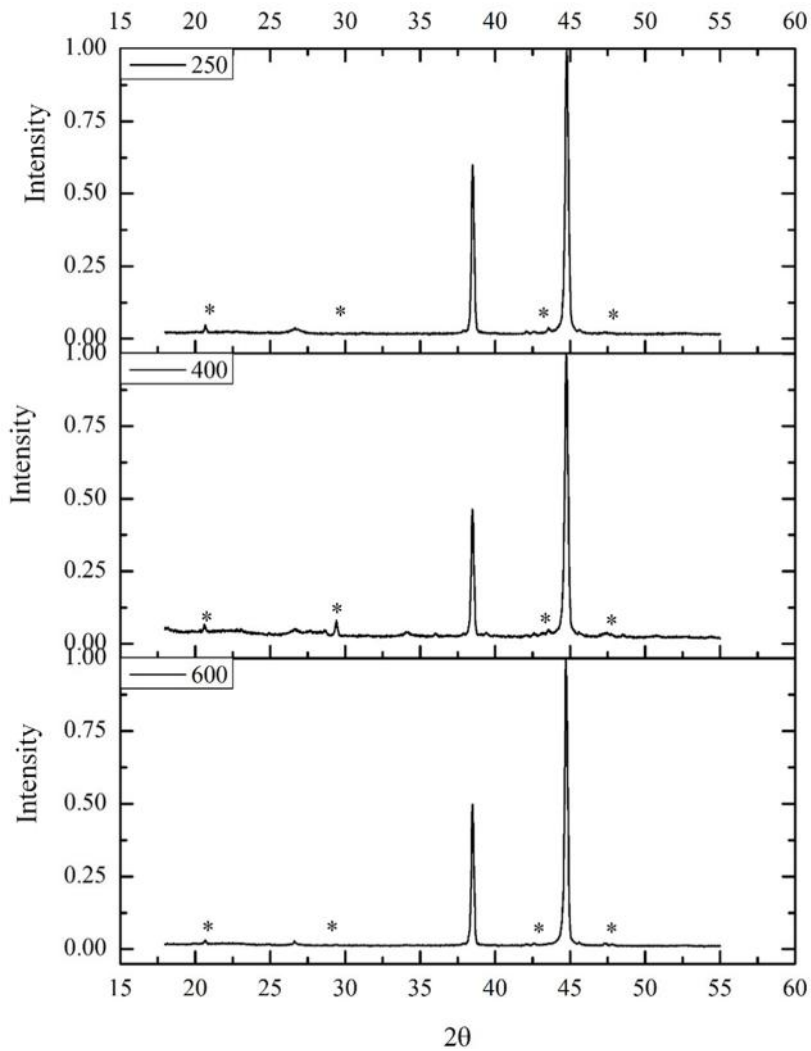


Figure 4.11 XRD data for 250, 400, and 600 rpm welds

(* denotes location of Al_2Cu peaks).

The results of the shear strain rate and temperature approximations, Table 4.3, indicated an increase in both the temperature and the shear strain rate as the rotational speed was increased.

Table 4.3 Estimated temperature and shear strain rates for each weld.

RPM	Torque (N-m)	Estimated Temperature (°C)	Estimated Shear Strain Rate (s⁻¹)
150	79	498	0.8 x 10 ⁴
200	72	510	1 x 10 ⁴
250	64	525	1.3 x 10 ⁴
400	45	560	2 x 10 ⁴
600	44	562	3 x 10 ⁴
800	36	577	4 x 10 ⁴
1000	32	584	5 x 10 ⁴

4.5 Discussion

When evaluating the quality of a welded panel, it was important to consider the microstructure of the material as a possible source of lower quality as well as the issues arising from insufficient consolidation. Some welds formed nuggets free of volumetric defects; however, the properties of the material indicated that the weld was not as high quality as some of the other rpm welds. This was evident at the 400 rpm range where there was a drop in nugget hardness. The variation in the hardness across the experimental panels can be explained by changes in the precipitate state in the nugget due to temperature and deformational changes occurring as the tool welds the panel. XRD confirmed that there was coarsening of the Al₂Cu precipitates from 250 to 400 rpm. In Figure 4.11, the peaks relating to Al₂Cu (denoted by *) increased in intensity from 250 to

400 rpm. In the 600 rpm weld, however, these peaks had diminished intensity. The increased intensity and lower hardness at 400 rpm indicated that the precipitates had coarsened and softened the material in the stir zone [15]. The alternative heat index was used to estimate the temperature in the shear surface based on the torque recorded during welding [29]. The temperature at 250 and 400 rpm were 525°C and 560°C, respectively. These temperatures were high enough to cause copper rich precipitates near the tool to coarsen causing the material to soften [14, 15]. The increase in the temperature and the strain rate at 600 rpm and above appeared to be high enough to drive the precipitates back into solution which in turn resulted in higher hardness in the weld stir zone [14].

Upon examination of the volumetric defects present at 200 and 1000 rpm, the mechanisms for volumetric defect formation appeared to be different. At 200 rpm, the volumetric defect had scalloped edges that coincided with the same markings that make up the onion ring structure. Each swath of material laid down by a rotation of the tool should have merged to form a solid weld nugget behind the tool, but at the lower rpm, the material did not fully consolidate behind the tool after each rotation. This left behind a small gap between the lobes of material moving around the tool [22, 23]. For each rotation where there was not consolidation, there was a scalloped edge in the transverse volumetric defect perimeter. For the 200 rpm weld, the parameters were such that the volumetric defect was present and varied in size along the length of the panel with the total void area increasing towards the end of the panel, Figure 4.9a. In the transverse sections of the weld, the largest gap between the lobes was close to the advancing side (AS) edge of the nugget and the gap was reduced moving away from the edge until it eventually disappeared resulting in a volumetric defect that was somewhat teardrop

shaped. Since the volumetric defect size varied along the panel, it was possible to form intermittent defects which produced regions in the weld with fully consolidated nuggets and regions with small volumetric defects as seen in the 250 rpm panel.

At 1000 rpm the volumetric defect was located higher in the transverse section, closer to the crown surface. The volumetric defects in this panel were actually clusters of smaller volumetric defects between two regions of heavily stirred material. There was a train of small defects leading from the cluster towards the center of the “onion.” The scalloped edges present in the 200 rpm weld were not as visible on the volumetric defects in the 1000 rpm weld. This may have been due to thinner deposited layers resulting from the increased rotational speed but constant travel speed.

In the 250 rpm weld, there was a scalloped line visible at the bottom of the weld nugget where the material from the lobes merged together fully. The scalloped line became less visible as the rpm increased.

To further understand the differences between the flow in the low rpm and high rpm ranges, the x-force and y-force have been plotted for several rotations of the tool for each weld panel, Figure 4.12. As the rotational speed increased, x-force decreased as expected since the increased rotational speed raised the temperature within the weld and thereby lowered the flow stress of the workpiece material [30]. The x-force minimum was reached at 800 rpm; however, at 800 rpm there was greater variation in the x-force than at 600 rpm. The y-force increased as the rotational speed increased.

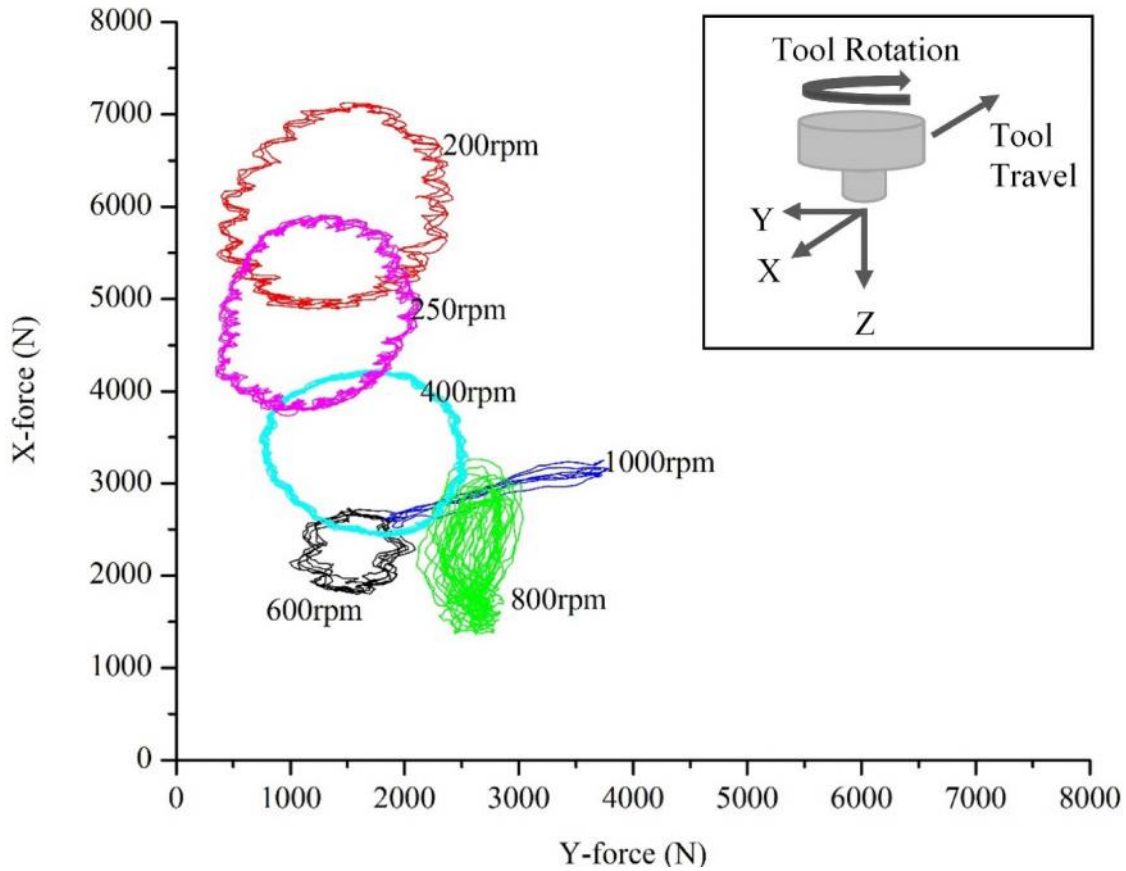


Figure 4.12 X-force vs Y-force plot for each rpm.

This data underscores the importance of high speed data collection to fully understand material flow during welding. The variations that occur during each rotation of the tool provide important information about how the material is moved around the tool.

For the 200 rpm - 600 rpm welds, the x-force and y-force variations per rotation were balanced which resulted in a circular plot in Figure 4.12. At 600 rpm, the circle had a small radius due to a lower magnitude variation in the forces. This balance did not continue as the rpm increased, however. At 800 rpm, there was less variation in the y-force than the x-force resulting in an oblong trace. The opposite was true at 1000 rpm

with there being greater variation in the y-force and much less change in the x-force. The resulting trace looked more like a diagonal line than the circular type shapes seen with the lower rpm welds.

The force plot indicated that there needs to be variation in the x and y forces to properly consolidate the weld joint. According to Gratecap et al., during FSWing, eccentricity in the tool leads to material moving around the tool in swaths during each rotation [22]. Once the material moves around the tool, it is stacked in layers behind the tool filling in the volume that was displaced when the tool moved through that area. One possible cause of the eccentricity, in addition to the eccentricity caused during the manufacture and installation of the tool in the machine, is the reactive forces on the tool during welding [22]. The changing variation of the x-force as the rotational speed was increased may show a change in the eccentricity of the movement of the tool. As the tool lost the front to back variation, the material being swept by the tool was no longer forged tightly together behind the tool. There was not enough force to compress the layers together and close up all of the volumetric defects. Above 250rpm, the oscillation in the tool was sufficient to press the layers together with each successive layer causing the layers behind to spread to fill any volumetric defects that may have been present. This was true until 1000rpm where the variation in the x-force decreased to the point where the layers are no longer forged together leaving small volumetric defects between the layers on the advancing side. The lack of variation in the x-force at 1000rpm may mean that there was not enough force pushing the material together behind the weld tool during each rotation. There was, however, variation in the y-force. This was interesting since the y-force variation was greater at 1000 rpm than it was at 600 or 800 rpm, but it was a

similar to the variation in the lower rpm 200, 250 and 400 rpm welds. Several researchers point to the y-force as having the most promise for indicating the presence of defects [19, 31, 32].

The variation in the y-force was at a minimum during the 600 and 800 rpm welds and the maximum at 200 and 1000 rpm. This implied that large variation in the y-force did not lead to good quality welds. When the y-force variation was lowest, there was not much movement of the tool in the y-direction. Oscillations of the tool in the y-direction may have led to excessive amounts of flash being pushed out on the sides of the weld by allowing material to escape from under the shoulder. When this happens, there is not enough material left in the weld nugget to fill in the gap behind the tool [12].

A balance between the x- and y-force variations with a minimized y-force variation provided the best weld quality for this series of welds. When the y-force variation was too great, defects were produced. When the x- and y- force variations are not balanced, there may not be enough x-force to prevent volumetric defect formation.

A summary of the resulting welds overlaid into the parameter window is shown in Figure 4.13. Based on the results of this study, the 600 rpm weld was considered the best quality weld of the series. At and below 250 rpm, the formation of volumetric defects resulted in low tensile strength. The 600 rpm weld had a high enough temperature to prevent softening due to over-aged precipitates. Above 600 rpm, the variations in the x- and y-forces result in material flow that led to defects as the rotational speed was increased. It is important to note that although the 800 rpm weld had the highest UTS of the series, there was a significant drop in strength at 1000 rpm due to the formation of defects in the weld. Examination of the x- and y- forces for the 600, 800, and 1000 rpm

welds indicated that significant changes were taking place in the material flow. A more balanced variation in the x- and y- force, which was not present in the 800rpm weld, appeared to result in a higher quality weld as seen in the 600 rpm weld.

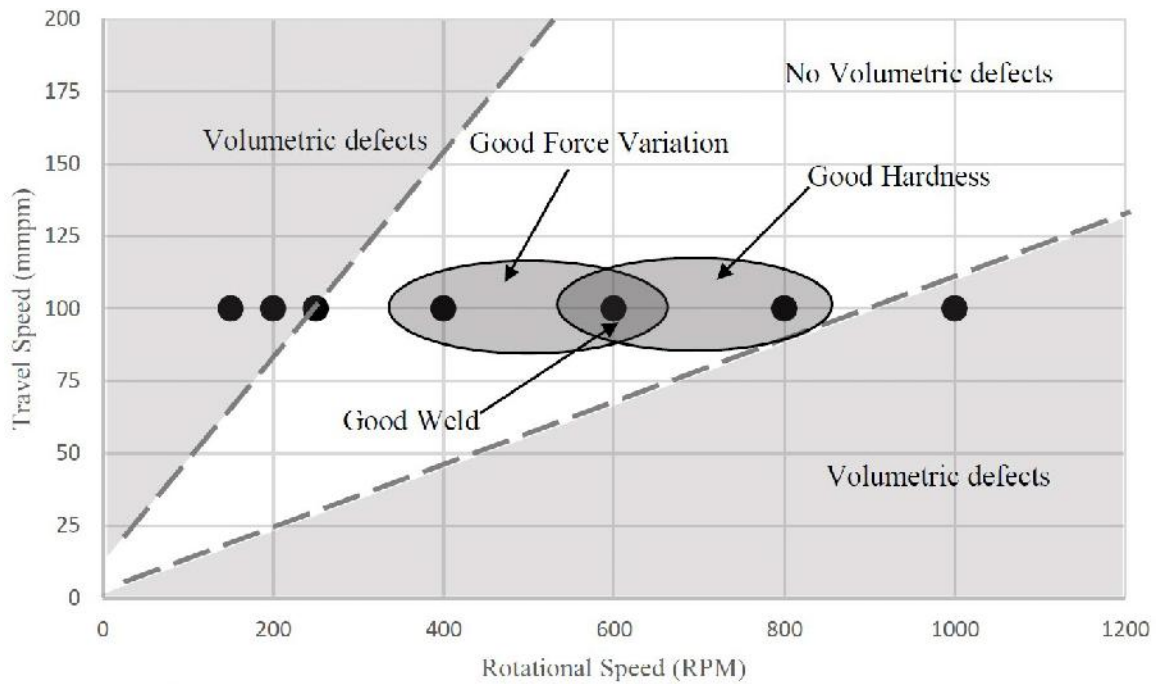


Figure 4.13 Summary of the parameter window.

4.6 Summary

1. The location of the volumetric defect depends on the material flow which can be affected by the rotational speed of the tool.
2. The formation of volumetric defects within the weld nugget is not due to insufficient material flow due to lack of heating within the workpiece material alone but is due to an imbalance between the amount of material being displaced by the tool and the amount of material deposited behind

the tool which can occur at any temperature. The proper amount of variation in the x-force and y-force is required to have sufficient force in the stir zone to consolidate the layers moving around the tool.

3. It is important to consider defects within the panel that are not visually obvious flow defects such as changes in precipitate state due to increased temperature and strain rate caused by increased rotational speed.
4. Choosing weld parameters to maximize the UTS may increase the likelihood of unexpected defective welds.

4.7 References

- [1] R.S. Mishra, Z.Y. Ma, *Mater. Sci. Eng. R Reports* 50 (2005) 1-78.
- [2] R.S. Mishra, M.W. Mahoney, *Friction Stir Welding and Processing*, ASM International, 2007.
- [3] W.J. Arbegast, in: R.S. Mishra, M.W. Mahoney (Eds.), *Frict. Stir Weld. Process.*, ASM International, Materials Park, OH, 2007, pp. 273–308.
- [4] J. Schneider, in: R.S. Mishra, M.W. Mahoney (Eds.), *Frict. Stir Weld. Process.*, ASM International, Materials Park, OH, 2007, pp. 37–49.
- [5] Y.G. Kim, H. Fujii, T. Tsumura, T. Komazaki, K. Nakata, *Mater. Sci. Eng.* 415 (2006) 250-254.
- [6] Y.-H. Zhao, S.-B. Lin, F.-X. Qu, L. Wu, *Mater. Sci. Technol.* 22 (2006) 45-50.
- [7] H.N.B. Schmidt, T.L. Dickerson, J.H. Hattel, *Acta Mater.* 54 (2006) 1199-1209.
- [8] A.J. Leonard, S.A. Lockyer, in: *Proc. 4th Int. Frict. Stir Weld. Symp.*, TWI, Park City, Utah, 2003.
- [9] F. Gratecap, G. Racineux, S. Marya, *Int. J. Mater. Form.* 1 (2008) 143-158.
- [10] K. Kumar, S.V. Kailas, *Mater. Sci. Eng.* 485 (2008) 367-374.
- [11] Z.W. Chen, T. Pasang, Y. Qi, *Mater. Sci. Eng.* 474 (2008) 312-316.
- [12] K. Elangovan, V. Balasubramanian, *Mater. Des.* 29 (2008) 362-373.
- [13] J. Seaman, B. Thompson, in: *Proc. Twenty-First 2011 Int. Offshore Polar Eng. Conf.*, International Society of Offshore and Polar Engineers, Maui, Hawaii, 2011.
- [14] B. Li, Y. Shen, *Mater. Des.* 32 (2011) 3796-3802.
- [15] J. Schneider, R. Stromberg, P. Schilling, B. Cao, W. Zhou, J. Morfa, O. Myers, *Weld. J.* (2013) .
- [16] R. Palanivel, P. Koshy Mathews, N. Murugan, I. Dinaharan, *Mater. Des.* 40 (2012) 7-16.
- [17] J. Querin, H. Rubisoff, J. Schneider, in: *Trends Weld. Res. Proc. 8th Int. Conf.*, ASM International, 2008, pp. 108–112.
- [18] K. Elangovan, V. Balasubramanian, *Mater. Sci. Eng.* 459 (2007) 7-18.

- [19] W.J. Arbegast, in: Z. Jin (Ed.), Hot Deform. Alum. Alloys III, 2003.
- [20] J.A. Schneider, A.C. Nunes Jr, Met. Mater. Trans. B 35 (2004) 777-783.
- [21] A.C. Nunes Jr, in: Proc. 9th Int. Frict. Stir Weld. Symp., TWI, Huntsville, Al, 2012.
- [22] F. Gratecap, M. Girard, S. Marya, G. Racineux, Int. J. Mater. Form. 5 (2011) 99-107.
- [23] E. Boldsaikhan, D.A. Burford, P.J.G. Britos, in: R. Mishra, M. W.honey, Y. Sato, Y. Hovanski, R. Verma (Eds.), Frict. Stir Weld. Process. VI, John Wiley & Sons, Inc., 2011, pp. 333–343.
- [24] W.J. Arbegast, Scr. Mater. 58 (2008) 372-308.
- [25] J. Schneider, R. Beshears, A.C. Nunes, Mater. Sci. Eng. 435-436 (2006) 297-304.
- [26] P.J. Ramulu, R.G. Narayanan, S.V. Kailas, J. Reddy, Int. J. Adv. Manuf. Technol. 65 (2012) 1515-1528.
- [27] A. Oosterkamp, L.D. Oosterkamp, A. Nordeide, Weld. J. 83 (2004) 225.
- [28] J. Schneider, A.C. Nunes Jr, M.S. Brendel, in: Proc. 8th Int. Frict. Stir Weld. Symp., Timmendorfen Strand, Germany, 2010.
- [29] J.A. Querin, J.A. Schneider, Weld. J. 91 (2012) 76s-82s.
- [30] G.W. Kuhlman, in: S.L. Semiatin (Ed.), ASM Handb., ASM International, Materials Park, OH, 2005, pp. 299–312.
- [31] P. Fleming, D. Lammlein, D. Wilkes, K. Fleming, T. Bloodworth, G. Cook, A. Strauss, D. DeLapp, T. Lienert, M. Bement, Sens. Rev. 28 (2008) 62-67.
- [32] P. Gimenez-Britos, C. Widener, E. Boldsaikhan, D.A. Burford, in: Proc. 8th Int. Frict. Stir Weld. Symp., TWI, Timmendorfen Strand, Germany, 2010.

CHAPTER V

IDENTIFICATION OF PERIODIC DEFECTS DUE TO MATERIAL FLOW VARIATIONS IN FSW USING POST-WELD DATA PROCESSING⁴

5.1 Abstract

Researchers have been seeking methods for better understanding and control of the FSW process since its invention. Currently, researchers are able to identify “good” and “bad” attributes of FSWs by applying analysis techniques post weld to the collected force data [1-5]. While the researchers were able to classify entire FSW panels as either all good or all bad, they did not attempt to isolate specific sections in a FSW that contained periodic defects. This spatially resolved data is necessary as it has been reported that intermittent defects can occur in long welds using processing parameters qualified on shorter panels [6]. For this study, several FSWs were produced within an identified parameter window to achieve good sections [7]. Force data was collected during welding and analyzed using an unsupervised matched filter (UMF) technique to classify segments of a weld based on their similarity or dissimilarity to other FSW segments. Destructive analysis of the FSW panels was used to determine the ability of

⁴ A version of this chapter was published in the proceedings of the 9th International Friction Stir Welding Symposium as: Doude, H., Schneider, Ma, B., J., Du, J. “Identification of periodic defects due to material flow variations in FSW using post-weld data processing.” *Proc. 9th International Symposium on Friction Stir Welding*, Huntsville, AL 2012.

UMF to correctly classify the weld segments. The results presented illustrate the feasibility of using digital data analysis techniques for post-process inspection of a FSW panel. By investigating individual weld segments within a panel, variations in material flow that correlate with either changing heat profile and/or possible formation of volumetric defects, can be spatially identified. These periodic flow variations or instabilities may result from either plunge preheat conditions or changes in the contact conditions between the weld tool and the workpiece. Validation of data analysis method will form the basis for in situ process control to ensure the quality of a FSW of any length.

5.2 Introduction

Establishment of acceptable FSW process parameter windows often use time consuming trial and error methods for new applications and rely on post-weld destructive and non-destructive testing to prove that the weld is acceptable. Because of the time and expense of testing, other ways of determining weld quality are necessary. One method is processing and interpretation of data signals collected during welding. Processing the force and torque data may provide information on the changes in the forces that can be related to material flow. Non-optimized material flow has been correlated with defect formation that is detrimental to the FSW strength [8-11].

Currently, researchers are able to identify “good” and “bad” weld panels by applying analysis techniques post-weld to the collected force data [1-5]. While the researchers were able to classify entire weld panels as either all good or all bad, they did not attempt to identify specific sections in a FSW that contained periodic defects. This spatially resolved data is necessary as it has been reported that intermittent defects can

occur in long welds that used parameters within a given processing window [6]. These types of defects are of concern as they are difficult to identify using traditional NDE methods [12]. The objective of this study was to identify periodic defect locations within a FSW panel produced within a production quality parameter window.

Tracer studies on C-FSWs have led to a better understanding of material flow during FSWing [10-11,13]. Lead and tungsten tracers suggest a stick-slip boundary condition at the tool/ work piece interface [12]. Even though the shoulder may appear to be in full contact with the work piece based on the tool marks on the surface, the shoulder may not be fully engaging the material through the panel thickness. An example of lack of shoulder engagement was seen in a series of self-reacting welds where the nugget showed evidence of less shoulder interaction in the weld with lower strength [14]. No visible defects were present in the low strength weld, but the nugget had an advancing side bulge and decreased shoulder engagement when compared to the higher strength weld. Figure 5.1 shows changes in shoulder contact at different rotational speeds. Figure 5.1a shows traces from the advancing side of transverse macrographs which allow a comparison between the nugget profile at 210 and 300 rpm. At 210 rpm, the profile is interpreted to result from increased material flow through the material thickness due to increased sticking at the shoulder. At 300rpm, the profile straightens indicating possible slipping at the shoulder which reduces the material movement through the material thickness.

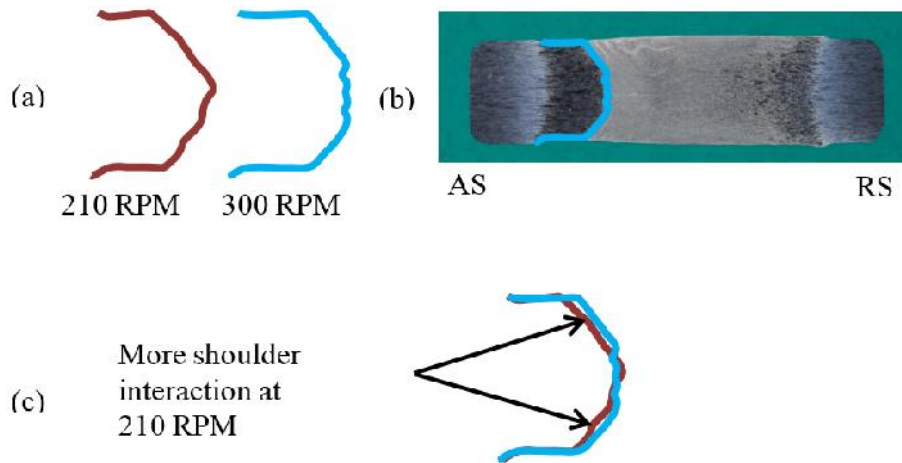


Figure 5.1 Shoulder contact comparison

(a) A comparison trace of the transverse advancing side of the nugget in FSWs made at 210 and 300 rpm. (b) This is shown for the 300 rpm weld in the transverse macrograph. (c) Overlaying the two advancing side traces shows more shoulder contact at 210 rpm than 300 rpm [14].

Volumetric defects are reported to form when the plunge force is insufficient to fully consolidate the material flowing around the tool [15-20]. One suspected cause of change in the plunge force is change in the amount of shoulder contact during FSWing. McClure [21] has previously shown that material flow is strongly affected by shoulder contact.

In previous studies, several plunge tests to varying depths were completed and macroscopic images were taken from transverse samples [14, 21]. Representative macrographs of the plunge section are shown in Figure 5.2a along with a corresponding force data plot versus time. These macrographs show that as the pin is lowered into the work piece in Figure 5.2b, material flow is concentrated around the pin tool/ workpiece interface and very little if any material movement occurs through the material thickness. Once the shoulder contacts the crown surface in Figure 5.2c, material begins to move in a

through thickness pattern near the bottom edge of the pin. It appears that a vortex of material in the shape of a ring is moving around the tool. The general shape of the vortex is similar to that of a doughnut revolving around the tool moving material through the thickness of the work piece. It has been proposed that a good quality FSW results from the interaction of these two flow fields [4]. If the shoulder is not fully engaged, insufficient material flow may result in volumetric defect formation.

Using the force data collected during the plunge stage of one study, each data set was transformed into the frequency domain using a fast fourier transform (FFT) analysis [14]. Figure 5.3a shows that when the pin only was engaged in the material, FFTs of the x, y, and z forces contain only peaks that represent the tool rotation frequency. In contrast, when the shoulder is fully engaged, Figure 5.3b shows FFT peaks which include both the tool rotation frequency but also low frequency peaks. The low frequency peaks are especially evident in the z force (plunge force) plot indicating that the plunge force maybe more sensitive to changes in material flow than the x and y forces and thereby a better indicator of weld quality in FSWs.

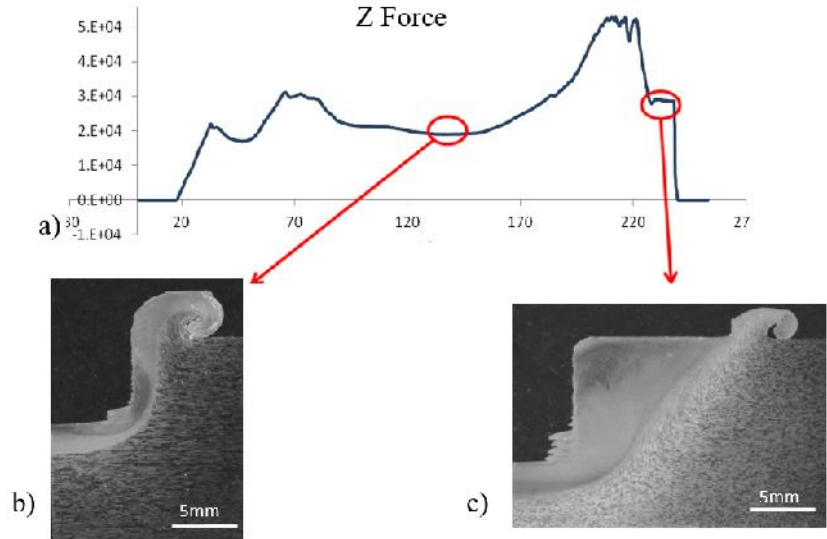


Figure 5.2 Variation in plunge force as tool shoulder is seated

(a) Continuous force data recorded during a plunge phase of a FSW, (b) transverse macro of the beginning of a plunge, and (c) at the end of the plunge as shoulder engages [14].

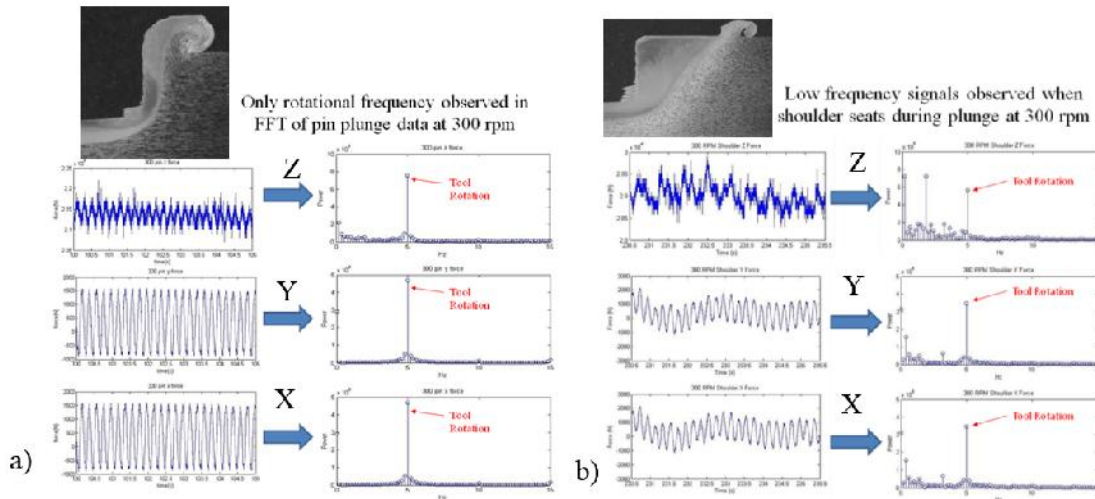


Figure 5.3 FFT results with and without shoulder contact

The plunge data is taken from 2 regions in the plunge phase: pin only and pin and shoulder contact. a) Taking the FFT of the load reveals that during the pin only portion, only the tool rotation frequency appears. b) Once the shoulder is fully seated however, other low frequency signals appear [14].

This study explores the use of a unsupervised matched filter (UMF) analysis to detect intermittent deviations in the force data and evaluate the ability to correlate these deviations with defects or low weld strength regions within a FSW panel, UMF uses only the given test data to determine which segments are most similar or different from the rest of the data. For this application, it is assumed that the majority of the weld is good with segment differences indicating changes in the flow. Destructive analysis will be used on segments identified as different to evaluate possible differences in nugget geometry and possible defects.

5.3 Methods

Four FSWed butt joints were made in 100mm by 610mm panels of 6.35mm thick AA2219-T87 using two different plunge routines and two different weld tools. The panels were welded longitudinally along the 610mm length after milling the faying surfaces to provide a smooth seam with clean surfaces. The welds were completed on a Manufacturing Technology Inc (MTI) Model RM1 FSW machine using tools with scrolled shoulders and threaded pins. Details of the weld tools are located in Table 5.1.

Table 5.1 Weld tool geometry

	Tool 1- Larger	Tool 2- Smaller
Pin length	5.9mm	5.7mm
Pin diameter	13mm	6mm
Pin thread pitch	1mm	2mm
Shoulder diameter	30mm	15mm
Shoulder scroll pitch	3mm	2mm

A National Instruments PXI 6123 data acquisition system was used to record the digitized data at a rate of 1024Hz. Force data was collected in the x, y, and z directions as well as the torque. A schematic in Figure 5.4 describes the direction of these forces in relation to the weld tool.

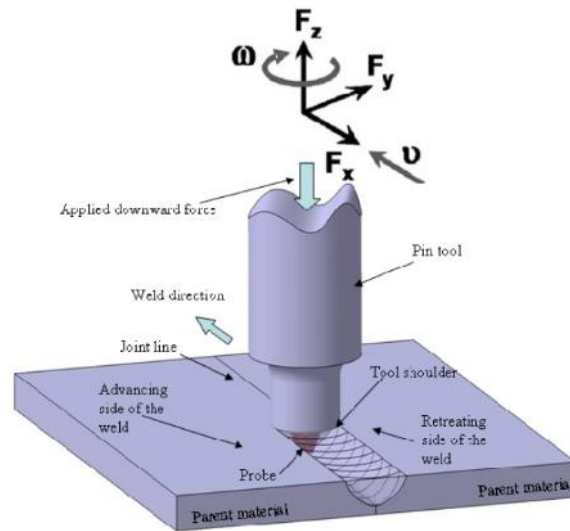


Figure 5.4 Weld schematic with x, y, and z forces and torque labeled [14]

The weld parameters are contained in Table 5.2 taking into account the limitation of the weld tool strength during pin only welds [7]. To determine the effects of the plunge preheat on the panel, two different plunge routines were used as summarized in Table 5.3-6. The slow plunge took approximately 3 min to complete before the tool travel was begun versus the faster plunge which took approximately 30 s to complete prior to initiating the tool travel.

Table 5.2 Weld parameters

	Tool 1- Larger	Tool 2- Smaller
Travel speed	229mmpm	100mmpm
Rotation speed	200rpm	400rpm
Control method	Position	Position

Table 5.3 Plunge parameters for Weld 1

Z Cmd (mm)	Rate (mm/min)	RPM	Control Mode	Force Setpoint (N)	Dwell (s)
-5	20	400	Position	---	1
-6.15	2	400	Position	---	1

(Slow Plunge (~3 min) Larger Tool)

Table 5.4 Plunge parameters for Weld 2

Z Cmd (mm)	Rate (mm/min)	RPM	Control Mode	Force Setpoint (N)	Dwell (s)
-5	20	400	Position	---	1
-1	15	400	Load	30KN	0
-5.1	15	400	Load	60kN	2

(Fast Plunge (~30 s) Larger Tool)

Table 5.5 Plunge parameters for Weld 3

Z Cmd (mm)	Rate (mm/min)	RPM	Control Mode	Force Setpoint (N)	Dwell (s)
-5	20	600	Position	---	1
-5.85	2	600	Position	---	1

(Slow Plunge (~3 min) Smaller Tool)

Table 5.6 Plunge parameters for Weld 4

Z Cmd (mm)	Rate (mm/min)	RPM	Control Mode	Force Setpoint (N)	Dwell (s)
-5	20	600	Position	---	1
-1	15	600	Load	30KN	0
-4.85	15	600	Load	60kN	2

(Fast Plunge (~30 s) Smaller Tool)

Once the FSW was completed, the panels were sectioned transversely into segments 19mm in width. Each 19 mm wide transverse segment was cut into two transverse segments where one was mounted and polished for metallurgical examination and one was reserved for later tensile testing.

The data file was parsed into corresponding subfiles of 5 seconds which corresponded to the length of the transverse sections. Due to the travel speed of 229 mmpm, 19 mm is travelled in 5 seconds resulting in data sections containing 5120 data points per segment. At 100 mmpm, the data segments contained 11776 points per segment.

To automate the parsing and comparison of the individual weld segments and subfiles, analysis techniques from pattern recognition were used. These combine techniques to reduce the dimensionality of the data set so that features within the reduced data set can be quickly characterized by an appropriate algorithm. These basics can be applied to large databases to understand great volumes of temporal data in directly informative terms and link with responsible phenomena.

The technique of principal component analysis (PCA) was first used to reduce the initial data set of 3 forces for a C-FSW to a smaller number of principal components.

PCA is a eigenvector-based multi-variant analysis technique which projects the data onto

an orthogonal coordinate system corresponding to the greatest variance in the data. This resulted in a transformation from the given set of variables into the principal components which are linearly independent. Applying PCA allowed the reduction of the number of variables while retaining the important information in the data. To reduce the number of variables, the principal components containing the most variance were extracted leaving a simplified data set that was still representative of the original data. This greatly reduced the dimensionality of the data set and provides a methodology for tracking or identification of changes. The low frequency data was then extracted to further reduce the data and focus on the frequencies of interest.

Reducing the dimensionality of the original data set using PCA prepared the data for further supervised or unsupervised analysis techniques to be applied to characterize the data. Since the process of FSW is not well understood at this time, unsupervised techniques were used to identify regions that are different within a FSW panel. The weld panel segments in this study were characterized using the unsupervised matched filter (UMF) analysis which compares subfiles within a given weld file with each other instead of using training data which is developed from well understood data from other welds.

Based on analysis indications, destructive evaluation was used to correlate these deviations with defects or low weld strength regions within a FSW panel.

5.4 Results

Four consolidated FSWed panels were obtained using the scrolled shoulder, threaded pin weld tools. The surfaces of the welds are available in Figure 5.5. Investigation of the transverse specimens from welds 1 and 2 using tool 1 revealed small volumetric defects ($\sim 0.025 \text{ mm}^2$ total void area per specimen) present at the advancing

side edge near the location of the bottom of the pin. These volumetric defects were intermittent along the length of the welds and varied from $\sim 0.16 \text{ mm}^2$ in void area at the largest to fully consolidated areas with no volumetric defects. Most specimens containing volumetric defects had 2 to 4 voids lined up in a series of differing sizes.

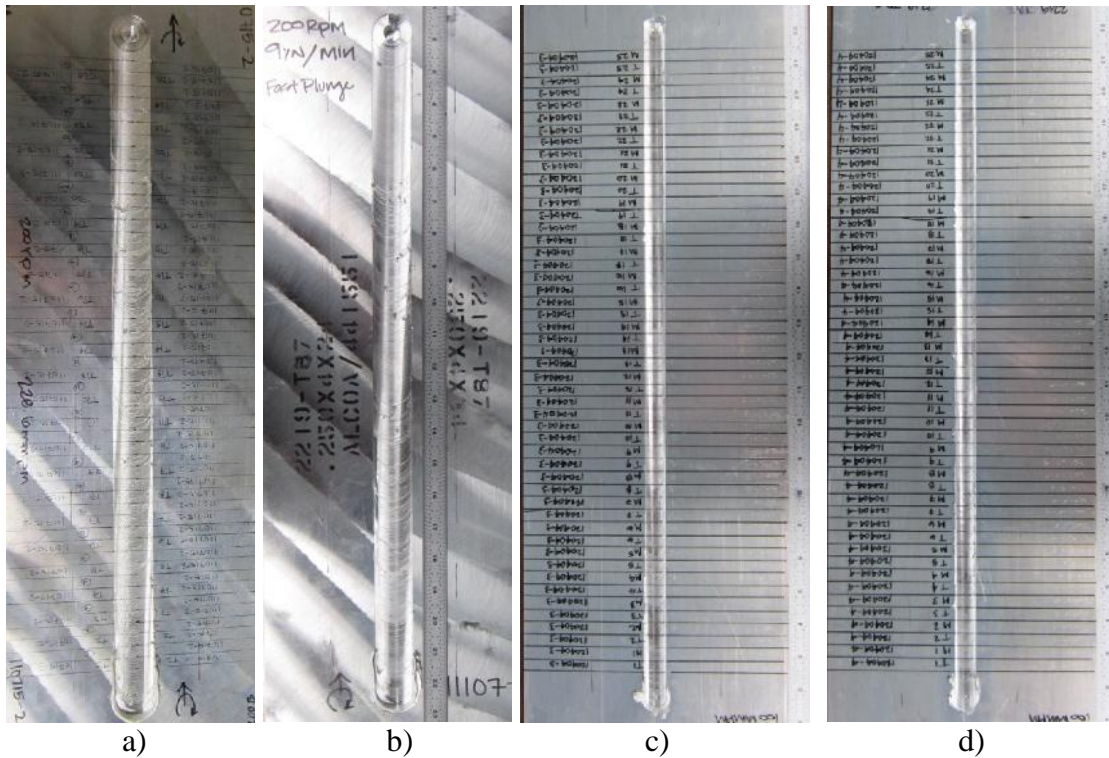


Figure 5.5 As-welded panels

a) Weld 1- slow plunge with larger tool, b) Weld 2- fast plunge with larger tool, c) Weld 3- plunge with smaller tool, and d) Weld 4- fast plunge with smaller tool.

Results of the data analysis in Figure 5.6 show that segment 16 of weld 1 with the slow plunge was identified as the most different from the rest of the panel when using UMF.

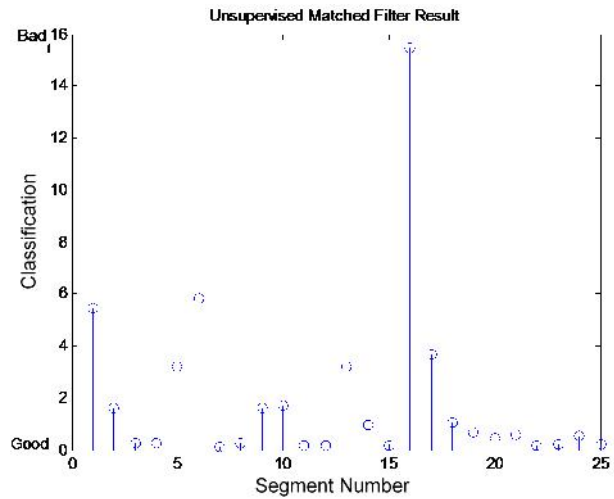


Figure 5.6 UMF analysis showing segment 16 as different from the other weld segments.

Figure 5.7 contains the transverse macrograph of the specimen classified as different from the rest of the weld. Specimen 16 had a total void area of 0.035 mm² which was above the average but well below the largest total void area of 0.197mm², and each volumetric defect in specimen 16 was smaller than the largest individual volumetric defects found in the weld.

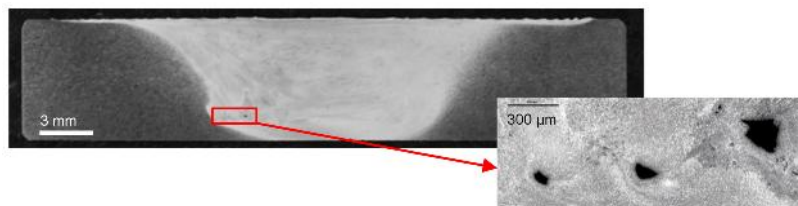


Figure 5.7 Macro and micro results of transverse inspection.

For weld 2 with the fast plunge test, segments 6 and 9 were identified as the most different using UMF to classify the segments as shown in Figure 5.8. Transverse macrographs of these sections, Figure 5.9, did not indicate volumetric defect sizes that were significantly different in size from the rest of the weld. However, after segment 9 (segments 10-25) only very small volumetric defects were apparent in the transverse segments.

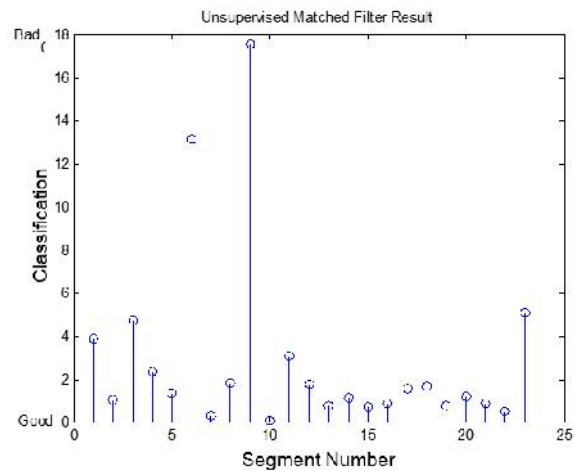


Figure 5.8 UMF results indicating segment 6 and 9 at different from the other segments.

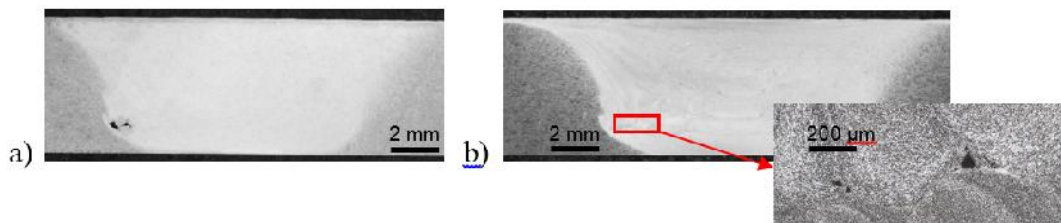


Figure 5.9 Macroscopic images of segments 6 and 9 from weld 2
Segments 6 (a) and 9 (b)

FSWs using tool 3 and 4, the smaller tool, were found to be free of volumetric defects. Representative macroscopic images are available in Figure 5.10.

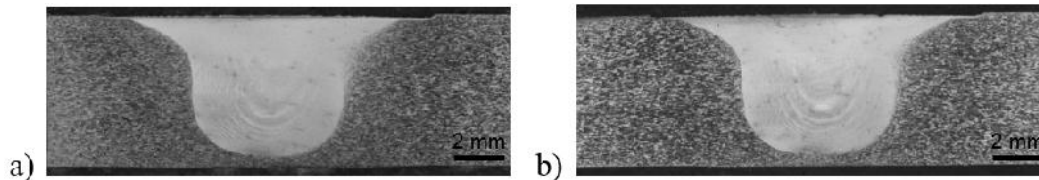


Figure 5.10 Defect free macro images for weld 3 and 4.

Weld 3 (a) and 4 (b).

UMF analysis, shown in Figures 5.11 and 5.12, of the defect free welds formed using the smaller tool had different results than the analyses of the previous welds using the larger tool. UMF for both welds, 3 and 4, indicated changes in forces near the starting position of the weld. These differences were reduced as the tool travel down the length of the weld. The resulting plots show that the collected weld force data was different at the start of the weld. For weld 3 with the slow plunge routine, there were 7 sections flagged as different from the rest of the weld. For weld 4 with the fast plunge routine, only 4 segments were indicated as different.

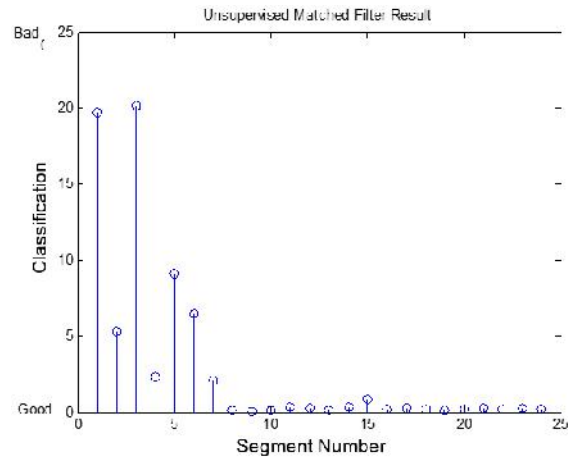


Figure 5.11 UMF analysis results from slow plunge using the smaller tool

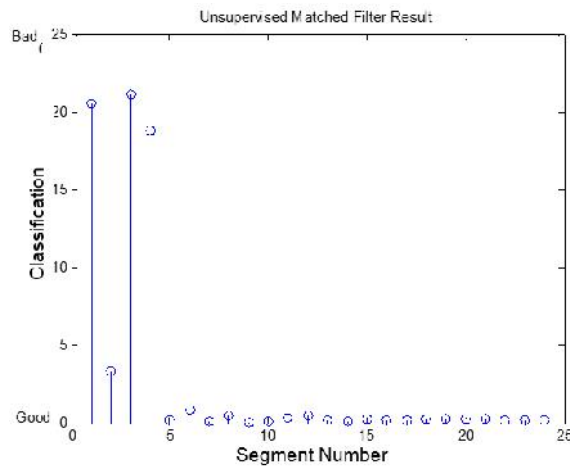


Figure 5.12 UMF analysis results from fast plunge using the smaller tool

5.5 Discussion

The volumetric defects at the bottom, advancing edge appear to result from a change in the flow due to the large diameter of the pin and shoulder relative to the material thickness. It appears as though there is not enough material under the tool to fully consolidate the weld material. The series of small volumetric defects are observed

to reside within an onion ring of material flow. This may indicate that there is a lack of material being moved during a tool rotation. To rectify this lack of material movement around the large pin, a smaller tool was used to produce two defect free welds (welds 3 and 4).

When comparing the UMF results from the two different tools it became obvious that there was a marked difference in the number of high peaks in the welds containing defects. UMF of welds 1 and 2 contain several peaks above 1 (arbitrary index of similarity). Thus it appears as though UMF is a good indicator of stabilized material flow. Areas where large peaks are present may indicate regions within the weld where the material flow is fluctuating. For welds 3 and 4, large peaks are only seen at the beginning of the weld. After a few centimeters of travel, the peaks approach zero indicating a region of very stable flow. In this stable region, volumetric defects were not expected nor observed as verified by macrographs of the transverse specimens.

After investigation of the flagged specimens from the series of welds, UMF did not detect exact defect locations but appears to provide an indication of unstable flow where defects may be likely to occur. One possible example is unstable flow may result as the tool traverses outside of the preheating region formed during the plunge routine.

As the tool is plunged into the weld material, the frictional and deformational heating raise the temperature of the material in the panel. This heat builds as the tool remains in one location but plunges deeper. During this time, the heat spreads into the panel and preheats an area that is to be welded. As the tool travels, it will eventually reach the edge of this preheated portion. As this happens, the loads on the tool will change due to changing material flow and contact conditions at the tool. The preheated

material is softer and has different contact conditions than the material at ambient temperatures. This temperature difference may be seen as a change in flow of the material.

To verify this, short and long plunge routines were used to study the effect temperature gradients on the data analysis. The long plunge routine with slower plunge speeds allows more time for heat buildup within the panel to move out ahead of the tool. The UMF results of weld 1 and 2 indicated that the transition between the preheated area and the rest of the panel may be indicated as specimen that is classified as very different from the weld. For weld 1, the highest peak is at segment 16 which is more than midway down the panel. Weld 2, with the faster plunge routine, has segments flagged much earlier in the weld with the first third of the panel. Welds 3 and 4 also exhibit this trend; however, more than just the transition is evident. The differences in the UMF results are most likely due to the existence of defects in welds 1 and 2. The intermittent occurrence of defects indicates changes in the material flow as the tool travels down the panel.

To further study this concept, heat models will be prepared using Rosenthal's equation for a moving heat source [22] and an alternative heat index during FSWing [23]. This should provide an estimated location of where the plunge preheating would be expected to be outrun by the tool travel.

5.6 Summary

The results presented illustrate the feasibility of using digital data analysis techniques such as PCA combined with UMF analysis for post-process inspection of a FSW. By investigating each weld segment, variations in material flow that correlate with volumetric defect formation can be detected. These periodic flow variations or

instabilities appear to correspond to changes in the heat profile in advance of the weld tool that may result from either plunge preheat conditions or changes in the contact conditions between the weld tool and the workpiece.

The current results indicate that by applying UMF to force data in the frequency domain, it is possible to identify regions in the weld where the material flow around the tool is changing. Further investigation is required to fully identify how the flow changes and why the changes occur. Expansion of this study will lead to a better understanding of the tool interaction with the material and how good welds are formed.

5.7 Acknowledgements

Funding was provided in part by the NASA Graduate Student Research Program Fellowship and the Mississippi Space Grant Consortium. The FSWing equipment was purchased through a NASA federal initiative. All welds were produced at Mississippi State University with the help of everyone in the friction stir weld group.

5.8 References

- [1] M. Guerra, C. Schmidt, J.C. McClure, L.E. Murr, A.C. Nunes, Jr., *Mat. Characterization*, 49 (2003) 95-101.
- [2] F. Contreras, E.A. Trillo, L.E. Murr, *J. Mat. Sci.*, 37 (2002) 89-99.
- [3] J.H. Ouyang, R. Kovacevic, *J. Mat. Eng. & Perf.*, 11 (2002) 51-63.
- [4] J.A. Schneider, A.C. Nunes, Jr., 7th Intl. Conf. Trends Welding Research, 2005.
- [5] Personal communication. Dr. Arthur C. Nunes, Jr. NASA MSFC. Jan 29, 2010.
- [6] H.R. Shercliff and P.A. Colegrove, *Friction Stir Welding & Processing II*. TMS, 2003.
- [7] J. Schneider, A.C. Nunes Jr, M.S. Brendel, in:, *Proc. 8th Int. Frict. Stir Weld. Symp.*, Timmendorfen Strand, Germany, 2010.
- [8] W.M. Thomas et al., International Patent Application No. PC7/GB92/02203 and G.B. Patent Application No. 9125978.9, 1991. U.S. Patent No. 5460317 Oct. 1995.
- [9] J. Schneider, in:, R.S. Mishra, M.W. Mahoney (Eds.), *Frict. Stir Weld. Process.*, ASM International, Materials Park, OH, 2007, pp. 37-49.
- [10] K. Colligan, *Welding Res. Suppl.*, July (1999) 229s-237s.
- [11] T.U. Seidel, A.P. Reynolds, *Met. & Mat. Trans.*, 32A (2001) 2879-2884.
- [12] J. Schneider, R. Beshears, A.C. Nunes, *Mater. Sci. Eng.* 435-436 (2006) 297-304.
- [13] A.P. Reynolds, *Sci. Tech. Weld. Join.*, 5 (2) (2000) 120-124.
- [14] Doude, H.R., et al. *Friction Stir Welding and Processing VI*. TMS 2011.
- [15] A.J. Leonard, S.A. Lockyer, in:, *Proc. 4th Int. Frict. Stir Weld. Symp.*, TWI, Park City, Utah, 2003.
- [16] A. C. Nunes, Jr., *Proc. Aluminum 2001*, Pub. TMS Intl., Materials Park, OH, (2001) 235-248.
- [17] F. Gratecap, G. Racineux, S. Marya, *Int. J. Mater. Form.* 1 (2008) 143-158.
- [18] J. Seaman, B. Thompson, in:, *Proc. Twenty-First 2011 Int. Offshore Polar Eng. Conf.*, International Society of Offshore and Polar Engineers, Maui, Hawaii, 2011.

- [19] K. Kumar, S.V. Kailas, Mater. Sci. Eng. 485 (2008) 367-374.
- [11] Z.W. Chen, T. Pasang, Y. Qi, Mater. Sci. Eng. 474 (2008) 312-316.
- [21] J. McClure, Summer Faculty Research Program Report. NASA Marshall Space Flight Center, 2004.
- [22] D. Rosenthal, Trans American Society Mech. Eng. 68 (1946) 849-866.
- [23] J.A. Querin, J.A. Schneider, Weld. J. 91 (2012) 76s-82s.

CHAPTER VI

CONCLUSIONS

This study was based on a kinematic model of material flow during FSWing as influenced by a threaded pin. This approach is material independent and does not consider the temperatures generated. Chapters II and IV emphasize the importance of proper material flow during welding to prevent defect formation. The rotational rate of the tool must be balanced with the travel rate as a function of the tool design. Not maintaining this balance affects the material flowing around the tool. It was found that increasing the rotation speed at a constant travel velocity leads to an imbalance of flow around the tool resulting in defects on the advancing side of the transverse section. This type of defect forms above the midpoint of the material depth and contains several small voids leading towards the center of the weld. The imbalance in material flow is evident in the x- vs y-force plot as an irregularly shaped plot with too much variation in the x or the y and insufficient variation in the opposite force. Properly balanced material flow results in a round plot of the x- and the y-force.

It is believed that decreased rotational speed leads to defects formed from insufficient force pressing each deposited layer together after each rotation. These defects are scalloped along the parameter showing each rotation's layer. The force plots for low rotational speed welds have a balanced variation in the x and y forces, but the magnitude of the x-force is excessive and not balanced with the y-force.

Also important in the formation of defects is the amount of shoulder contact as discussed in Chapters III and IV. The amount of shoulder contact can depend whether or not the material is sticking or slipping on the tool. The amount of sticking and slipping varies along the length of the panel and therefore changes the material flow pattern as the weld tool travels. This is a potential cause of intermittent defects in FSWs if the weld parameters are near the edge of the acceptable parameter window; therefore, it is important to design weld schedules that are well within the acceptable parameter window. Another potential source of defects in precipitate strengthened aluminum alloys is coarsened precipitates which lower the hardness and strength of the weld nugget. This occurs within the range of weld parameters that produces a fully consolidated weld and can be an unexpected cause of low weld strength.

Because not all defects are related to a lack of consolidation or proper forces on the weld material, it is difficult to use the collected force data to identify regions of lower weld quality within the weld. It is possible to use UMF to identify regions where material flow changes, but understanding the effect of those changes will require more investigation. An understanding of the temperature during welding in precipitate strengthened materials would allow for a better method for identifying suspect regions.

Various schemes are currently being investigated to calculate the temperature from the FSW torque [1]. However, these techniques also make assumptions regarding the contact conditions between the tool and the workpiece. These contact conditions also will affect the assumed efficiency of conversion from mechanical to thermal energy.

6.1 References

- [1] J.A. Querin, J.A. Schneider, *Weld. J.* 91 (2012) 76s-82s.

CHAPTER VII

FUTURE WORK

Heat transfer during FSW needs further investigation as a method for identifying regions of lower weld quality. As discussed in Chapter IV, the precipitate state of materials such as AA2219 impacts the mechanical properties of the material. Identifying regions where the temperature has been high enough to coarsen the precipitates may be possible by monitoring changes in the material flow by studying the forces on the tool during welding, but a more straightforward method would be monitoring the heat transfer during weld. Since direct measurement is difficult and post-weld investigation is destructive, a more exact heat transfer model of the FSW process would be beneficial for determining whether or not the material had reached a temperature that could cause lower performance of the weld. If this model could be applied real-time, the parameters of the weld could be adjusted to detect or prevent regions where temperatures could adversely affect the weld quality.

APPENDIX A
TEMPERATURE AND STRAIN ESTIMATION

A.1 Shear Strain Rate Estimation

The shear strain rate was estimated in Chapter VI using equation 4.1:

$$\dot{\gamma} = \frac{R * \omega}{\delta}$$

Radius of the pin (R) = 3 mm

Tool rotation rate () from 150 to 1000 rpm

Shear surface thickness () = 0.06 mm

A.2 Temperature Calculation

The temperature during FSWing was estimated in Chapter IV using equation 4.2:

$$T = T_{mp} - \frac{T}{2\pi m_t R^3 \left[\frac{1}{3} \left(\frac{R_s}{R} \right)^3 + \frac{H}{R} \right]}$$

Melting temperature of 2219 (T_{mp}) = 917 K

Change in the shear stress (m_t) = 0.45 MPa/K

Radius of the shoulder (R_s) = 7.5 mm

Radius of the pin (R) = 3 mm

Length of the pin (H) = 5.75 mm

Torque (T) =

79 N-m at 150 rpm

72 N-m at 200 rpm

64 N-m at 250 rpm

45 N-m at 400 rpm

44 N-m at 600 rpm

36 N-m at 800 rpm

32 N-m at 1000 rpm

APPENDIX B
WELD PARAMETER WINDOW APPROXIMATION

The equation used to estimate the nugget bulge for C-FSWs using the pin in Chapter IV contains the pin radius, the travel speed, the rotational speed and the pitch of the thread on the pin.

$$Nugget\ Bulge\ (mm) = R_p \left[1 - \cos \left(\frac{Pitch * \omega}{V * \pi} \right) \right] \quad (B.1)$$

Pin radius (R_p) = 6 mm

Pin Pitch (Pitch) = 2 mm

Rotational Speed () from 150-1000 rpm

Travel Speed (V) from 100-500 mmpm

This calculation was repeated over the range of travel speeds and rotational speeds of interest to obtain nugget bulge estimates for the full range of parameters.

APPENDIX C
EXAMPLE DATA PROCESSING PROGRAM

Representative program to load the raw data files into Matlab:

```
% this program loads weld data 130123-3 as test data

close all, clear all, clc

% FSW project directory
FSWpath = 'k:\Graduate School\FSW Data\FSW\130123-3\';

ForceName = {'X-Force', 'Y-Force', 'Z-Force', 'Torque', 'A-
Pulse', 'Z-Pulse'};
Fs = 1024;%frequency of data collection
interval = 256*46;%number of data points per segment

%% load Weld #130123-3 as test data

filename = [FSWpath '130123-3.txt'];
fid = fopen(filename);
tline = fgetl(fid);
temp = fscanf(fid, '%f');
fclose(fid);
clear fid;

temp = reshape(temp,11,[]);
data = temp([4:6],:);%gets x,y,z data from col. 4,5,6

% select X, Y, Z forces and Torque to process
testdata = data(1:3, :);% x,y,z forces not torque

f = Fs*linspace(0, 1, interval+1);
num1 = floor(size(testdata, 2)/interval);
```

Unsupervised match filter program:

```
function [output] =
MUUseFeatureAll2(file1,s,Nontarget,N,opt1,opt2)

x = file1(:,1:N);
R = zeros (N,N);
[rowN,colN] = size(Nontarget);

if strcmp(opt1,'cov')
    R = cov(Nontarget);
elseif strcmp(opt1,'corr')
    R = Nontarget.' * Nontarget/(N-1);
end

ra = rank(R);
if (ra==N)
%     disp('Full rank!')
    RInverse = inv (R);
else
%     disp('Not full rank!')
    [V,D]= eig(R);
    V=fliplr(V);
    D=flipud(fliplr(D));
    V3= V(:,1:ra);
    D3 = D(1:ra,1:ra);
    RInverse = V3*inv(D3)*V3';
end

if strcmp(opt2,'re')
    meanNontarget = mean(Nontarget);
    s = s - meanNontarget;
    x = x - repmat(meanNontarget,size(x,1),1);
end

if size(x,1) > 1
    output = (s * RInverse * x')/(s*RInverse*s');
elseif size(x,1) == 1
    output = (x * RInverse * x');
end
```

Representative program to apply FFT and UMF:

```
% unstructured matched filter to process data 130123-3

loadData1301233

i=3; % finds the fft of the z force (1=x, 2=y, 3=z)
for j = 1:num1
    Ftestdata(j,:) = abs(fft(testdata(i,(j-
1)*interval+1:j*interval)))/interval;
    nFtestdata(j,:) = Ftestdata(j,2:interval/160);
%adjust the frequency range here
end

% creates bins for fft plots
x =0.087:0.087:0.087*(interval/160-1);

% plots the fft for each segment and saves it as a jpg
for i=1:num1
h=figure, stem(x,abs(nFtestdata(i,:)));
axis([0 6.5 0 400])
xlabel('Frequency (Hz)');
ylabel('Amplitude');
title(sprintf('FFT 130123-3 %i', i));
print(h, '-djpeg', sprintf('FFT 130123-3 %i', i));
end

% Method Unsupervised Matched Filter
[score coef junk] = pca1([nFtestdata]);
PCs = 1:3; % changes the number of principle components
used in UMF
for j = 1:size(score,1)
    MFresult(j) = MUseFeatureAll2(score(j,PCs), score(j,
PCs), score(:, PCs), length(PCs), 'cov', 're');
end
figure, stem(1:length(MFresult), MFresult);
title('Unsupervised Matched Filter Result');
```

APPENDIX D
COPYRIGHT PERMISSION

Submit Form

PROMOTING THE GLOBAL SCIENCE AND ENGINEERING PROFESSIONS CONCERNED WITH MINERALS, METALS AND MATERIALS

Obtaining Permission to Reproduce TMS Materials

TMS PUBLICATIONS PERMISSION REQUEST FORM

Name: Hayley Rubisoff Doude
Company or Organization: Mississippi State University
Mailing Address: P.O. Box 9552
City: Mississippi State State: MS Zip: 39759
Phone Number: _____ Fax: _____
E-mail: har15@msstate.edu
Are you a TMS member? YES NO
Are you the author of the TMS material for which permission is being requested? YES NO

CONTENT YOU ARE REQUESTING

TMS title from which you'd like to reprint [For permits, please provide the journal name and not the individual article title.]

*Control of reproduction of materials for which through a trademark theory of trade flow. *Proc. Fabric. Str. Welding and Processing in TMS 2009 Annual Meeting and Exhibition, San Francisco, CA, 2009

If this title is a book, please provide the following:

Primary Author or Editor: _____ ISBN: _____

If this title is a journal, please provide the following:

Month: _____ Year: 2009 Volume: _____ Issue Number: _____

Specific page numbers, figures/tables, and/or total word count you wish to reproduce: _____
149-158

WHERE CONTENT IS BEING USED

Your Publisher: Mississippi State University (dissertation)

Book Title and/or Chapter Title (if applicable): Understanding the mechanisms leading to FSW property variations to aid in defect formation identification via post-weld data processing

Journal Title and Article Title: _____

Projected Publication Date: 12/2013 If Book, Projected Print Run: _____

Format of Your Work: (Check all that apply)

Print CD-ROM World Wide Web


If World Wide Web:

URL: http://library.msstate.edu/

Is the site password protected? YES NO

How long will the material be posted? From indefinitely To _____

Permission granted: YES NO

TMS Signature: 
Matt Baker, Publications Manager

Date: November 7, 2013